Copyright Warning & Restrictions

The copyright law of the United States (Title 17, United States Code) governs the making of photocopies or other reproductions of copyrighted material.

Under certain conditions specified in the law, libraries and archives are authorized to furnish a photocopy or other reproduction. One of these specified conditions is that the photocopy or reproduction is not to be "used for any purpose other than private study, scholarship, or research." If a, user makes a request for, or later uses, a photocopy or reproduction for purposes in excess of "fair use" that user may be liable for copyright infringement,

This institution reserves the right to refuse to accept a copying order if, in its judgment, fulfillment of the order would involve violation of copyright law.

Please Note: The author retains the copyright while the New Jersey Institute of Technology reserves the right to distribute this thesis or dissertation

Printing note: If you do not wish to print this page, then select "Pages from: first page # to: last page #" on the print dialog screen

ABSTRACT

MEMS APPROACHES IN INFRARED IMAGING

by
George Papavieros

The design and performance simulation of a novel Microelectromechanical System (MEMS) based infrared detector, that utilizes coefficient of thermal expansion, is discussed. The detector design uses a variety of thermal expansion coefficient materials, including alloys which are connected to ambient through a thermal conducting bridge. The thermal flux, due to the incident IR photons, is determined by the Extended Blackbody Calculator (BBC). These materials are physically interfaced with different types of piezoelectric resonators, constructed using the MEMS process. The expansion due to heating, applies stress to the piezoelectric resonator material. This thermally induced stress forces the resonator to alter its physical frequency and produces a voltage across its ends, as dictated by the piezoelectric effect. The device performance is characterized in terms of the resonator frequency and voltage as a function of the focal plane array's (pixel's) temperature. The detector performance is comparable to that of commonly used IR imaging systems currently available in the MWIR and LWIR spectral range.

MEMS APPROACHES IN INFRARED IMAGING

by
George Papavieros

A Thesis
Submitted to the Faculty of
New Jersey Institute of Technology
and Rutgers University - Newark
in Partial Fulfillment of the Requirements for the Degree of
Master of Science in Applied Physics

Federated Department of Physics

January 2014

APPROVAL PAGE

MEMS APPROACHES IN INFRARED IMAGING

George Papavieros

Dr. Nuggehalli M. Ravindra Advisor Professor of Physics, NJIT	Date
Dr. Keun Hyuk Ahn, Committee Member Associate Professor of Physics, NJIT	Date
Dr. Cristiano Luis Dias, Committee Member Assistant Professor of Physics, NJIT	Date
Peter Kaufman, Committee Member Chairman of the Board, Public Service Solutions Inc, Fresh Meadows, NY	Date

BIOGRAPHICAL SKETCH

Author: George Papavieros

Degree: Master of Science

Date: January 2014

Undergraduate and Graduate Education:

- Master of Science in Applied Physics,
  New Jersey Institute of Technology, Newark, NJ, 2014

- Bachelor of Science in Physics,
  University of Athens, Athens, Greece, 2012

Major: Physics

Presentations and Publications:

- Modeling and Simulation of TCE Based Infrared Imager (in preparation for publication)

To my loving Parents and Grandparents to whom I owe everything I have achieved in my life so far and who guided me to where I am today

ACKNOWLEDGMENTS

Foremost, I would like to express my sincere gratitude to my advisor Prof. Nuggehalli M. Ravindra for the continuous support he provided me during my Master's study and research. His patience, motivation and enthusiasm, along with his immense knowledge and guidance helped me throughout the time of the research and writing of this thesis. He became my mentor, my family and my friend.

I would also like to thank Peter Kaufman for the guidance, comments and support he provided me throughout my research. I thank the rest of my thesis committee members: Prof. Keun Hyuk Ahn and Prof Chistiano Luis Dias for their encouragement, insightful comments, and questions.

Last but not the least, I would like to thank my friends and fellow lab-mates: Vijay Kasi Somayajula and Chiranjivi Lamsal for their comments, insights, ideas and all the stimulating discussions we had.

TABLE OF CONTENTS

TABLE OF CONTENTS
(Continued)

TABLE OF CONTENTS
(Continued)

LIST OF TABLES

LIST OF TABLES
(Continued)

LIST OF FIGURES

LIST OF FIGURES
(Continued)

LIST OF FIGURES
(Continued)

CHAPTER 1

INTRODUCTION

In this study, the design and simulation of a Microelectromechanical (MEMS) based infrared (IR) detector is discussed. The detector consists of two parts; a heat-sensitive metal and a piezoelectric component that interfaces with the metal.

In Chapter 2, the fundamentals of thermal expansion as well as the effects of temperature on the thermal and mechanical properties of materials are discussed. The isotropic and anisotropic behavior of materials is analyzed by introducing the thermal expansion coefficients and elastic properties.

In Chapter 3, the fundamentals of piezoelectricity are discussed. A general discussion of the effects of pressure on materials precedes the introduction to ferroelectricity and dielectric properties of materials. The piezoelectric effect and its potential uses in sensors, actuators and resonators are presented in light of MEMS technology.

In Chapter 4, the device under consideration, in this study, is introduced. The device components are analyzed utilizing the theory discussed in Chapters 2 and 3. Simulations of the thermal, voltage and frequency response are presented. The simulations consider various material candidates for both the components of the detector. Results and discussion are presented in Chapter 4.

The conclusions of the present study, in Chapter 5, presents a summary of the results obtained along with future work and development of the proposed detector configuration.

CHAPTER 2

FUNDAMENTALS OF THERMAL EXPANSION

2.1 Introduction to Thermal Expansion

In this Chapter, the fundamentals of thermal expansion as well as the effects of temperature on the mechanical properties of materials are discussed.

When a material is heated, it will, in most cases, expand and when it is cooled, it will shrink. This is the fundamental physical phenomenon of thermal expansion. However, the increase in volume, upon heating, is not an absolute effect for every material. The result due to heating a material can be the exact opposite due to complex magnetic and phonon properties. In other words, there are materials that contract on heating [1].

Thermal expansion is caused by the anharmonicity of lattice vibrations. This means that the springs (bonds) that hold the atoms together do not exactly follow Hooke's law. In order to investigate this further, because of Pauli's Exclusion Principle, the atoms cannot get extremely close to each other. Therefore, the potential energy diverges when the inter-atomic distance, Δr, approaches zero. This asymmetry favors longer distances between the atoms rather than shorter ones (Figure 2.1). As a result, interatomic distances increase when a material is heated [1, 2].

The coefficient of thermal expansion, α, is given by:

$$\alpha = \frac{\gamma C_{Debye}}{3KV} \tag{2.1}$$

where, γ is Grüneisen's parameter, C_{Debye} is the Debye specific heat, V is the volume and K is the bulk modulus.

$$\gamma = -\frac{\partial ln\theta}{\partial lnV} \quad , \theta \text{ is the Debye temperature} \tag{2.2}$$

The bulk modulus (K) along with the other elastic constants, Young's modulus (E), Poisson's ratio (ν) and shear modulus (G), describe the elastic properties of the material.

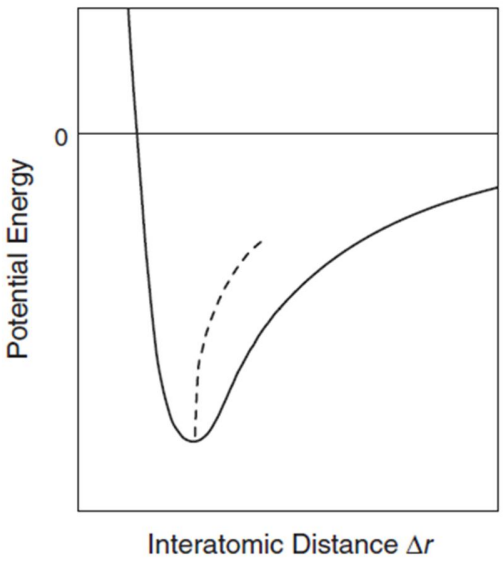

--------- Potential energy

- - - - - average interatomic distance

Figure 2.1 Potential energy for a typical bond as a function of interatomic distance. Source: [2]

K and γ depend weakly on temperature while α shows a strong dependence similar to C_{Debye}.

$$C_{Debye} = 9Nk_B(\frac{T}{\theta})^3 \int_0^{\theta/T} \frac{x^4 e^x}{(e^x-1)^2} dx \quad (2.3)$$

Therefore, the Volume is:

$$V(T) = V_o + \frac{9Nk_B\gamma}{K} T(\frac{T}{\theta})^3 \int_0^{\theta/T} \frac{x^3}{e^x-1} dx \quad (2.4)$$

This is the theoretical thermal expansion which is used to fit the corresponding experimental data with refinement of θ, when γ and K are known.

The coefficient of thermal expansion describes changes in physical dimensions with change in temperature. Specifically, it measures the fractional change in size per degree change in temperature at a constant pressure. Several types of coefficients have been developed to express this mathematically: volumetric, area, and linear. The choice of the coefficient depends on the particular application and the dimensions that are considered to be important in that particular application. For solids, one might only be concerned with the change in length, or over some area (that may include grains, grain boundaries, defects, dislocations etc.).

The coefficient of volume expansion (α_v) is the most basic thermal expansion coefficient. In general, substances expand or contract when their temperature changes, with expansion or contraction occurring in all directions. Substances that expand at the same rate, in every direction, are called isotropic. For isotropic materials, the area and linear coefficients may be calculated from the coefficient of volume expansion as will be shown in the following sections.

2.2 General Volumetric Thermal Expansion Coefficient

In general, the coefficient of volume expansion is given by:

$$\alpha_v = \frac{1}{V}\left(\frac{\partial V}{\partial T}\right)_p \tag{2.5}$$

where, p is the pressure, held constant during heating of the material, which leads to the expansion. Especially when dealing with the influence of heat on gas, the constant pressure plays an important role because it affects volume as well.

In this study, the influence of heat on solids is considered. As described above, materials react to temperature fluctuations by changing their size. Commonly engineered solids have coefficients of thermal expansion that do not vary significantly over a range of temperatures. Because of this, high accuracy is not critical and calculations of change in physical dimensions can be made based on a constant average value of the coefficient.

The change in physical dimensions can be distinguished in accordance with the way the solid reacts to the temperature change. The expansion can be volumetric, linear or area.

2.2.1 Volumetric Expansion

For a solid, the volumetric thermal expansion coefficient is given by:

$$\alpha_v = \frac{1}{V}\frac{dV}{dT} \tag{2.6}$$

where, V is the volume of the solid and dV/dT is the rate of change in volume.

Using the above equation and provided that the coefficient, α_v, is known and does not change with temperature, the change in volume can be calculated using:

$$\frac{\Delta V}{V} = \alpha_v \Delta T \tag{2.7}$$

where, $\Delta V/V$ is the factional change in volume and ΔT is the change in temperature.

If the coefficient of thermal expansion does change with temperature, then the integral form of the above has to be used. It is given by [3]:

$$\frac{\Delta V}{V} = \int_{T_0}^{T_0+\tau} \alpha_V(T) T dT \tag{2.8}$$

where, T_0 is the initial temperature and $T_0+\tau$ is the final temperature.

2.2.2 Area Expansion

In area expansion, the areal thermal expansion coefficient is connected with the change in the area dimensions of the heated material. It is given by:

$$\alpha_A = \frac{1}{A}\frac{dA}{dT} \tag{2.9}$$

where, A is the area of interest and dA/dT is the change in area per unit change in temperature.

Similarly, the areal thermal expansion coefficient can be used to calculate the change in area.

$$\frac{\Delta A}{A} = \alpha_A \Delta T \tag{2.10}$$

If the coefficient, α_A, changes with temperature, the above equation needs to be modified as [3]:

$$\frac{\Delta A}{A} = \int_{T_0}^{T_0+\tau} \alpha_A(T) T dT \quad (2.11)$$

2.2.3 Linear Expansion

For one dimensional change in the material, the linear coefficient of thermal expansion, which describes the change in length per degree of change in temperature, is utilized [3, 4]:

$$\alpha_L = \frac{1}{L}\frac{dL}{dT} \quad (2.12)$$

where, L is the length of the material and dL/dT is the rate of change of the dimension L per unit change of the temperature.

Again provided that α is known, change in length can be calculated using the equation:

$$\frac{\Delta L}{L} = \alpha_L \Delta T \quad (2.13)$$

In this case, if α changes with temperature, integration is required:

$$\frac{\Delta L}{L} = \int_{T_0}^{T_0+\tau} \alpha_L(T) T dT \quad (2.14)$$

Table 2.1 Coefficient of Thermal Expansion for Common Elements at 20 ^{0}C

Substance	Linear Coefficient	Volumetric Coeff.
	α (1/ ^{o}C)	β = 3α (1/ ^{o}C)
Aluminum	24 x 10^{-6}	72 x 10^{-6}
Brass	19 x 10^{-6}	57 x 10^{-6}
Copper	16.6x 10^{-6}	51 x 10^{-6}
Zn	29.7 x 10^{-6}	27 x 10^{-6}
ZnO	4.31 x 10^{-6}	9 x 10^{-6}
Iron/Steel	12 x 10^{-6}	36 x 10^{-6}
Lead	29 x 10^{-6}	87 x 10^{-6}
Ice	51 x 10^{-6}	153 x 10^{-6}
Diamond	1.18x10^{-6}	950 x 10^{-6}
Mercury		180 x v
AlN	5.27x 10^{-6}	15.81 x 10^{-6}

Source: [4, 5]

2.3 Isotropic and Anisotropic Materials

Isotropy, in general, means uniformity in all directions/orientations. In materials science, isotropic materials are those that have identical properties in all directions. Metals are good examples of isotropic materials.

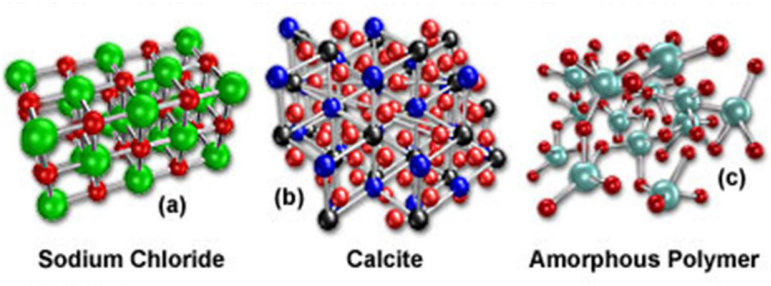

Figure 2.2 Crystalline structures of isotropic and anisotropic materials.
Source: [6]

Most metallic alloys are considered isotropic. Such materials, as mentioned earlier, have four elastic constants: Young's modulus (E), shear modulus (G), bulk modulus (K) and the Poisson's ratio (ν). The relationship between the elastic constants can be reduced to two independent equations:

$$K = E/[3(1-2\nu)] \tag{2.15a}$$

$$G = E/[2(1+\nu)] \tag{2.15b}$$

The simplest crystalline lattice structure is the cubic, as illustrated by the molecular model of sodium chloride in Figure 2.2 (a), an arrangement where all of the sodium and chloride ions are ordered with uniform spacing along three mutually perpendicular axes. Each chloride ion is surrounded by (and electrostatically bonded to) six individual sodium ions and vice versa for the sodium ions. It is a perfect example of an isotropic crystal [2, 6].

For Isotropic materials, and for small expansions, because of the uniformity in all directions, the volumetric thermal expansion coefficient is three times the linear expansion coefficient.

$$\alpha_V = 3\alpha_L \tag{2.16}$$

To further investigate the above, the volume composition of these materials has to be analyzed. In isotropic alloys, three mutually orthogonal directions are found. Therefore, for small changes in the material's size, one third of the volumetric expansion is placed on each of the three axes.

For a metal cube with side length L, $= L^3$. After the metal is heated, the new volume will become:

$$V + \Delta V = (L + \Delta L)^3 = L^3 + 3L^2\Delta L + 3L\Delta L^2 + \Delta L^3 ,$$

$$\Delta L^2 << 1 \text{ and } \Delta L^3 << 1 \Rightarrow$$

$$L^3 + 3L^2\Delta L = V + 3V\frac{\Delta L}{L} \rightarrow L^3 + L^3\alpha_V\Delta T = L^3 + 3L^3\alpha_L\Delta T \Rightarrow$$

$$\alpha_V = 3\alpha_L$$

The terms ignored are due to the fact that small changes in volume and temperature are considered. If large changes are utilized, then the third and fourth term have to be taken into consideration.

Similarly, the relationship between areal and linear coefficient is derived:

$$A + \Delta A = (L + \Delta L)^2 = L^2 + 2L\Delta L + \Delta L^2$$

$$\Delta L^2 << 1 \Rightarrow$$

$$L^2 + 2L\Delta L = A + 2A\frac{\Delta L}{L} \rightarrow L^2 + L^2\alpha_A\Delta T = L^2 + 2L^2\alpha_L\Delta T \Rightarrow$$

$$\alpha_A = 2\alpha_L$$

Anisotropic materials behave differently. They have anisotropic structure which leads to different values of properties being obtained when specimens are probed from several directions within the same material. Observed properties often vary depending on whether the observed phenomena are based on optical, acoustical, thermal, magnetic, or electrical properties. As mentioned earlier, isotropic properties remain symmetrical, regardless of the direction of measurement. In the section on thermal property, the linear expansion coefficient, α_L, is different in different directions. The result is that, upon heating, they will expand unequally among the three axes [6].

The lattice structure illustrated in Figure 2.2 (b) represents the mineral calcite (calcium carbonate), which consists of a rather complex, but highly ordered three-dimensional array of calcium and carbonate ions. Calcite has an anisotropic crystalline lattice structure that interacts with light in a totally different manner than isotropic crystals. The polymer illustrated in Figure 2.2 (c) is amorphous and devoid of any recognizable periodic crystalline structure. Polymers often possess some degree of crystalline order and may or may not be optically transparent.

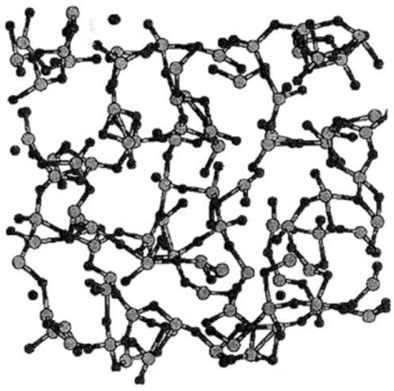

Figure 2.3 Silica Glass - No long range order of SiO_4 tetrahedra.
Source: [7]

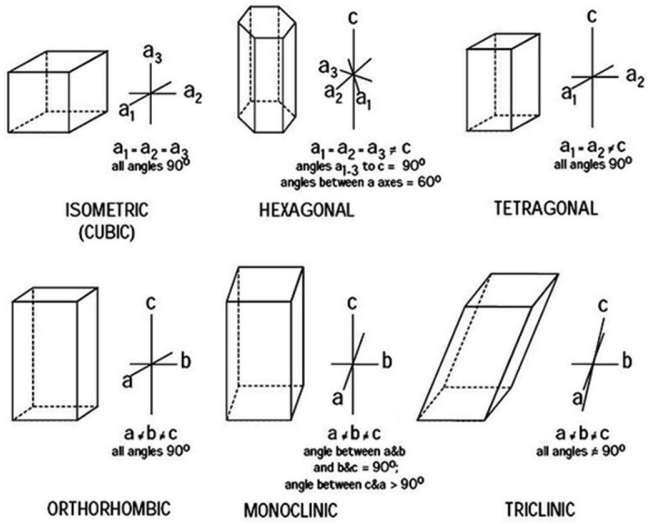

Figure 2.4 Crystal structures.
Source: Image taken from http://www4.nau.edu/meteorite/meteorite/book-glossaryc.html, Glossary c by James Wittke (2009), Northern Arizona University, Meteorite page, College of Engineering, Forestry & Natural Sciences. Accessed October 2 2013

If the crystal symmetry is monoclinic or triclinic, even the angles between these axes are subject to changes due to thermal cycles. In such cases, the coefficient of thermal expansion is treated as a tensor, with up to six independent elements. A good way to determine the elements of the tensor is to study the expansion by powder diffraction.

2.4 Mechanical Properties

2.4.1 Young's Modulus Of Elasticity

Young's modulus or elastic modulus is a way to measure stiffness and is a property that can be used to characterize materials. Elasticity is a material property which will restore its original shape after distortion. A spring is an example of an elastic object which, when stretched, exerts a restoring force which tends to bring it back to its original length. This

restoring force is, in general, proportional to the stretch described by Hooke's Law. Young's modulus is defined as the ratio of the stress along a specified axis over the strain along the same axis. In solid mechanics, the slope of the stress-strain curve at any point is called the tangent modulus. The tangent modulus of the initial, linear portion of a stress-strain curve is called Young's modulus and it can be experimentally determined from the slope of a stress-strain curve created during tensile tests conducted on a sample of the material. In anisotropic materials, Young's modulus may have different values depending on the direction of the applied force with respect to the material structure [8].

Young's modulus can be used to calculate the change in dimensions of an isotropic elastic material and predict how much the material extends under tension or how much it contracts under pressure and vice versa.

Young's modulus is not always the same in all directions depending on the nature of the material. Most metals and ceramics are isotropic; thus, their mechanical properties will remain the same no matter the orientation. If we consider the impurities that can be found in metals and grain structures, then, in such cases, the materials are anisotropic and the corresponding Young's modulus is different depending on the direction of the strain or force vector.

The calculation of Young's modulus is performed by dividing the tensile stress by the tensile strain [9]:

$$E = \frac{\sigma}{\varepsilon} = \frac{F/A_o}{\Delta L/L_o} \tag{2.17}$$

where, E is the Young's modulus, F is the force under tension, A_o is the cross sectional area where the force is applied, ΔL is the change in length, L_o is the materials' original length.

The force produced under specific strain is determined by:

$$F = \left(\frac{EA_o}{L_o}\right)\Delta L = kx \text{ , where, } \left(\frac{EA_o}{L_o}\right) = k \text{ and } \Delta L = x \qquad (2.18)$$

The above equation can be used to calculate the force that the material applies in one direction after thermal expansion. In (Table 2.2) the Young's modulus and elastic properties of some common materials are summarized.

Table 2.2 Young's Modulus and Elastic Properties of some Common Materials

Material	Young's Modulus (Modulus of Elasticity)		Ultimate Tensile Strength	Yield Strength
	- E -		- Su -	- Sy -
	(106 psi)	(109 N/m2, GPa)	(106 N/m2, MPa)	(106 N/m2, MPa)
ABS plastics		2.3	40	
Acrylic		3.2	70	
Aluminum	10	69	110	95
Aluminium Bronze		120		
Antimony	11.3			
Aramid		70 - 112		
Beryllium (Be)	42	287		
Bismuth	4.6			
Bone, compact		18	170	
			(compression)	
Bone, spongy		76		
Boron				3100
Brass		102 - 125	250	
Brass, Naval		100		
Bronze		96 - 120		
Cadmium	4.6			
Carbon Fiber Reinforced Plastic		150		
Carbon nanotube, single-walled		1000+		
Cast Iron 4.5% C, ASTM A-48			170	
Chromium	36			
Cobalt	30			
Concrete		17		
Concrete, High Strength (compression)		30	40	
			(compression)	
Copper	17	117	220	70
Diamond (C)		1220		
Douglas fir Wood		13	50	
			(compression)	
Fiberboard, Medium Density		4		
Flax fiber		58		
Glass		50 - 90	50	
			(compression)	
Glass reinforced polyester matrix		17		
Graphene		1000		
Grey Cast Iron		130		
Gold	10.8	74		
Granite		52		
Hemp fiber		35		
Iridium	75			
Iron	28.5	210		
Lead	2			
Magnesium metal (Mg)	6.4	45		
Manganese	23			
Marble			15	
MDF - Medium-density fiberboard		4		
Mercury				
Molybdenum (Mo)	40	329		
Nickel	31	170		
Niobium (Columbium)	15			
Nylon		4-Feb	75	45
Oak Wood (along grain)		11		
Osmium (Os)	80	550		
Phosphor Bronze		116		
Pine Wood (along grain)		9	40	
Platinum	21.3			
Plutonium	14	97		
Polycarbonate		2.6	70	
Polyethylene HDPE (high density)		0.8	15	
Polytehylene, LDPE (low density)		0.11 - 0.45		
Polyethylene Terephthalate, PET		2 - 2.7	55	
Polyimide		2.5	85	
Polypropylene, PP		1.5 - 2	40	
Polystyrene, PS		3 - 3.5	40	

Table 2.2 Young's Modulus and Elastic Properties of some Common Materials (Continued)

Material	Young's Modulus (Modulus of Elasticity)		Ultimate Tensile Strength	Yield Strength
	- E -		- Su -	- Sy -
	(106 psi)	(109 N/m2, GPa)	(106 N/m2, MPa)	(106 N/m2, MPa)
Potassium				
Rhodium	42			
Rubber, small strain		0.01 - 0.1		
Sapphire		435		
Selenium	8.4			
Silicon	16	130 - 185		
Silicon Carbide		450		3440
Silver	10.5			
Sodium				
Steel, stainless AISI 302		180	860	502
Steel, Structural ASTM-A36		200	400	250
Steel, High Strength Alloy ASTM A-514			760	690
Tantalum	27			
Teflon. PTFE		0.5		
Thorium	8.5			
Tin		47		
Titanium	16			
Titanium Alloy		105 - 120	900	730
Tooth enamel		83		
Tungsten (W)		400 - 410		
Tungsten Carbide (WC)		450 - 650		
Uranium	24	170		
Vanadium	19			
Wrought Iron		190 - 210		
Zinc	12			

- $1\ N/m^2 = 1x10^{-6}\ N/mm^2 = 1\ Pa = 1.4504x10^{-4}\ psi$
- $1\ psi\ (lb/in^2) = 144\ psf\ (lb_f/ft^2) = 6{,}894.8\ Pa\ (N/m^2) = 6.895x10^{-3}\ N/mm^2$

Source: [10]

2.4.2 Poisson's Ratio

When a material is compressed in one dimension, it tends to expand in the two perpendicular directions to the direction it was compressed. This phenomenon is called the Poison effect. The ratio of transverse contraction strain to longitudinal extension strain in a stretched bar is called Poison's Ratio (ν). In case of a material that is being stretched, it tends to contract in the perpendicular directions. Again, here, Poison's ratio is the ratio of relative contraction to relative stretching and will have the same value as in the previous case. If the material shrinks in the transverse direction when compressed (or expand when stretched), then the Poison's ratio will yield a negative value [11, 12].

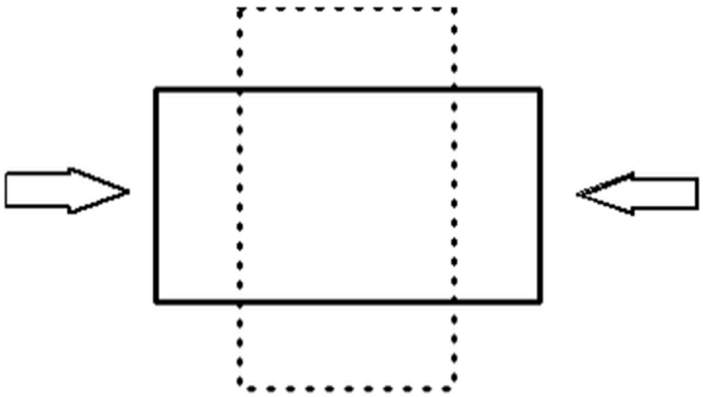

Figure 2.5 Representation of poison's effect.
Source: [11]

Mathematically,

$$\nu = -\frac{d\varepsilon_{trans}}{d\varepsilon_{axial}} = -\frac{d\varepsilon_y}{d\varepsilon_x} = -\frac{d\varepsilon_z}{d\varepsilon_x} \tag{2.19}$$

where, ν is Poisson's ratio, ε_{trans} is the transverse strain and ε_{axial}, the axial strain.

For a rod with thickness d under longitudinal tension, it will cause a change ΔL in its thickness given by:

$$\Delta L' = -d \cdot \nu \frac{\Delta L}{L} \tag{2.20}$$

If we consider a cube stretched in the x-direction with ΔL representing the change in length in x direction and $\Delta L'$ is the change in length in y and z directions, then the infinitesimal diagonal strains for each axis will be as follows:

$$d\varepsilon_x = \frac{dx}{x} \tag{2.21a}$$

$$d\varepsilon_y = \frac{dy}{y} \tag{2.21b}$$

$$d\varepsilon_z = \frac{dz}{z} \tag{2.21c}$$

$$-\nu \int_L^{L+\Delta L} \frac{dx}{x} = \int_L^{L-\Delta L'} \frac{dy}{y} = \int_L^{L-\Delta L'} \frac{dz}{z} \tag{2.21d}$$

The above equations yield the relationship between ΔL and $\Delta L'$:

$$(1 + \frac{\Delta L}{L})^{-\nu} = 1 - \frac{\Delta L'}{L} \tag{2.22}$$

For ΔL, $\Delta L' << 1 \rightarrow \nu \approx \frac{\Delta L'}{\Delta L}$

The relative change in volume, ΔV/V, of the cube is given by:

$$V = L^3 \tag{2.23a}$$

$$V + \Delta V = (L + \Delta L)(L - \Delta L')^2 \tag{2.23b}$$

$$\frac{\Delta V}{V} = \left(1 + \frac{\Delta L}{L}\right)\left(1 - \frac{\Delta L'}{L}\right)^2 - 1 \tag{2.23c}$$

We obtain:

$$\frac{\Delta V}{V} = \left(1 + \frac{\Delta L}{L}\right)^{1-2\nu} - 1 \rightarrow \frac{\Delta V}{V} \approx (1 - 2\nu)\frac{\Delta L}{L} \tag{2.23d}$$

Hooke's law can now be generalized in three dimensions; for an isotropic material, the deformation in one axis can cause deformations along the perpendicular axes in three dimensions:

$$\varepsilon_\iota = \frac{1}{E}[\sigma_i(1 + \nu) - \nu(\sigma_x + \sigma_y + \sigma_{z)}] \tag{2.24}$$

where, ε_x, ε_y, ε_z are strains in the directions x, y, z; σ_x, σ_y, σ_z represent stress in the directions x, y and z, E is the Young's modulus and ν is the Poison's ratio.

2.4.3 Bulk Modulus

Bulk modulus (K) measures the physical reaction of materials to uniform compression. It is defined as the ratio of the change in pressure to the fractional volume compression:

$$K = V\frac{\Delta P}{\Delta V} \tag{2.25}$$

where, P is the pressure and V is the volume.

Bulk modulus is proportional to the amount of energy that can be stored in a material [13].

2.4.4 Shear Modulus

Shear modulus (G) defines the rigidity of the material. It describes the response of a substance to shear or strain. It quantifies the deformation of a solid when an external force is applied parallel to one of its surfaces, while its opposite face experiences an opposite force.

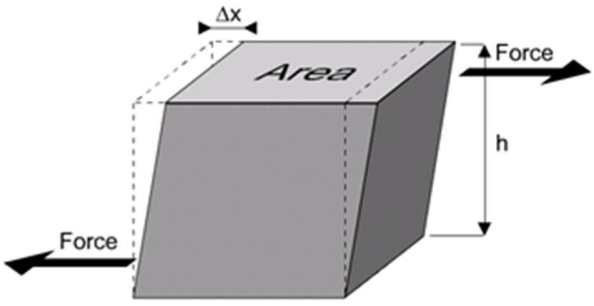

Figure 2.6 Shear deformation.
Source: www.spaceflight.esa.int/impress/text/education/Mechanical%20Properties/MoreModuli.html
Access date: 10/02/2013

$$G = \frac{F/A}{\Delta x/l} \tag{2.26}$$

where, F/A is the shear stress, F is the force, A is the area, Δx is the transverse displacement and l is the original length. The Shear modulus for some common materials is presented in Table 2.3.

Table 2.3 Shear Modulus of some Common Materials

Material	Typical values for Shear Modulus (Gpa) at 298 K
Diamond	478
Steel	79.3
Copper	44.7
Titanium	41.4
Glass	26.2
Aluminium	25.5
Polyethylene	0.117
Rubber	0.0006

Source: http://homepages.which.net/~paul.hills/Materials/MaterialsBody.html, http://www.thefreelibrary.com/Cure+system+effect+on+low+temperature+dynamic+shear+modulus+of...-a0111451108 Access date: 11/02/2013 [14]

2.5 Negative Thermal Expansion (NTE)

As mentioned earlier, in nature, there are materials that have an opposite response to heat; i.e., instead of expanding with temperature rise, they contract. For the past two decades, the field of NTE has undergone a rapid expansion. The potential for applications of NTE materials in controlled thermal expansion composites has been thoroughly investigated and a number of possible applications in electronics, fiber optics and others have been proposed. Some of the common NTE materials are presented in Table 2.4 [2, 15].

Table 2.4 Typical NTE Materials

Materials	α (ppm K^{-1})	T_{oper} (K)	Category	Method[a]	References
β-eucryptite	−1 to −6[b]	300–900	1	D	[1, 4, 15]
α-ZrW_2O_8	−9	<425	1	D/N	[20]
β-ZrW_2O_8	−6	425–1030	1	D/N	[20]
$Cd(CN)_2$	−33.5	170–375	1	X	[27]
ReO_3	−0.5	<220	1	N	[10]
ReO_3	−0.7	600–680	1[b]	N	[10]
$(HfMg)(WO_4)_3$	−2[b]	Room temp. ~ 1070	1	D	[11]
$Sm_{2.75}C_{60}$	−100[b]	<30	2	X	[29]
$Bi_{0.95}La_{0.05}NiO_3$	−82[b]	320 ~ 380	2	D	[35]
Invar (Fe-36Ni)	0.1–1	<500	3	D	[37, 38]
Invar (Fe_3Pt)	−6 to −30	100–420	3	D	[49, 50]
$Tm_2Fe_{16}Cr$	−9[b]	340–380	3	X	[47]
CuO nano particles	−36[b]	<150	3[b]	X	[48]
$Mn_3Cu_{0.53}Ge_{0.47}N$	−16	265–340	3	D	[73]
$Mn_3Zn_{0.4}Sn_{0.6}N_{0.85}C_{0.15}$	−23	270–335	3	D	[75]
$Mn_3Zn_{0.5}Sn_{0.5}N_{0.85}C_{0.1}B_{0.05}$	−30	280–340	3	D	[76]

[a] D, dilatometry; N, neutron diffraction; X, x-ray diffraction.
[b] The thermal expansion is anisotropic and α is the averaged value.
[c] Details of the mechanism are unknown. The classification is temporary (see text).

Source: [2]

The mechanisms for NTE can be separated into three categories. (i) flexible network (transverse vibrational modes), (ii) atomic radius contraction, (iii) magneto volume effect.

2.5.1 Flexible Network

The materials in this category are characterized by strong atomic bonds. As bonds strengthen, the corresponding potential well becomes more symmetric and the vibrations more harmonic. If the bonds are very strong, then it is possible not to experience any expansion at all. Negative thermal expansion occurs when dynamic deformation takes over free space in the crystal lattice provided that the thermal expansion of the core unit is suppressed.

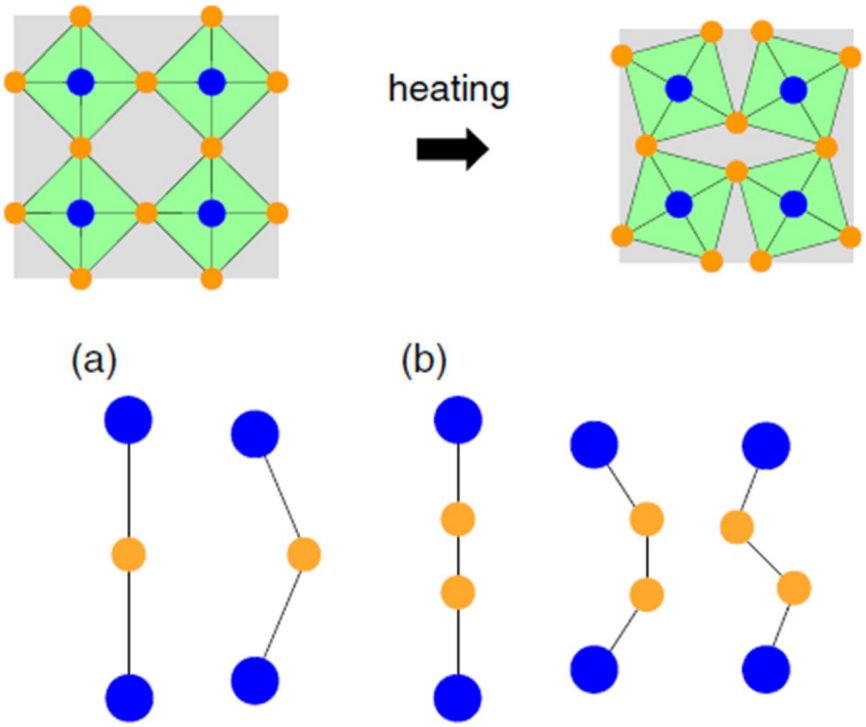

Figure 2.7 Flexible network mechanism.
Source: [2]

Structural allowance in necessary for this mechanism [2, 15].

2.5.2 Atomic Radius Contraction

This type of NTE occurs from the variation of the atomic radius depending on the valency. When an atom accepts a charge (electron), it expands and when it loses one, it shrinks. This variation depends on the electronic configuration of the element. The total net volume will contract if the expansion of an electron –accepting atom is relatively smaller than the contraction of an electron-donating atom. NTE can occur when this electron transfer is thermally induced.

Generally though, the atomic radius depends also on the spin configuration of the atom. So, for a given valency, the high spin state has a larger radius than that with a low

spin because of the Pauli's exclusion principle that forbids to put the electrons in the same orbital and the same state [2].

2.5.3 Magneto Volume Effect

A large volume of a magnetic metal is likely to have a magnetic moment. The magneto volume effect is the induced change in volume due to a variation in the amplitude of the magnetic moment. From the electronic theory of solids, it can seen that an increase in volume suppresses the overlap of electronic orbitals and therefore reduces the width of electronic bands. Narrowing of the bandwidth can increase the density of states ρ(E) with Fermi energy E_f, which favors magnetism [2].

Magneto volume effect corresponding to a lattice expansion can be defined as:

$$\omega_s \frac{\partial F_m(M,T,V)}{\partial V} / K \tag{2.27}$$

where, ω_s is the spontaneous volume magnetostriction, F_m(M,T,V) is the magnetic contribution of free energy, M is the amplitude of the magnetic moment and K is the bulk modulus.

$$F_m(M,T,V) = \frac{1}{2} a(T,V) M^2 + \frac{1}{4} b(T,V) M^4 + \cdots \tag{2.28}$$

where, a, b are coefficients that depend on the density of states near the Fermi energy.

Combining the above equations yields:

$$\omega_s = CM^2/K \tag{2.29}$$

where, $C = -\frac{1}{2}\frac{\partial a(T,V)}{\partial V}$ is the magnetovolume coupling constant.

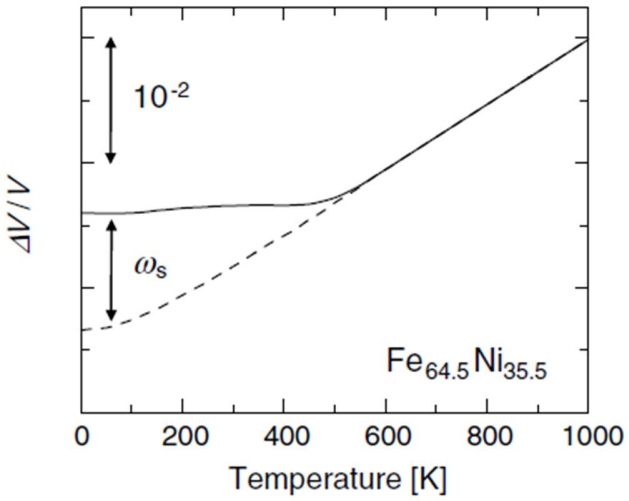

Figure 2.8 Volume thermal expansion $\Delta V/V$ of Fe64.5Ni35.5.
Source: [2]

ω_s can be estimated by subtracting the ideal lattice thermal expansion (equation 2.4) from the measured value.

2.6 Effect of Temperature on Resistance and Resistivity

The electrical resistance (R) of a conducting material is the impedance to an electrical current through the conducting material. The inverse is the electrical conductance (G) which shows instead how easy the current flows through the conductor [4].

The resistance of a conductor is the ratio of the applied voltage to the current that runs through it:

$$R = \frac{V}{I} \quad , G = \frac{I}{V} \tag{2.30}$$

The resistance of a conductor depends on the shape of the material. It is inversely proportional to the cross-sectional area and proportional to its length:

$$R = \rho \frac{l}{A}, \; G = \sigma \frac{A}{l} \tag{2.31}$$

where, l is the length, A is the cross sectional area, ρ is the electrical resistivity and σ is the conductivity.

The resistivity and conductivity are proportionality constants ($\rho = 1/\sigma$) and depend on the material. Resistivity is a measure of the material's ability to oppose electric current. It is given by:

$$\rho = R \frac{A}{l}, \; \sigma = G \frac{l}{A} \tag{2.32}$$

Resistivity determines if the material under consideration is a metal, semimetal, semiconductor, insulator or superconductor.

Metals are characterized by delocalized or free electrons. These electrons are free to move within the metal. The resistivity of metals increases with temperature. This can be explained in many ways. A simple explanation is that, at high temperatures (energies), the atoms of a metal vibrate more (phonon energy increases); therefore, it is more likely

for a collision to occur as the electrons move, hence higher resistance/ resistivity. Another way to look at it is by examining the number of free electrons in a metal. Upon heating, more electrons are liberated from the atoms. More electrons mean more collisions and therefore bigger resistance. An even better explanation is on the level of quantum theory in combination with the above. In order for an electron to interact with an atom and lose some of its energy, there needs to be an appropriate change in energy level. When the temperature increases, the distribution of energy level in an atom widens and the possibilities for such interaction multiply. In this way, the energy gets lost quicker; this is the same as the resistance being larger.

If the temperature does not vary too much, then a linear approximation can be made for the resistance:

$$R(T) = R_o[1 + \alpha'(T - T_o)] \tag{2.33}$$

α' is the temperature coefficient of resistance (different reference temperatures), T_o is the fixed temperature of reference, R_o is the resistance at T_o [4].

2.7 Effect of Temperature on Semiconductor Band Gap

In semiconductors, upon heating, the electrons move from the valence energy band to the conduction energy band due to the thermal energy. This leads to both the electrons moving free in the conduction band and the holes they leave behind also to flow freely in the valence band. Hence, the resistivity decreases with increasing temperature.

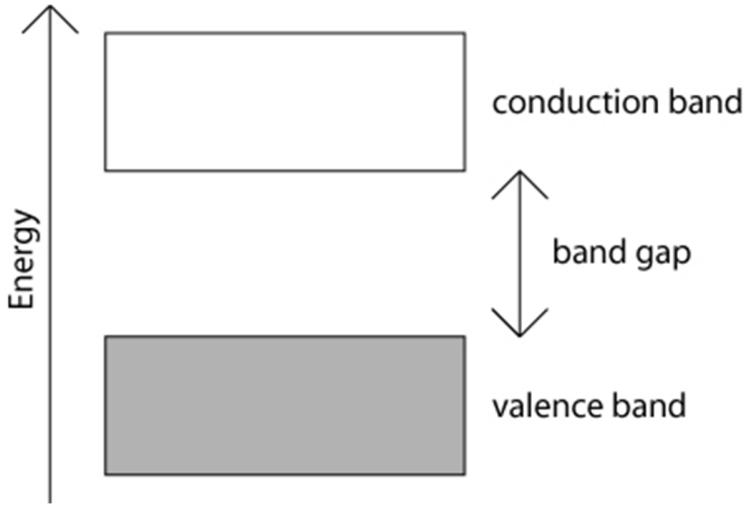

Figure 2.9 Semiconductor band structure.

The electrical resistance of an undoped semiconductor decreases exponentially with temperature:

$$\rho = \rho_o e^{-aT} \tag{2.34}$$

An even better approximation of the temperature – resistivity relation is given by the Steinhart-Hart equation:

$$\frac{1}{T} = A + Bln(\rho) + C(\ln(\rho))^3 \tag{2.35}$$

where, A, B, C are the Steinhart-Hart coefficients.

Unlike metals, in semiconductors, there are not as many free electrons. At absolute zero, a semiconductor behaves like a perfect insulator. When it is heated, because of the creation of electron-hole pairs, the resistivity decreases as temperature increases [4, 16].

Generally, the band-gap energy of semiconductors tends to decrease with increasing temperature. When temperature increases, the amplitude of atomic vibrations

increases, leading to larger interatomic spacing. The interaction between the lattice phonon and the free electrons and holes will also affect the band gap to a smaller extent. The relationship between band gap energy and temperature can be described by Varshni's empirical expression.

$$E_g(T) = E_g(0) - \frac{aT^2}{T+\beta} \tag{2.36}$$

where, $E_g(0)$, a, β are material constants [16].

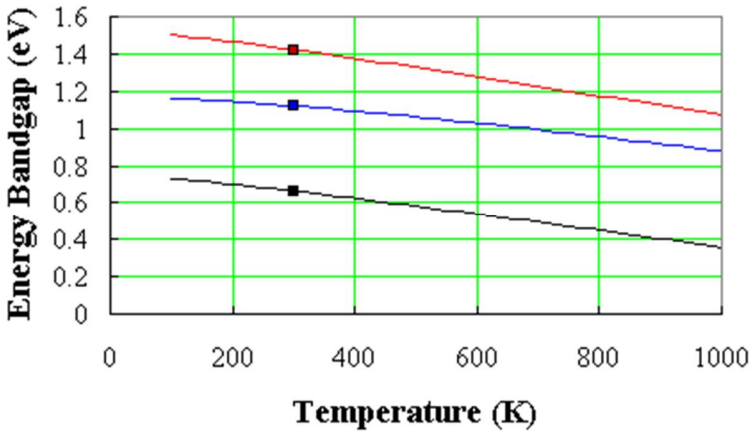

Ge (bottom/black curve), Si (blue curve) and GaAs (top/red curve)

Figure 2.10 Temperature dependence of the energy bandgap of germanium, silicon and Gallium Arsenide.
Source: [16]

2.8 Effect of Temperature on Reflectivity, Refractive Index and Absorption

The electron-phonon collision frequency in a metal depends on the temperature of the material because of the temperature dependence of the phonon population. This is because, when a metal is heated, the lattice vibrations increase and hence, the free

electrons collide with the atoms. The temperature dependence of the collision frequency determines the optical properties of metals [4].

In order to investigate the effects of temperature on the optical properties of metals, the optical constants and their dependence on temperature need to be examined. We consider an average collision frequency of the free electrons with the vibrating lattice ω_c. These electrons moving between the lattice atoms are under the influence of an electric field of optical perturbation. The dielectric constant is given by:

$$\varepsilon = \varepsilon_1 + j\varepsilon_2 = 1 - \frac{\omega_p^2}{\omega^2+\omega_c^2} - j\frac{\omega_p^2\omega_c}{(\omega^2+\omega_c^2)\omega} \tag{2.37}$$

where, ε_1, ε_2 are the real and imaginary parts of the dielectric constant, respectively, and ω_p is the electron plasma frequency.

The above result is due to the Drude model. The reflectivity (R) in terms of the complex refractive index is:

$$R = \left|\frac{\varepsilon^{1/2}-1}{\varepsilon^{1/2}+1}\right|^2 \tag{2.38}$$

ω_c and ω_p are temperature dependent parameters. However, due to volume expansion, if small temperature dependence of ω_p is ignored and there is no induced band structure with temperature rise, then the only term that depends on temperature is ω_c. When temperature rises, ω_c increases. This is because, from the Debye phonon spectrum model, ω_c is:

$$\omega_c(\vec{k}) = K\left|\vec{k}\right|T^5 \int_0^{\theta/T} \frac{z^4}{e^z-1} dz \tag{2.39}$$

where, $\vec{k}$ is the wave vector, K is a constant including the total scattering cross section of an isolated atom, the ion mass, the ion density, the Debye wave number, the Debye temperature (θ), and T is the temperature in Kelvin. Here, it is assumed that θ does not change with temperature. ω_c is the average of $\omega_c(\vec{k})$.

For most metals, because k_BT is small compared to the Fermi energy (k_B is the Boltzman constant), even near the melting point, we can assume that the electron distribution remains the same as the temperature changes. So we can write:

$$\omega_c = K'T^5 \int_0^{\theta/T} \frac{z^4}{e^z-1} dz \tag{2.40}$$

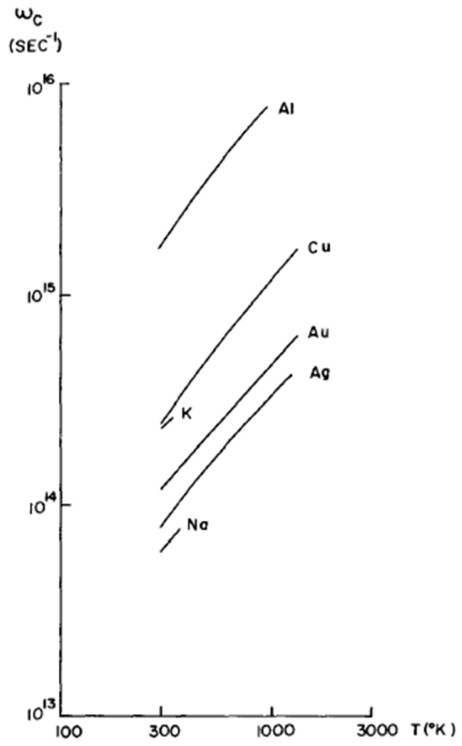

Figure 2.11 Electron-phonon collision frequency with temperature.
Source: [1]

The above discussions show that the phonon population increases with temperature and so does the electron scattering in the lattice. The real part of the dielectric constant ε_1 is negative and gives a large absolute value at room temperature and is an increasing function of ω_c and T. ε_2 is always negative and, at T=0 (absolute), it approaches zero. It reaches a minima at $\omega_c=\omega$.

Writing ω_c in terms of ε_1, ε_2 yields:

$$(\varepsilon_1 - 1 + \omega_p^2/2\omega^2)^2 + \varepsilon^2 = \omega_p^4/4\omega^4 \tag{2.41}$$

This is a circle with the circumference being the point (ε_1, ε_2), with a center $(1 - \frac{\omega_p^2}{2\omega^2}, 0)$ and radius $\omega_p^2/2\omega^2$. As temperature rises, the point moves counterclockwise [1].

The refractive index and the absorption coefficient are given by:

$$\varepsilon^{\frac{1}{2}} = n - jk \tag{2.42}$$

$$n = \left\{\frac{1}{2}\left[\varepsilon_1 + (\varepsilon_1^2 + \varepsilon_2^2)^{1/2}\right]\right\}^{1/2} \tag{2.43}$$

$$k = \left\{\frac{1}{2}\left[(\varepsilon_1^2 + \varepsilon_2^2)^{1/2} - \varepsilon_1\right]\right\}^{1/2} \tag{2.44}$$

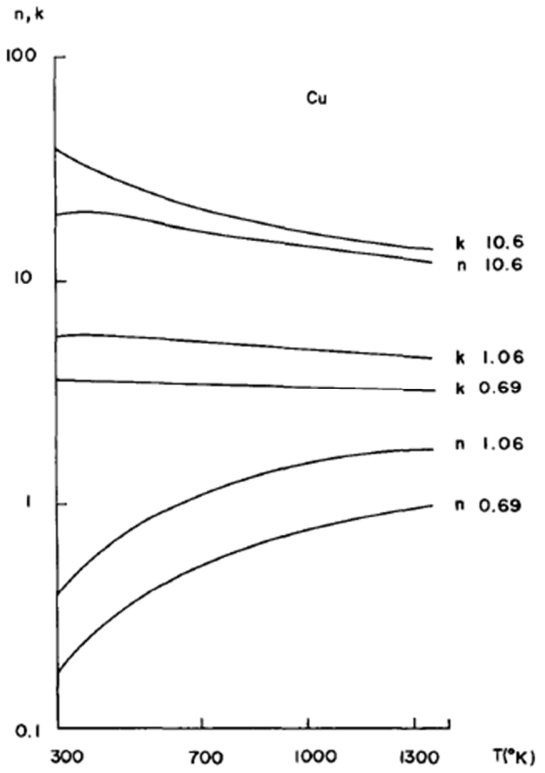

Figure 2.12 Refractive index and absorption coefficient with temperature for Cu.
Source: [1]

CHAPTER 3

FUNDAMENTALS OF PIEZOELECTRICITY

3.1 Introduction

In this chapter, the fundamentals of Piezoelectricity will be discussed. The objective is to present the effects of pressure on materials, introduce the piezoelectric effect and discuss the potential applications of piezoelectricity.

3.2 Effect of Pressure on Materials

Pressure is an important thermodynamic variable. The application of pressure in materials processing is vital to most experiments and, like temperature, it plays a critical role in materials science and technology.

Pressure has a variety of influence on materials. Depending on the material and the intensity of the applied pressure, it may cause catastrophic results. In order to analyze the effects of pressure on materials, one has to investigate the mechanical properties of materials. Perhaps the most natural test can be that of the *tension test,* in which a sample of the material, having a length L and a cross sectional area A, is subjected to a load P at one of its ends. As the load increases, the displacement δ of the specimen increases. After a certain load, the material will experience catastrophic results such as breaking into one or more parts if critical fracture load is exceeded, or fail mechanically in other ways. The length of the specimen will be different at the end of the experiment. Also, the material

fracture load will be different now, which means that, besides the dimensional change, the load has influenced the material microstructure.

This is an outcome of the fact that the strength of a uniaxially loaded object is proportional to the magnitude of its cross sectional area or to the number of bonds available.

The strength of a material loaded in tension is:

$$\sigma_f = \frac{P_f}{A_0} \tag{3.1}$$

where, σ_f is the ultimate tensile stress, P_f is the breaking load and A_0 is the original cross sectional area. If the load P is less than the breaking limit, then the tensile stress is given by:

$$\sigma = \frac{P}{A_0} \tag{3.2}$$

Tensile stress is a fundamental measurement of internal force within the material [9].

In the field of superconductors, high temperature studies have shown that the superconducting transition temperature T_c (temperature at which the electrical resistivity drops to zero) decreases under pressure [17].

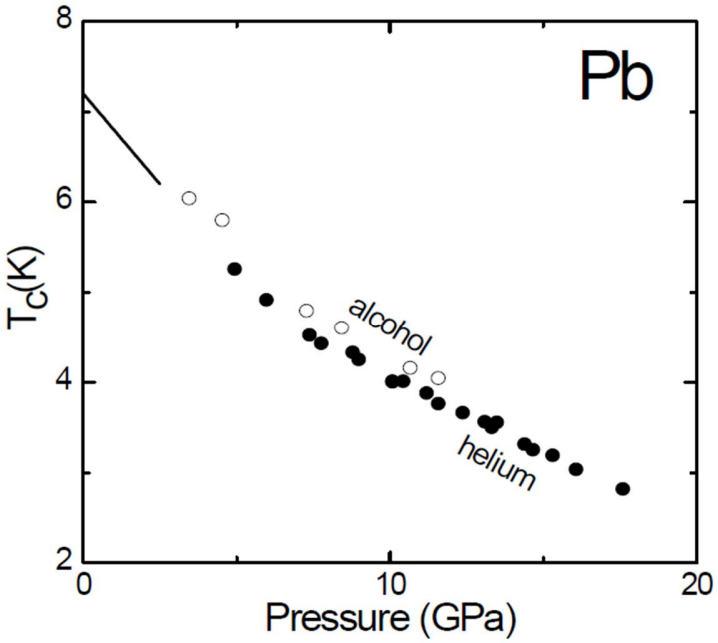

Figure 3.1 Pressure dependence of T_c for Pb.
Source: [17]

In semiconductors, we find a temperature and pressure dependence of the dielectric constant. The pressure effect is due to the change in the polarizability with volume. Generally, the dielectric constant can be written as:

$$\varepsilon = \varepsilon_{\infty} + \frac{4\pi N e_T^2}{\bar{m}\omega_{TO}^2} \tag{3.3}$$

where, ε_{∞} is the high-frequency or optical (electronic) dielectric constant, N is the number of unit cells per unit volume, $\bar{m}$ is the reduced mass of the crystal, e_T is the transverse dynamic effective charge, and ω_{TO} is the long-wavelength transverse optical (TO)-mode frequency.

The second term is defined as ε_l and is the pressure and temperature dependent component obtained by $\varepsilon(T,P)$:

$$\left(\frac{\partial ln\varepsilon}{\partial T}\right)_P = \left(\frac{\varepsilon_\infty}{\varepsilon}\right)\left(\frac{\partial ln\varepsilon_\infty}{\partial T}\right)_P + \left(\frac{\varepsilon_l}{\varepsilon}\right) \tag{3.4}$$

where, ε_l is the lattice contribution [18].

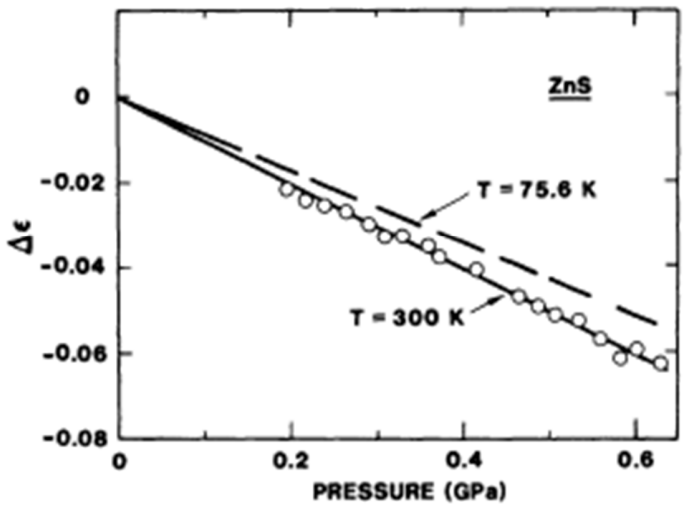

Figure 3.2 Hydrostatic pressure dependence of the static dielectric constant of cubic ZnS at two temperatures.
Source: [19]

In some ferroelectric materials (like $BaTiO_3$), an applied pressure will produce a voltage across the material, which, as we will see in the following section, results from a change in the population of negative and positive charge centers by different amounts.

3.3 Ferroelectricity and Piezoelectricity

3.3.1 Ferroelectricity and Dielectric Properties

The dielectric constant determines the storage capacity (capacitance C) of a dielectric material inserted between two parallel plates of a capacitor or in an electric field [4].

$$C = \varepsilon\varepsilon_0 \frac{A}{L} \tag{3.5}$$

$$\varepsilon = \frac{C}{C_{vac}} \tag{3.6}$$

where, A is the area of the plates, L is the distance between the plates, ε_0 is the permittivity of empty space, C_{vac} is the capacitance of vacuum.

The increasing capacitance of a dielectric, when inserted in an electric field, is due to certain processes that take place in the dielectric. Under the influence of an external electric field, dipoles (negatively charged electron cloud displaced with respect to the positive core) are created which possess an electric dipole moment p.

$$p = q \cdot x \tag{3.7}$$

where, x is the distance between positive and negative charge and q is the total electronic charge.

This dipole formation process is called polarization. The electric field lines within the material are effectively weakened due to polarization and therefore,

$$E = \frac{E_{vac}}{\varepsilon} \tag{3.8}$$

Within the material, the field is replaced by the displacement, D given by:

$$D = \varepsilon\varepsilon_o E = \frac{q}{A}\text{, A is the surface} \tag{3.9}$$

The displacement is also the superposition of:

$$D = \varepsilon_o E + P \tag{3.10}$$

where, P is the dielectric polarization.

Table 3.1 DC Dielectric Constants of some Common Materials

Potassium tantalate niobate	6,000	
Barium titanate ($BaTiO_3$)	4,000	Ferroelectric
Potassium Niobate ($KNbO_3$)	700	
Rochelle salt ($NaKC_4H_4O_6 \cdot 4H_2O$)	170	
Water	81.1	
Acetone	20	
Silicon	11.8	
GaAs	10.9	
Marble	8.5	
Soda-lime-glass	6.9	
Porcelain	6.0	
Epoxy	4.0	
Fused silica	4.0	Dielectric
Nylon 6,6	4.0	
PVC	3.5	
Ice	3.0	
Amber	2.8	
Polyethylene	2.3	
Paraffin	2.0	
Air	1.000576	

Source: [4]

Table 3.2 Electrical Properties of Nitride Piezoelectric Materials

Sample	Layer	R (Ω)	C (pF)	ρ (Ω m)	ϵ_r	t
AlN on	AlN	634×10^3	130	1.1×10^6	8.42	450 nm
Si(111)	Si	100	0	0.26	3.7	0.3 mm
GaN/AlN	GaN	218×10^3	442	1.2×10^6	8.9	140 nm
on Si(111)	Si	300	0	0.785	3.7	0.3 mm
GaN/AlN	GaN	804×10^3	446	4.5×10^6	8.99	140 nm
on Si(100)	Si	400	0	1.05	3.7	0.3 mm

Source: [20]

Certain materials exhibit spontaneous polarization. This behavior occurs in the absence of an external E-field and such a field can be used to reverse that behavior. These materials possess dielectric dipoles. For this reason, their dielectric constants are much larger than those of common materials of non-polar dielectrics by many magnitudes (Table 3.2).

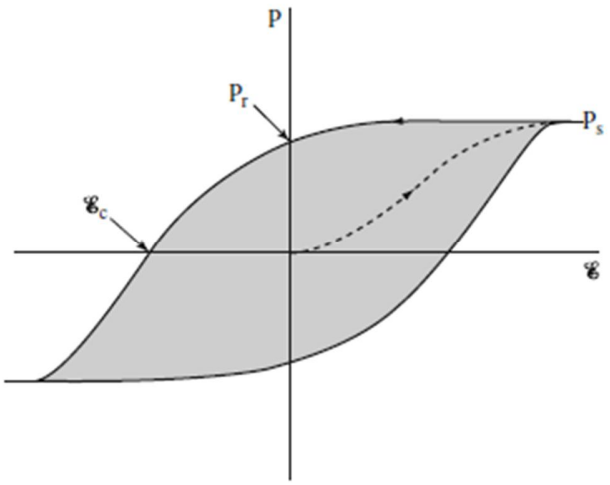

Figure 3.3 Representation of a hesteresis loop for a ferroelectric material in an E- Field. Source:[4]

In ferroelectric materials, in the presence of an external field, these dipoles can be reoriented. If the applied field is strong enough, the dipoles can become increasingly aligned with the field and almost all of them end up being close to parallel to the field. As a result, we have a saturation of polarization P_s. If the external field is removed, then a remnant polarization, P_r, is left behind. This can be removed only by applying a reversed field. By increasing the strength of the reversed field, a hysteresis loop can be obtained (Figure 3.3).

There is a critical temperature above which the ferroelectric effects are destroyed and the material becomes paraelectric. This temperature is known as the Curie Temperature T_c. Above T_c, the temperature dependence of the dielectric permittivity follows a Curie-Weiss law:

$$\frac{\varepsilon}{\varepsilon_0} = \frac{C}{T - T_0} \tag{3.11}$$

Below T_c, the dependence of the displacement D on the electric field E is highly nonlinear and shows a characteristic hysteresis loop (Figure 3.3) [21].

As mentioned above, there are materials that can possess spontaneous polarization. A perfect example is $BaTiO_3$. This can be explained by examining its structure (Figure 3.4).

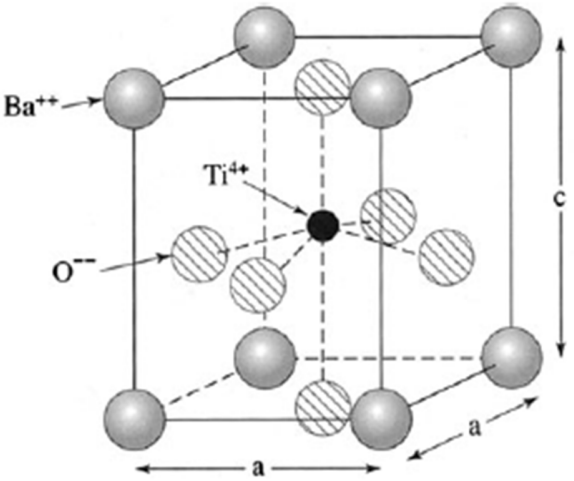

Figure 3.4 Tetragonal crystal structure of $BaTiO_3$ (Room temperature).
Source: [4]

The negatively charged oxygen ions and the positively charged titanium ion are displaced slightly from their symmetrical positions and therefore a permanent dipole moment exists along the c axis.

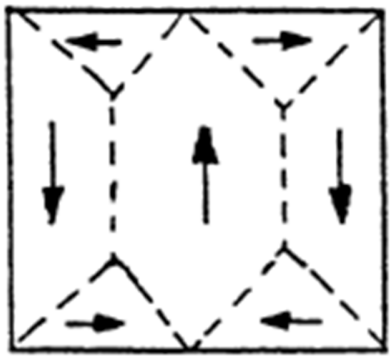

Figure 3.5 Spontaneous alignments of dipoles within a domain and random alignment of the dipole moments of several domains in a ferroelectric material.
Source: [4]

Within a ferroelectric material, a number of these dipoles line up in domains. Without an external E field, the domains have random orientation so that there is no total

polarization. When an external field is applied, it causes a reorientation of the spontaneous polarization. At the same time, it orients the favorably oriented domains parallel to E so that the domains with a favorable orientation to the polarity field direction grow at the expense of those that have unfavorable orientation. The domain walls are shifted in the crystal lattice. After polarization, most of the reorientations are preserved even without the application of an electric field (Figure 3.5) However, a small number of the domain walls are shifted back to their original position, e.g., due to internal mechanical stresses [22].

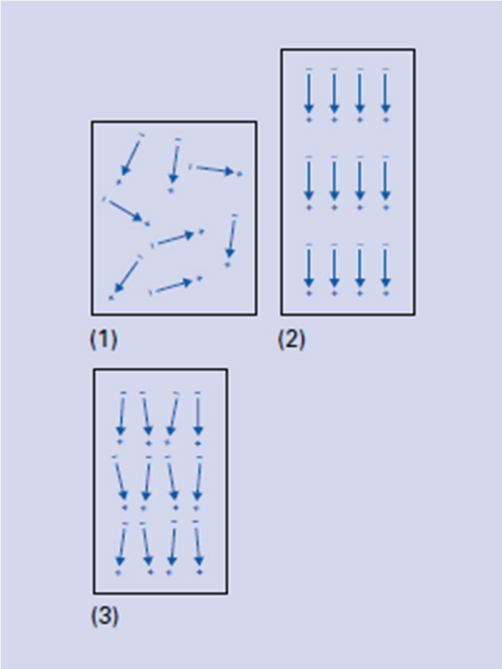

(1) Unpolarized ceramic,
(2) Ceramic during polarization and
(3) Ceramic after polarization

Figure 3.6 Orientation of the spontaneous polarization within a piezo ferroelectric ceramic.
Source: [22]

Application of pressure on some ferroelectric materials such as $BaTiO_3$ results in the generation of a small voltage across the sample. This is due to the displacement of the negative and positive charge centers by different amounts, because of the mechanical deformation, which causes a change in the polarization. This effect is called *Piezoelectricity*. The piezoelectric effect in which stress is used to generate voltage to the material is called *direct piezoelectric effect* whereas if the converse mechanism is considered, where an applied voltage to the piezo-material will induce a change to its dimensions, then the effect is called *converse piezoelectric effect*.

3.3.2 Piezoelectric Effect

Piezoelectricity is mathematically described in the materials' constitutive equations. Constitutive equation defines how the materials' stress (T), charge displacement (D), strain (S) and electric Field (E) interact.

In order to form the equation, the following are considered:

a) Hooke's law:

$$S = s \cdot T \tag{3.12}$$

where, s is the compliance (the inverse of stiffness)

b) The equation for common dielectrics, since piezoelectric materials have electrical properties, is given by:

$$D = \varepsilon \cdot E \tag{3.13}$$

where, D is the electrical displacement, ε is the permittivity and E, the electrical field.

Combining the above equations, we have the piezoelectric constitutive law.

$$S = s_E \cdot T + d^t \cdot E \tag{3.14}$$

$$D = d \cdot T + \varepsilon_T \cdot E \tag{3.15}$$

where, the matrix d contains the piezoelectric coefficients of the material and is the matrix for the direct piezoelectric effect, d^t is the matrix for the converse piezoelectric effect, ε_T is the permittivity and s_E is the elasticity constant.

In order to model a piezoelectric material, we must know its mechanical properties (compliance or stiffness), its electrical properties (permittivity) and its piezoelectric coupling properties [23].

Generally, *D* and *E* are Cartesian tensors of rank-1 and permittivity ε is Cartesian tensor of rank 2. Strain and stress are, in principle, also rank-2 tensors. Because strain and stress are all symmetric tensors, the subscript of strain and stress can be re-labeled in the following fashion: 11 → 1; 22 → 2; 33 → 3; 23 → 4; 13 → 5; 12 → 6.

There are totally four piezoelectric coefficients: d_{ij}, e_{ij}, g_{ij}, h_{ij}

$$d_{ij} = \left(\frac{\partial D_i}{\partial T_j}\right)^E = \left(\frac{\partial S_j}{\partial E_i}\right)^T \tag{3.16}$$

$$e_{ij} = \left(\frac{\partial D_i}{\partial S_j}\right)^E = -\left(\frac{\partial T_j}{\partial E_i}\right)^S \tag{3.17}$$

$$g_{ij} = -\left(\frac{\partial E_i}{\partial T_j}\right)^D = \left(\frac{\partial S_j}{\partial D_i}\right)^S \tag{3.18}$$

$$h_{ij} = -\left(\frac{\partial E_i}{\partial S_j}\right)^D = -\left(\frac{\partial T_j}{\partial D_i}\right)^S \tag{3.19}$$

where, d_{ij} defines the ratio of strain in j direction to the electric applied field in the i direction for constant external strains, g_{ij} is the ratio of strain applied in j direction to the

charge deposited perpendicular to i direction, e_{ij} is the dielectric coefficient and h_{ij} is the ratio of mechanical stress to applied electric displacement or electric field to mechanical strain. The first set of terms corresponds to the direct effect and the rest of them to the converse piezoelectric effect.

A wide variety of materials are piezoelectric, including poled polycrystalline ceramics (e.g., lead zirconate titanate, PZT), single-crystal or highly oriented polycrystalline ceramics (e.g. zinc oxide and quartz), organic crystals (e.g., ammonium dihydrogen phosphate), and polymers (e.g. polyvinylidiene fluoride) [23, 24]. In Table 3.3, some common piezoelectric materials are listed along with their piezoelectric properties.

Table 3.3 Properties of some Piezoelectric Materials

Material	Formula	Form	Piezoelectric constant (pm/V or pC/N)
Ammonium dihydrogen phosphate (ADP)	$NH_4H_2PO_4$	Single crystal	$d_{36} = 48$
Barium titanate	$BaTiO_3$	Single crystal	$d_{15} = 587$
Barium titanate	$BaTiO_3$	Polycrystalline ceramic	$d_{15} = 270$
Lead zirconate titanate (PZT)	$PbZr_{0.6}\ Ti_{0.40}O_3$	Polycrystalline ceramic	$d_{33} = 117$
Lead lanthanum zirconate titanate (PLZT)	$Pb_{0.925}La_{0.5}Zr_{0.56}Ti_{0.44}O_3$	Polycrystalline ceramic	$d_{33} = 545$
Polyvinylidene fluoride	$(CH_2CF_2)_n$	Oriented film	$d_{31} = 28$
Potassium dihydrogen phosphate (KDP)	KH_2PO_4	Single crystal	$d_{36} = 21$
Quartz	SiO_2	Single crystal	$d_{11} = 2.3$
Zinc oxide	ZnO	Single crystal	$d_{33} = 12$

Source: [24]

3.4 Microelectromechanical Systems (MEMS) Technology

Microelectromechanical systems (MEMS) refers to devices that, have a characteristic length between 1μm and 1mm, combine electrical and mechanical components and are fabricated using integrated circuit batch processing technologies. This field has grown exponentially over the past decades and the devices that are being manufactured using this technology are numerous. Electromagnetic, pneumatic, magnetic and thermal actuators, motors, valves, switches and many more of a size less than 100μm have been fabricated using MEMS technology. The devices can be used as sensors for temperature, velocity and pressure, among many other physical quantities.

Like all new technologies, over the past dozen years, MEMS emphasized on new materials and manufacturing methods in order to construct new microdevices. The technological advantages of MEMS are due to the contributions of various researchers whose focus has been on the mechanical testing of materials that are used to fabricate MEMS devices. These mechanical properties of materials include three main categories: elastic, inelastic and strength.

The strength of the material must be known so that the allowable operating limits can be set while the elastic properties are important in order to predict the amount of deflection from an applied force, or *vice versa* as it will be utilized for the IR detector considered in this research. Also, if the material is ductile, then the inelastic behavior is important. In any case, for the design and fabrication of any MEMS device, the relationship between processing and properties of the materials need to be considered [25].

3.5 Piezoelectric Sensors

Utilizing the piezoelectric effect, piezoelectric transducers are suitable for sensor applications. In this section, the performance characteristics of a piezoelectric sensor will be investigated.

Under small field conditions, the constitutive relations for a piezoelectric material can be rewritten as:

$$\begin{bmatrix} D \\ S \end{bmatrix} = \begin{bmatrix} \varepsilon_T & d \\ d^T & s_E \end{bmatrix} \begin{bmatrix} E \\ T \end{bmatrix} \tag{3.20}$$

When a piezoelectric element is subjected to a stress field, and assuming there is no electric field applied, the resulting displacement vector can be written as:

$$D = dS \tag{3.21}$$

where, $D = \begin{bmatrix} D_1 \\ D_2 \\ D_3 \end{bmatrix}$, $S = \begin{bmatrix} S_1 \\ S_2 \\ S_3 \\ S_4 \\ S_5 \\ S_6 \end{bmatrix} = \begin{bmatrix} S_{11} \\ S_{22} \\ S_{33} \\ S_{23} \\ S_{31} \\ S_{12} \end{bmatrix}$ and $d = \begin{bmatrix} 0 & 0 & 0 & 0 & d_{15} & 0 \\ 0 & 0 & 0 & d_{24} & 0 & 0 \\ d_{31} & d_{32} & d_{33} & 0 & 0 & 0 \end{bmatrix}$

$D_{1,2,3}$ are the electrical displacements in all 3 directions. For a sheet of piezo material, the poling direction is usually along the thickness (3-axis) and 1,2 are the plane axis. The above equation summarizes the principle of operation of piezo sensors. That is, a stress field generates an electric displacement because of the piezoelectric effect. The electric displacement D is now related to the generated charge by:

$$q = \iint [D_1 \;\; D_2 \;\; D_3] \begin{bmatrix} dA_1 \\ dA_2 \\ dA_3 \end{bmatrix} \tag{3.22}$$

where, $dA_{1,2,3}$ are the infinitesimal electrode areas in the 1-2, 2-3 and 1-3 planes respectively. As viewed, the charge depends on the dA area normal to the displacement D.

The charge q and the voltage V are connected by the capacitance of the sensor C_p by the following equation [26]:

$$V = q/Cp \tag{3.23}$$

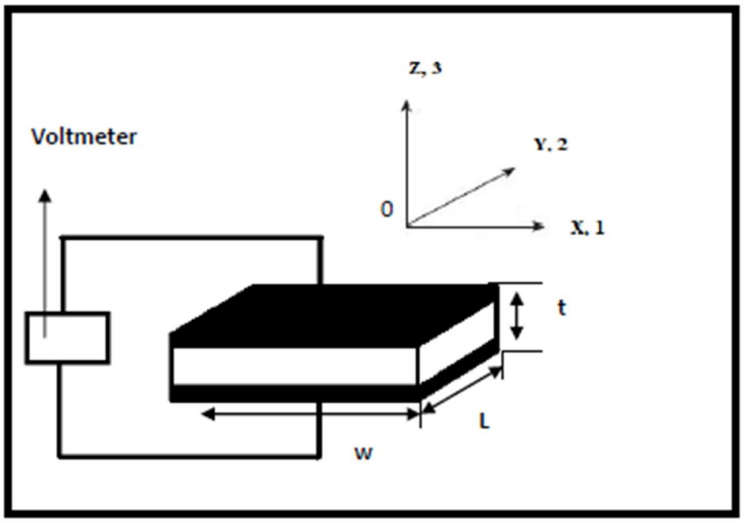

Figure 3.7 Piezoelectric sensors.
Source: [27]

If the strain/stress is applied along 1-axis, we have:

$$D = Ed_{31}\varepsilon_{11} \tag{3.24}$$

$$q = DdA \tag{3.25}$$

By combining the above,

$$V = \frac{E d_{31} \varepsilon_{11} dA}{C} \tag{3.26}$$

where, the normal to the plane induced strain can be calculated from equations:

$$\varepsilon = \frac{\sigma}{E} \tag{3.27a}$$

$$\varepsilon = \frac{\Delta L}{L} \tag{3.27b}$$

where, σ is the applied stress, normal to the plane (A):

$$\sigma = F/A \tag{3.28}$$

The generated voltage from a piezoelectric material can be also calculated from the following equation [27, 28]:

$$V = S_V \cdot P \cdot D \tag{3.29}$$

where, V is the Piezoelectric generated voltage (Volts), S_V is the voltage sensitivity of the material (V*m / N), P is the pressure (N/m^2) and D is the thickness of material (m). S_v is provided by the material manufacturer.

3.6 Piezoelectric Resonators

When exposed to an AC voltage, a piezoelectric ceramic element changes dimensions with the same frequency of the voltage. This change in dimensions can be viewed as a vibration**.** The frequency at which the material vibrates most readily or converts electrical energy into mechanical energy most efficiently is called resonance frequency.

The pattern of an element's response is depicted in Figure 3.8. As the frequency is increased, the element's oscillations first approach a frequency at which impedance is minimum (maximum admittance). This minimum impedance frequency, f_m, approximates the series resonance frequency, f_s, the frequency at which impedance in an electrical circuit, describing the element, is zero, if resistance caused by mechanical losses is ignored. The minimum impedance frequency is also the resonance frequency, f_r. The maximum impedance frequency is also the *anti-resonance frequency*, f_a. Maximum response from the element will be at a point between f_m and f_n. The composition of the ceramic material and the shape and volume of the element determine the resonance frequency. Generally, a thicker element has a lower resonance frequency than a thinner element of the same shape [29]

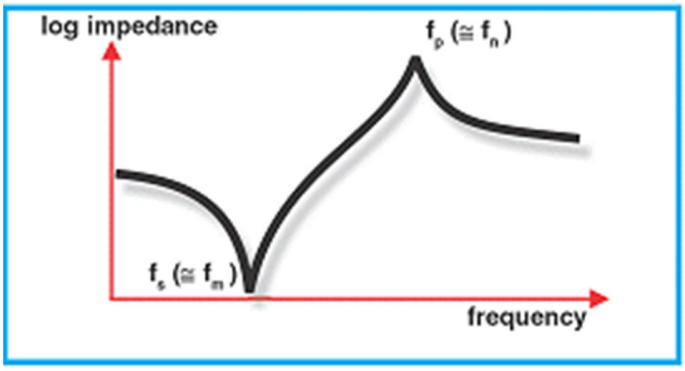

Figure 3.8 Impedance as a function of frequency.
Source: [29]

As the cycling frequency is further increased, impedance increases to a maximum (minimum admittance). The maximum impedance frequency, f_n, approximates *the parallel resonance frequency*, f_p, the frequency at which parallel resistance in the equivalent electrical circuit is infinite, if resistance caused by mechanical losses is ignored. The maximum impedance frequency is also the anti-resonance frequency, f_a. Maximum response from the element will be at a point between f_m and f_n. Values for minimum impedance frequency, f_m, and maximum impedance frequency, f_n, can be determined by measurements [29].

For a piezoelectric structure, the resonance frequency depends on the material size (or the distance between the electrodes), Young's modulus E_{eq} and the density of the material as shown in Equation 3.30:

$$f = \frac{1}{2\lambda}\sqrt{\frac{E_{eq}}{\rho_{eq}}} \tag{3.30}$$

where, f is the resonance frequency, λ is the distance between the electrodes on the piezoelectric material or the material length, E_{eq} and ρ_{eq} are the materials' Young's modulus and density respectively. It is clear that, in the presence of a stress force, the distance between the electrodes will alter; hence, this will cause a change in the resonance frequency [30].

Piezoelectric resonators are electronic components designed for electronic oscillators. They can be:

- Crystal
- Ceramic
- MEMS

Crystal oscillators use the mechanical resonance of a piezo crystal to create electrical signals of precise frequencies. Likewise, ceramic resonators can generate oscillations at specific frequencies when combined with appropriate components. When voltage is applied to them, their piezoelectric vibration produces oscillating signals. MEMS structures, as well, produce highly stable reference frequencies and have a range of advantages over crystal resonators.

Electrical Characteristics of a lossless ceramic resonator can be expressed by unified formulae with three basic parameters: clamped capacitance, electromechanical coupling factor and the gravest resonant or antiresonant frequency. While valid for a wide frequency range, these formulae are not easy to calculate due to transcendental functions involved. There are two types of piezoelectric vibrational modes, stiffened and unstiffened (Figures 3.9 and 3.10) [31].

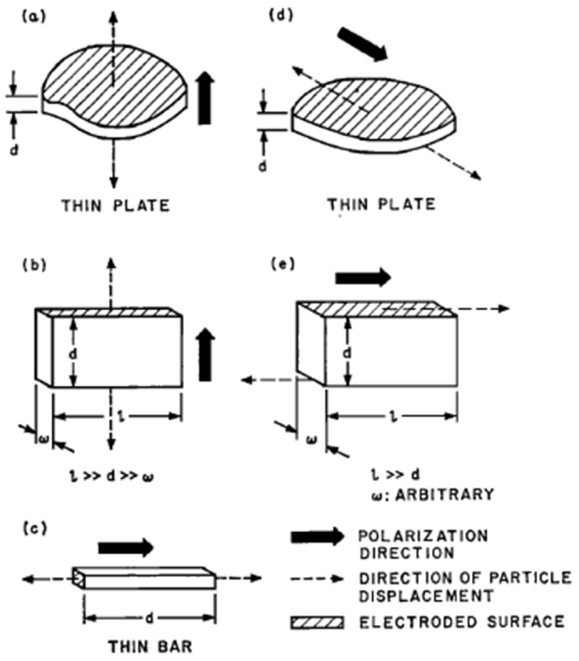

Figure 3.9 Resonators vibrating in piezoelectrically stiffened mode.
Source: [31]

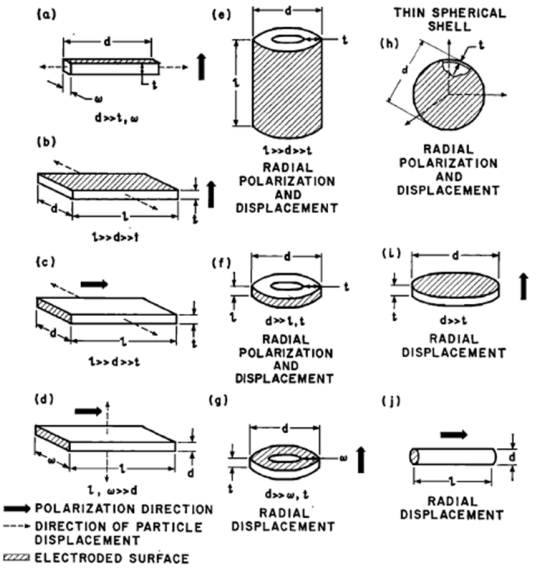

Figure 3.10 Resonators vibrating in piezoelectrically unstiffened modes.
Source: [31]

3.6.1 Unstiffened Mode

In the unstiffened mode, the electric field is transverse to the elastic wave's direction; so there is no effect on the shape of vibration. The electrical admittance V of the resonator is:

$$Y = j\omega C_D \left\{1 + \left[\frac{k^2}{1-k^2}\right] M(X)\right\} \tag{3.31}$$

where, k is the coupling factor, C_D is the clubbed capacitance, ω the angular frequency and M(X) a function of the normalized frequency X:

$$C_D = \varepsilon_D(\frac{A}{t}) \tag{3.32}$$

$$X = \frac{\omega d}{2u} = X_1(\frac{f}{F_R}) \tag{3.33}$$

where, ε_D is the dielectric constant, d is the frequency determining dimension of the resonator, u is the face velocity of the elastic wave, A and t are the area and thickness of

the resonator respectively, f is the frequency and F_r and X_1 are the gravest resonant frequency and its normalized value [31].

3.6.2 Stiffed mode

In stiffed mode, the electric field is parallel to the direction of the elastic wave and it affects the shape of vibration. Here [31]:

$$Y = j\omega C_D/(1 - k^2 M) \tag{3.34}$$

$$M = tanX/X \tag{3.35}$$

$$X = \frac{\omega d}{2u} = (\frac{\pi}{2})(\frac{f}{F_A}) \tag{3.36}$$

3.6.3 Approximate Formulae

As mentioned earlier, because of the difficulty in calculations, approximate formulae need to be derived. The approximation is based on the expansion of M:

$$M = \frac{C_{-1}}{n} + C_0 + C_{1n} + C_{2n^2} + \cdots \approx \frac{C_{-1}}{n} + C_0 \tag{3.37}$$

$$n=(X-X_1)/X_1 \text{ (normalized frequency deviation)} \tag{3.38}$$

From equations (3.31) and (3.37), we get:

$$\frac{1}{k^2} = a\left(\frac{F_R}{\Delta F}\right) + b \tag{3.39}$$

The coefficients $\alpha=-C_{-1}$ and b depend on the mode. When the coupling factor is low, b can be neglected and we can write [31]:

$$k^2 = (\frac{1}{a})\left(\frac{\Delta F}{F_R}\right) \tag{3.40}$$

3.7 Applications

Piezoelectric materials are widely used in electromechanical sensors and actuators like telephone sensors (transmitters and receiver insets) in handsets, ultrasonic transducers for medical imaging or transducers sensitive in other frequency ranges like upper MHz range, robotic sensors, surface acoustic wave devices and many more.

Piezoelectricity is utilized in devices that are designed to convert mechanical strain into electricity. These devices are called transducers. Sonar transducers apply an electrical pulse to a piezoelectric crystal to create a pressure wave and then produce a current when the reflected wave deforms the crystal. The time gap between the two currents is used to estimate distances. Small piezoelectric crystals can produce enough voltage to create a spark large enough to ignite gas. These igniters are used in many gas-powered appliances such as ovens, grillers, room heaters, and water heaters. One of the best known applications is the electric cigarette lighter. While pressing the button in an electric cigarette lighter, a spring-enabled hummer is released to hit a piezoelectric crystal. The strain is transformed by the crystal to a high voltage electric current that flows to a small spark gap, which eventually lights the igniting gas. Applications also include strain gauges, phonographs, microphones among many others.

Devices that utilize the converse effect (converse piezoelectric effect) can also be designed. The magnitude of the converse effect can be up to $6x10^{-10}$ m/V for $PbZrO_3$ and $PbTiO_3$ materials. Industrial inkjet printers use the converse piezoelectric effect to move ink through the hundreds of nozzles in their print heads fuel injectors. An electric current makes a tiny crystal in each nozzle bend, creating a pressure pulse that forces the ink out. Ink is drawn into the nozzle when the current stops and the crystal relaxes. We can also

find examples in earphones and diesel fuel injectors. One of the most important applications is the quartz crystal resonator, which is used in electronic devices as a frequency selective element. Specifically, a periodic strain is applied to a quartz crystal by an alternating electric field, which excites this crystal to vibrations. These vibrations are monitored, in turn, by piezoelectricity. If the applied frequency coincides with the natural resonance frequency of the molecules, then amplification occurs. In this way, very distinct frequencies are produced, which are utilized for clocks or radio frequency signals [4].

During recent years, the study of micro-electromechanical systems (MEMS) has shown that there are significant opportunities for microsensors and microactuators based on various physical mechanisms such as piezoresistive, capacitive, piezoelectric, magnetic, and electrostatic. MEMS themes include miniaturization, multiplicity, and microelectronics manufacturing and integration. These devices can replace bulky actuators and sensors with micro-scale devices that can be produced in integrated circuit photolithography. MEMS are miniature versions of traditional electrical and mechanical devices (Figures 3.11 and 3.12) - such as valves, pressure sensors, hinged mirrors, gears etc. The principle of sensors is based on a variety of physical phenomena: piezoresistive, capacitance, resonance, piezoelectric, pyroelectric and thermoelectric. Microactuators use mainly these phenomena: thermal expansion forces, shape memory alloys, piezoelectric layers, electrostatic and electromagnetic forces [32]. Huge technology opportunities for MEMS are present in automotive applications including: medicine, defense, controls, and communications. Other applications include biomedical pressure sensors and projection displays [24].

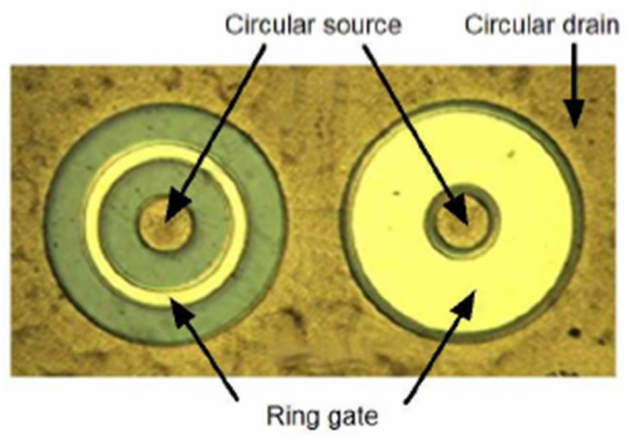

Figure 3.11 Microscopic view of C-HEMT structure – MEMS pressure sensor.
Source: [32]

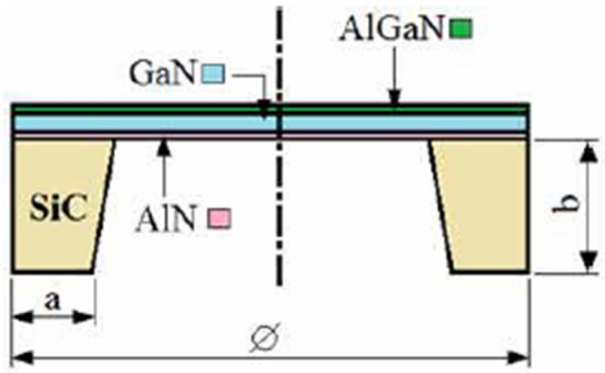

Figure 3.12 SiC substrate and AlGaN/GaN/AiN layers of MEMS sensor.
Source: [32]

MEMS can be classified into two major categories: sensors and actuators. MEMS sensors, or microsensors, usually rely on integrated microfabrication methods to realize mechanical structures that predictably deform or respond to a specific physical or chemical variable. Such responses can be observed through a variety of physical detection methods including electronic and optical effects. Structures and devices are designed to be sensitive to changes in resistance (piezoresistivity), changes in

capacitance, and changes in charge (piezoelectricity), with amplitude usually proportional to the magnitude of the stimulus sensed. Examples of microsensors include accelerometers, pressure sensors, strain gauges, flow sensors, thermal sensors, chemical sensors and biosensors.

A really good example of a thermal detector (Figure 3.12) was introduced by Northeastern University.

"Here a heat absorbing element and a temperature sensitive microelectromechanical system (MEMS) resonator are perfectly overlapped but separated by a microscale air gap. This unique design guarantees efficient and fast (10s;µs) heat transfer from the absorbing element to the temperature sensitive device with a thermal power as low as 150nW and enables high resolution thermal power detection (nW), thanks to the low noise performance of the high quality factor (Q¼2305) MEMS resonant thermal detector" [33].

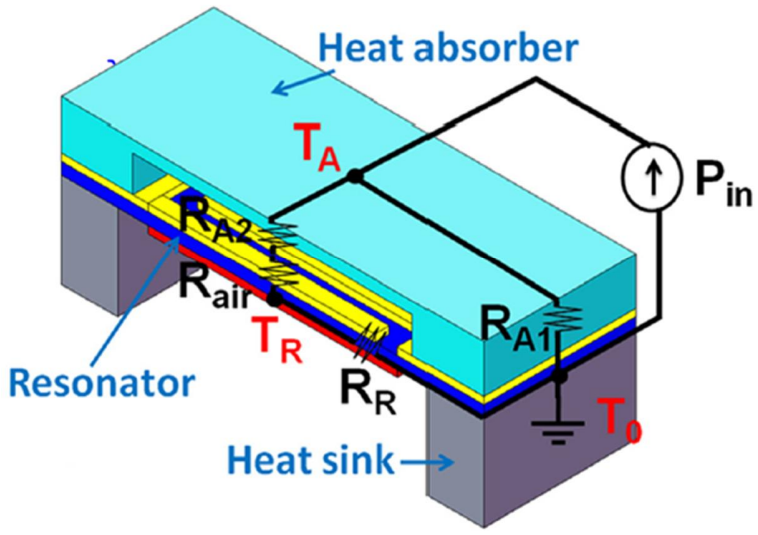

Figure 3.13 3-D schematic representation of the proposed micromechanical resonant thermal detector and its equivalent thermal circuit
Source: [33]

Table 3.4 PI Ceramic Material Properties

	PIC151	PIC153	PIC255/252	PIC050
Physical and Dielectric Properties				
Density ρ [g/cm^3]	7.8	7.6	7.8	4.7
Curie temperature T_c [°C]	250	185	350	>500
Relative permittivity in the polarization direction $\varepsilon_{33}^T/\varepsilon_0$	2400	4200	1750	60
Perpendicular to the polarization $\varepsilon_{11}/\varepsilon_0$	1980		1650	85
Dielectric loss factor tan δ [10^{-3}]	20	30	20	<1
Acousto-Mechanical Properties				
Elastic compliance coefficient				
s_{11}^E [10^{-12} m^2/N]	15		16.1	
s_{33}^E [10^{-12} m^2/N]	19		20.7	
Mechanical quality factor Qm	100	50	80	
Electro-Mechanical Properties				
Piezoelectric deformation coefficient, piezo modulus*				
d_{31} [pm/V]	-210		-180	
d_{33} [pm/V]	500	600	400	40
d_{15} [pm/V]			550	80

Source: [22]

MEMS actuators or microactuators are usually based on electrostatic, piezoelectric, magnetic, thermal, and pneumatic forces. Examples of microactuators include positioners, valves, pumps, deformable mirrors, switches, shutters, and resonators [24]. In Table 3.4, the physical and dielectric properties of some actuator materials (from PI Ceramic) are summarized.

3.7.1 Actuators

Actuators can be divided into four categories depending on their displacement mode.

3.7.1.1 Longitudinal Stack Actuators. "In longitudinal piezo actuators, the electric field in the ceramic layer is applied parallel to the direction of polarization. This induces an expansion or displacement in the direction of polarization. Individual layers provide relatively low displacements. Many individual layers are mechanically connected in

series and electrically connected in parallel (Figure 3.13), in order to achieve technically useful displacement values"[22].

$$\Delta L_{long} = n d_{33(GS)} V \tag{3.41}$$

where, ΔL is the displacement, $d_{33(GS)}$ is the longitudinal piezoelectric large-signal deformation coefficient [m/V], n is the number of stacked ceramic layers and V is the operating voltage.

"Longitudinal stack actuators (Figure 3.14) are highly efficient in converting electrical energy to mechanical energy. They achieve nominal displacements of around 0.1 to 0.15% of the actuator length. The nominal blocking forces are on the order of 30 N/mm^2 in relation to the cross-sectional area of the actuator. Values of up to several 10,000 Newtons can thus be achieved in the actuator. Longitudinal stack actuators are excellently suited for highly dynamic operation due to their high resonant frequencies. A mechanical preloading of the actuator suppresses dynamically induced tensile forces in brittle ceramic material, allowing response times in the microsecond range and a high mechanical performance" [22].

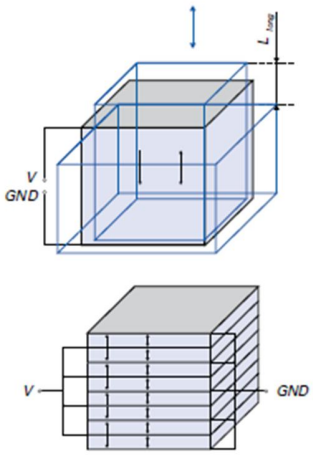

Figure 3.14 Longitudinal actuators.
Source: [22]

3.7.1.2 Shear Actuators. "In piezoelectric shear actuators (Figure 3.15), the electric field in the ceramic layer is applied orthogonally to the direction of polarization; so the displacement is in the direction of polarization. The displacement of the layers, added up as in stacked actuators, is given by" [22]:

$$\Delta L_{shear} = n d_{15(GS)} V \tag{3.42}$$

where, ΔL is the shear displacement, $d_{15(GS)}$ is the shear piezoelectric large-signal deformation coefficient [m/V], n is the number of stacked ceramic layers and V is the operating Voltage.

"The shear deformation coefficients d_{15} are normally the largest piezoelectric coefficients. When controlled with nominal voltages, PIC ceramics achieve $d_{15(GS)}$ values of up to 2000 pm/V. The permissible controlling field strength is limited in order to prevent a reversal of the vertically oriented polarization. When lateral forces act on the

actuator, the shear motion is additionally superimposed by bending. The same effect occurs in dynamic operation near the resonant frequency. Furthermore, shear stresses cannot be compensated by a mechanical preload. Both limit the practical stacking height of shear stacks. Shear actuators, combined with longitudinal actuators, yield very compact XYZ stacks with high resonant frequencies" [22].

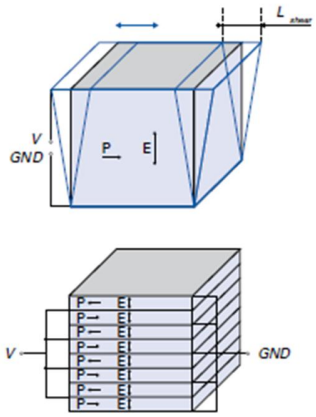

Figure 3.15 Shear actuators.
Source: [22]

3.7.1.3 Tube Actuators. "Tube actuators are radially polarized and take advantage of the transversal piezoelectric effect to generate displacement. The electrodes are applied on the outer surfaces, so that the field parallel to the polarization also runs in a radial direction. Axial displacements or changes in length (Figure 3.16a), lateral motions such as changes in the radius (Figure 3.16b), as well as bending (Figure 3.16c) are all possible. In order to cause a tube to bend, the outer electrode is segmented into several sections" [22]:

$$\Delta L_{axial} = d_{31(GS)} \frac{l}{t} V \tag{3.43}$$

$$\Delta L_{radial} = d_{31(GS)} \frac{ID}{2t} V \tag{3.44}$$

$$\Delta L_{lateral} = 0.9 d_{31(GS)} \frac{l^2}{ID} V \tag{3.45}$$

where, ΔL_{axial} is the axial displacement, ΔL_{radial} the radial displacement, $\Delta L_{lateral}$ the lateral tube displacement, l the tube length, ID the internal tube diameter and t the thickness of the tube.

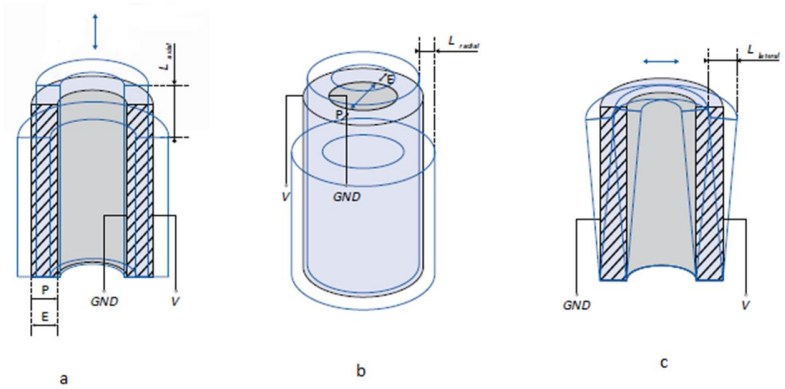

a)axial displacement b)Radial Displacement c)Bending actuator XY scanning tubes
Figure 3.16 Tube actuators.
Source: [22]

"When the respectively opposite electrodes are controlled, the tube bends in a lateral direction. Undesirable tilting or axial motions that occur during this process can be prevented by more complex electrode arrangements" [22].

3.7.1.4 Contracting Actuators. "Typically, piezo contracting actuators are low-profile components. Their displacement occurs perpendicularly to the polarization direction and to the electric field. Like in the case of tube actuators, the displacement of contracting

actuators is based on the transversal piezoelectric effect. Multilayer elements offer decisive advantages over single-layer piezo elements in regard to technical realization. Due to the larger cross-sectional area, they generate higher forces and can be operated with a lower voltage" [22] (Figure 3.17):

$$\Delta L_{trans} = d_{31(GS)} \frac{l}{h} V \tag{3.46}$$

where, ΔL_{trans} is the transversal displacement, l the length of the piezo ceramic and h the height of the ceramic layer.

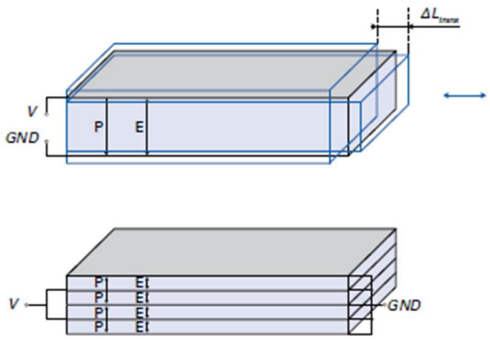

Figure 3.17 Contracting actuators.
Source: [22]

As a result of the contraction, tensile stresses occur that can cause damage to the brittle piezo ceramic.

3.7.1.5 Bending Actuators. "When attached to a substrate, contracting actuators can act as bending actuators (Figure 3.18). For the construction of all-ceramic benders, two active piezoceramic elements are joined and electrically controlled. For example, if a passive substrate made of metal or ceramic material is used, one refers to them as composite benders" [22].

$$\Delta L_{bend} = \frac{3}{8} nd \frac{l_f^2}{h_p^2} V \quad (3.47)$$

The piezoceramic elements can be designed as individual layers or as multilayer elements. Piezoelectric bending actuators function according to the principle of thermostatic bimetals.

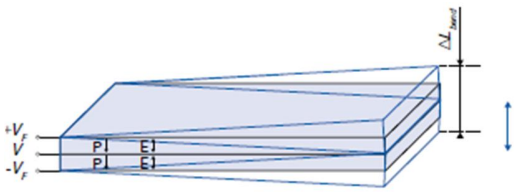

Figure 3.18 Bending actuators.
Source: [22]

"When a flat piezo contracting actuator is coupled to a substrate, the driving and contraction of the ceramic creates a bending moment that converts the small transversal change in length into a large bending displacement vertical to the contraction. Depending on the geometry, translation factors of 30 to 40 are attainable, although at the cost of the conversion efficiency and the force generation. With piezoelectric bending actuators, displacements of up to several millimeters can be achieved with response times in the millisecond range. However, the blocking forces are relatively low. They are typically in the range of milli Newton to a few Newton" [22].

CHAPTER 4

DEVICE MODELING, SIMULATIONS AND DISCUSSION

4.1 Introduction

Infrared Imaging technology has made impressive progress during the past decades. Various types of cooled and uncooled infrared (IR) detectors have been designed including diodes, quantum wells (InGaAs, HgCdTe), thermoelectrics, bolometers, piezoelectrics, Schottky barrier detectors and many others. Present CMOS, Charge Couple Devices (CCD) and microbolometer detectors require complex and precise photon to electron conversion techniques at the quantum semiconductor level. This complexity and precision means that reliable manufacturing techniques are utilized and hence the costs to set up, build and maintain such devices is big. In this chapter, the fundamentals described in the previous two chapters are utilized and combined in order to present and discuss the design concept of a MEMS based IR detector [34].

Every pixel of the device has two parts: the metal-piezoelectric component (Figures 4.1 and 4.2) and the optics (for example, microlens) (Figure 4.3), constructed using the MEMS process, for improved performance of the metal-piezoelectric detector. The metal part uses the thermal expansion coefficient of a metal to translate the temperature change in the metal (due to the incident IR radiation) into a stress induced in the piezo. The piezoelectric material utilizes the applied strain from the metal to produce a voltage which is indirectly related to the scene temperature. The optics part of the device consists of an infrared (micro) lens which also works as a band pass filter operating in the wavelength range of 8 to 14 microns.

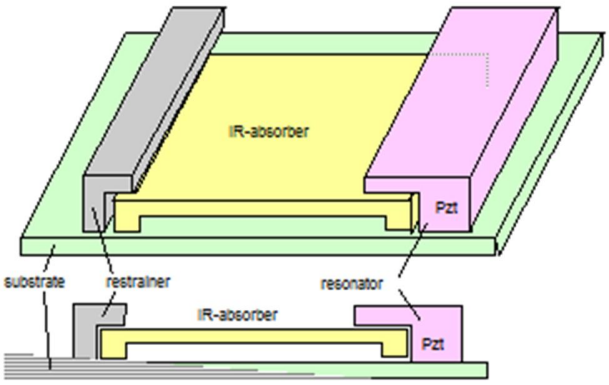

Figure 4.1 MEMS detector schematic.
Source: [34]

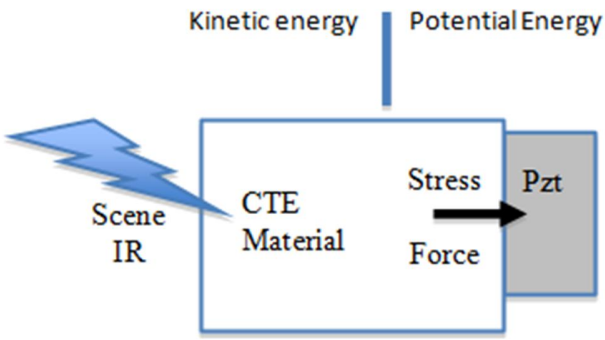

Figure 4.2 Schematic of the detector.
Source: [34]

4.2 Optics

The modeling of the optics is done by utilizing the *Blackbody Calculator (BBC)* [35]. An extended blackbody source is assumed, with specific lens (Optics), dewar window (Window), and filter transmission values. The filter can have up to two different wavelength bands. The blackbody temperature and the various elements that determine the system are manually inputted by the user and have the ability to specify the units for the resulting values on the focal plane area that corresponds to the location of the pixel. If

a unit is changed, the value displayed is converted according to the new units. The calculated parameters are shown in the beige box in real-time and include the total integrated focal plane flux (*or radiance*) in photon or *power* units along with the sensitivity of this flux (*radiance*) to a 1 K temperature change [35]. The BBC is shown in Figure 4.3.

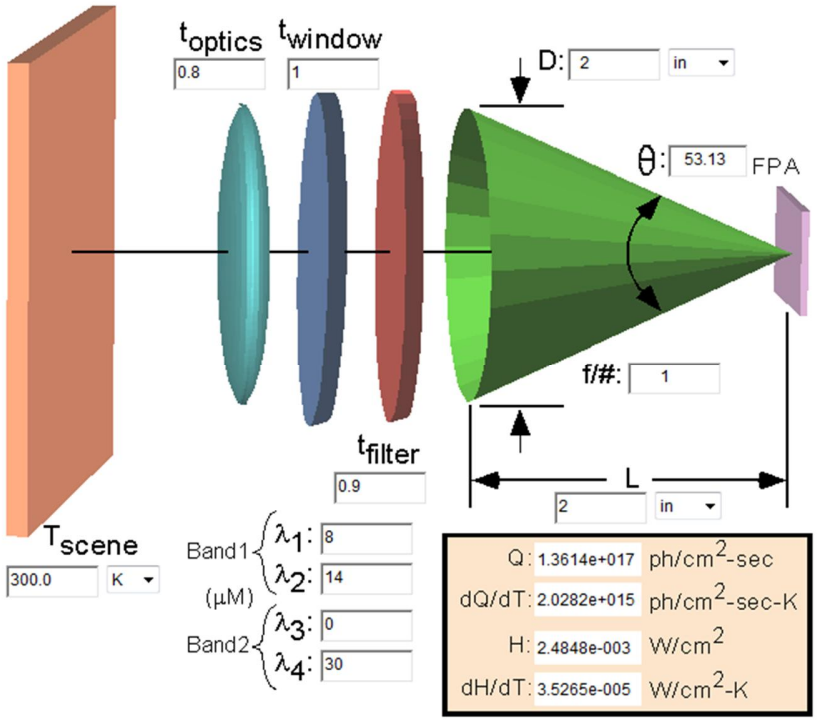

Figure 4.3 Blackbody Calculator (BBC).
Source: [35] http://www.sbfp.com/fluxcalc/fluxcalculator.html Access Date: 10/25/2013

For a black body scene temperature of 300 K, a bandwidth of 8 to 14 μm and the rest of the parameters set for maximum performance, the corresponding thermal flux on the pixel is 2.48×10^{-3} Watts/cm^2.

4.3 Interaction of IR Radiation with Metal-Piezo Detector Configuration

For the pixel, a simple linear model is assumed, where the pixel (absorber) is a block that is thermally connected to ambient by a thermally conductive PbSe multiple bridge design. Convection and radiation are ignored. The detector dimensions are chosen to be 50x50x10 microns and the bridge to be consisting of 50 bridges of 5μm (length) x 1μm^2. Therefore, the total amount of energy available to the detector at 300 K is 2.48×10^{-9} W/cm^2. In order to determine the temperature of the detector, the thermal conductivity of the bridge, along with its thermal resistance, must be considered.

For a metal, the thermal conductance is given by:

$$c = \frac{C_T A}{L} \tag{4.1}$$

where, C_T is the material's thermal conductivity, A is the detector's incident area and L the thickness.

Thermal resistance is the inverse of conductance and is given by:

$$R_T = \frac{1}{c} \tag{4.2}$$

To calculate the pixel temperature (above ambient), the product of the bridge's thermal resistance and the energy available to the detector is determined. Copper is considered to be the material of the detector and, for a scene temperature range of 300 to 370 K (with a step of 5 degrees), by acquiring the thermal flux for each scene temperature, the pixel temperature is calculated. In Table 4.1, the material thermal properties are presented. The calculated results are summarized in Table 4.2. In Figures 4.4 and 4.5, the pixel temperature, above ambient, with respect to the scene temperature and pixel temperature, with respect to detector displacement, respectively are presented.

Table 4.1 Thermal Properties of Materials

Metal	Cu	Zinc	Brass	PbSe	PbTe	PbS
Thermal Conductivity (W/mK) (300K)	401	116	109	1.6	2.1	2.55
Melting point (K)	1358	692	1193			
(CTE) linear	$16.6*10^{-6}$	$29.7*10^{-6}$	$18.7*10^{-6}$			$5.27*10^{-6}$
(CTE) Area	$33.2*10^{-6}$	$5.94x10^{-5}$	$3.74x10^{-5}$			
(CTE) Volume	$49.8*10^{-6}$	$89.1*10^{-6}$	$56.1*10^{-6}$			

Source: [36]

Table 4.2 Pixel Temperature and Detector Displacement with Respect to Scene Temperature

Scene temp (K)	**thermal flux* (Watts/cm^2)**	**pixel flux (Watts)(50x50)**	**pixel temp above ambient (K) (50x50)**	**Detectors displacement (m)**
300	2.48E-03	6.20E-08	9.69E+00	1.61E-09
305	2.68E-03	6.70E-08	1.05E+01	1.74E-09
310	2.88E-03	7.20E-08	1.13E+01	1.87E-09
315	3.09E-03	7.72E-08	1.21E+01	2.00E-09
320	3.31E-03	8.28E-08	1.29E+01	2.15E-09
325	3.54E-03	8.85E-08	1.38E+01	2.30E-09
330	3.78E-03	9.45E-08	1.48E+01	2.45E-09
335	4.05E-03	1.01E-07	1.58E+01	2.63E-09
340	4.28E-03	1.07E-07	1.67E+01	2.78E-09
345	4.54E-03	1.14E-07	1.77E+01	2.94E-09
350	4.81E-03	1.20E-07	1.88E+01	3.12E-09
355	5.10E-03	1.28E-07	1.99E+01	3.31E-09
360	5.39E-03	1.35E-07	2.11E+01	3.50E-09
365	5.68E-03	1.42E-07	2.22E+01	3.68E-09
370	5.99E-03	1.50E-07	2.34E+01	3.88E-09

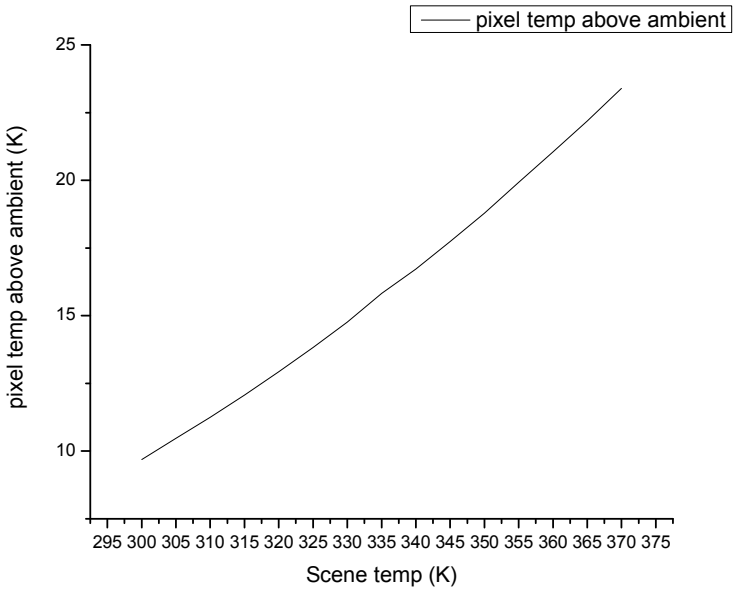

Figure 4.4 Pixel temperature as a function of scene temperature for Cu using a PbSe multiple thermal bridge.

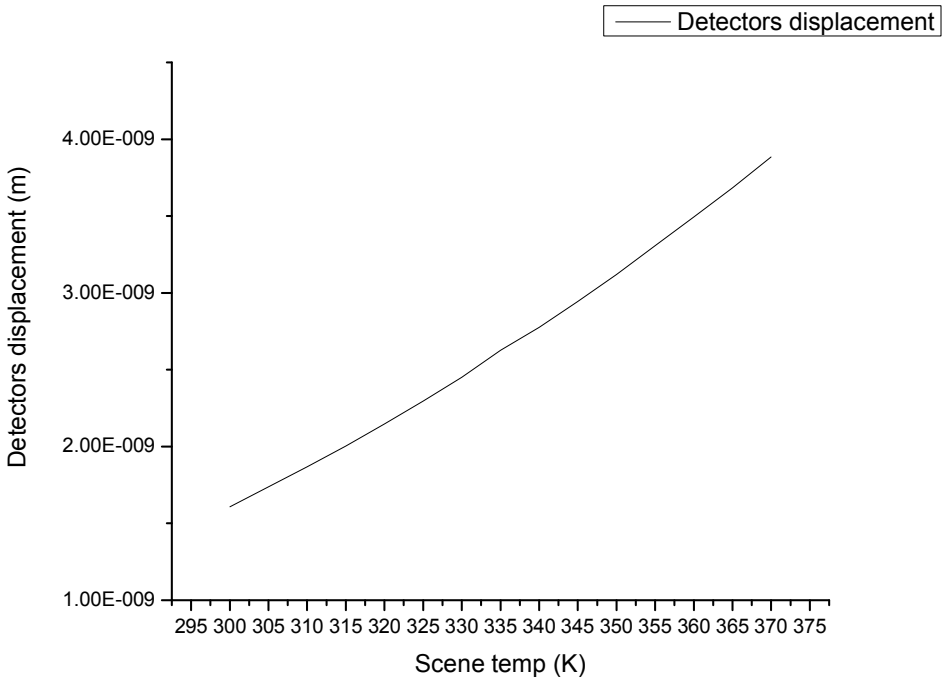

Figure 4.5 Detector displacement as a function of scene temp.

4.4 Performance Analyses of Candidates for Metal- Piezo Detector Configuration

As mentioned above, the detector's pixel consists of a metal part physically interfaced to a piezo part. The structure is constructed using the MEMS process and its schematic is presented in Figures 4.1 and 4.2.

Chapter 1 of this thesis presented an overview of the reaction of metals to heat, i.e., change in their dimensions according to their coefficient of thermal expansion (CTE). Most materials are isotropic and change their dimensions uniformly in all directions. This change in dimensions with temperature can be used to create a stress force applied to other materials such as piezoelectrics as will be seen in the following section.

4.4.1 Metal and Thermal Response

In this section, calculations for three different metals are presented: copper, zinc and brass. We consider two different sizes for the materials: 1x1x1 microns and 10x10x10 microns. Taking into consideration the coefficient of thermal expansion for each metal and equations (2.7), (2.9) and (2.13), linear, area and volume displacements are calculated for each metal. A range of temperatures is used so as to not to exceed 60% of their melting point. Using Young's modulus and Equation (2.18), the stress force due to the expansion of each material is derived. In Table 4.1, the thermal properties of the three metals, under consideration, are presented. In Tables 4.3, 4.4 and 4.5, the calculated results with the corresponding plots (Figures 4.6, 4.7 and 4.8) of the linear displacement of the metals with temperature are presented.

Table 4.3 Copper - Results 1x1x1 and 10x10x10 (microns)

	1x1x1 (micron)			
T (K)	Δl (m)	ΔA (m^2)	ΔV (m^3)	Stress force (N)
300	3.32E-11	6.64E-17	9.96E-23	3.88E-06
304	9.96E-11	1.99E-16	2.99E-22	1.17E-05
308	1.66E-10	3.32E-16	4.98E-22	1.94E-05
312	2.32E-10	4.65E-16	6.97E-22	2.72E-05
316	2.99E-10	5.98E-16	8.96E-22	3.50E-05
320	3.65E-10	7.30E-16	1.10E-21	4.27E-05
324	4.32E-10	8.63E-16	1.29E-21	5.05E-05
328	4.98E-10	9.96E-16	1.49E-21	5.83E-05
332	5.64E-10	1.13E-15	1.69E-21	6.60E-05
336	6.31E-10	1.26E-15	1.89E-21	7.38E-05
340	6.97E-10	1.39E-15	2.09E-21	8.16E-05
344	7.64E-10	1.53E-15	2.29E-21	8.93E-05
348	8.3E-10	1.66E-15	2.49E-21	9.71E-05
352	8.96E-10	1.79E-15	2.69E-21	1.05E-04
356	9.63E-10	1.93E-15	2.89E-21	1.13E-04
360	1.03E-09	2.06E-15	3.09E-21	1.20E-04
364	1.1E-09	2.19E-15	3.29E-21	1.28E-04
368	1.16E-09	2.32E-15	3.49E-21	1.36E-04
372	1.23E-09	2.46E-15	3.69E-21	1.44E-04
376	1.29E-09	2.59E-15	3.88E-21	1.51E-04
380	1.36E-09	2.72E-15	4.08E-21	1.59E-04
384	1.43E-09	2.86E-15	4.28E-21	1.67E-04
388	1.49E-09	2.99E-15	4.48E-21	1.75E-04
392	1.56E-09	3.12E-15	4.68E-21	1.83E-04
396	1.63E-09	3.25E-15	4.88E-21	1.90E-04
400	1.69E-09	3.39E-15	5.08E-21	1.98E-04

	10x10x10(micron)			
T (K)	Δl (m)	ΔA (m^2)	ΔV (m^3)	Stress Force (N)
300	3.32E-10	6.64E-15	9.96E-20	3.88E-04
304	9.96E-10	1.99E-14	2.99E-19	1.17E-03
308	1.66E-09	3.32E-14	4.98E-19	1.94E-03
312	2.32E-09	4.65E-14	6.97E-19	2.72E-03
316	2.99E-09	5.98E-14	8.96E-19	3.50E-03
320	3.65E-09	7.30E-14	1.10E-18	4.27E-03
324	4.32E-09	8.63E-14	1.29E-18	5.05E-03
328	4.98E-09	9.96E-14	1.49E-18	5.83E-03
332	5.64E-09	1.13E-13	1.69E-18	6.60E-03
336	6.31E-09	1.26E-13	1.89E-18	7.38E-03
340	6.97E-09	1.39E-13	2.09E-18	8.16E-03
344	7.64E-09	1.53E-13	2.29E-18	8.93E-03
348	8.30E-09	1.66E-13	2.49E-18	9.71E-03
352	8.96E-09	1.79E-13	2.69E-18	1.05E-02
356	9.63E-09	1.93E-13	2.89E-18	1.13E-02
360	1.03E-08	2.06E-13	3.09E-18	1.20E-02
364	1.10E-08	2.19E-13	3.29E-18	1.28E-02
368	1.16E-08	2.32E-13	3.49E-18	1.36E-02
372	1.23E-08	2.46E-13	3.69E-18	1.44E-02
376	1.29E-08	2.59E-13	3.88E-18	1.51E-02
380	1.36E-08	2.72E-13	4.08E-18	1.59E-02
384	1.43E-08	2.86E-13	4.28E-18	1.67E-02
388	1.49E-08	2.99E-13	4.48E-18	1.75E-02
392	1.56E-08	3.12E-13	4.68E-18	1.83E-02
396	1.63E-08	3.25E-13	4.88E-18	1.90E-02
400	1.69E-08	3.39E-13	5.08E-18	1.98E-02

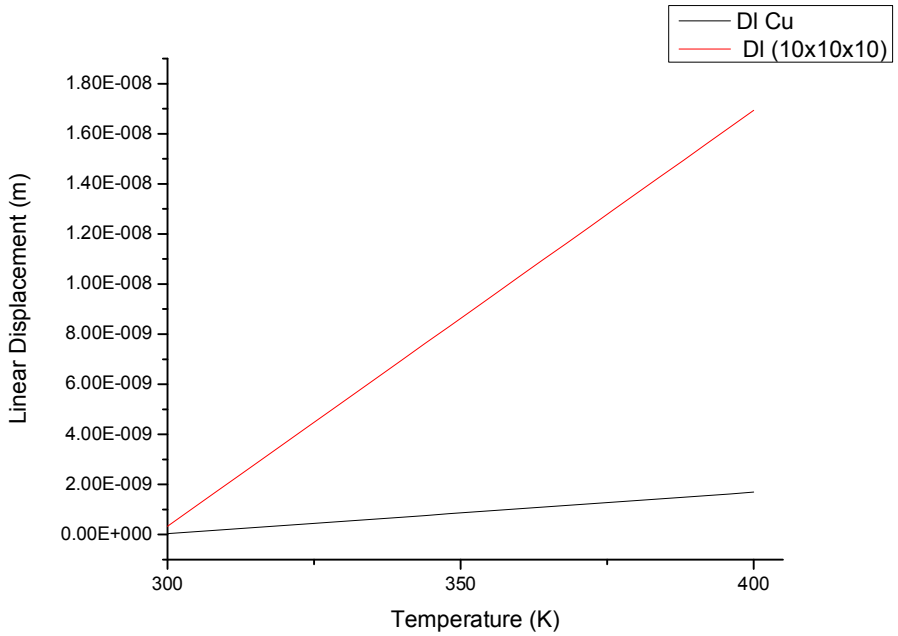

Figure 4.6 Linear displacement of Copper as a function of temperature.

Table 4.4 Zinc - Results 1x1x1 and 10x10x10 (microns)

	1x1x1 (micron)			
T (K)	Δl (m)	ΔA (m^2)	ΔV (m^3)	Stress force (N)
300	5.94E-11	1.19E-16	1.78E-22	4.91E-06
304	1.78E-10	3.56E-16	5.35E-22	1.47E-05
308	2.97E-10	5.94E-16	8.91E-22	2.46E-05
312	4.16E-10	8.32E-16	1.25E-21	3.44E-05
316	5.35E-10	1.07E-15	1.60E-21	4.42E-05
320	6.53E-10	1.31E-15	1.96E-21	5.40E-05
324	7.72E-10	1.54E-15	2.32E-21	6.39E-05
328	8.91E-10	1.78E-15	2.67E-21	7.37E-05
332	1.01E-09	2.02E-15	3.03E-21	8.35E-05
336	1.13E-09	2.26E-15	3.39E-21	9.33E-05
340	1.25E-09	2.49E-15	3.74E-21	1.03E-04
344	1.37E-09	2.73E-15	4.10E-21	1.13E-04
348	1.49E-09	2.97E-15	4.46E-21	1.23E-04
352	1.6E-09	3.21E-15	4.81E-21	1.33E-04
356	1.72E-09	3.45E-15	5.17E-21	1.42E-04
360	1.84E-09	3.68E-15	5.52E-21	1.52E-04
364	1.96E-09	3.92E-15	5.88E-21	1.62E-04
368	2.08E-09	4.16E-15	6.24E-21	1.72E-04
372	2.2E-09	4.40E-15	6.59E-21	1.82E-04
376	2.32E-09	4.63E-15	6.95E-21	1.92E-04
380	2.44E-09	4.87E-15	7.31E-21	2.01E-04
384	2.55E-09	5.11E-15	7.66E-21	2.11E-04
388	2.67E-09	5.35E-15	8.02E-21	2.21E-04
392	2.79E-09	5.58E-15	8.38E-21	2.31E-04
396	2.91E-09	5.82E-15	8.73E-21	2.41E-04
400	3.03E-09	6.06E-15	9.09E-21	2.51E-04

	10x10x10(micron)			
T (K)	Δl (m)	ΔA (m^2)	ΔV (m^3)	Stress Force (N)
300	5.94E-10	1.19E-14	1.78E-19	4.91E-04
304	1.78E-09	3.56E-14	5.35E-19	1.47E-03
308	2.97E-09	5.94E-14	8.91E-19	2.46E-03
312	4.16E-09	8.32E-14	1.25E-18	3.44E-03
316	5.35E-09	1.07E-13	1.60E-18	4.42E-03
320	6.53E-09	1.31E-13	1.96E-18	5.40E-03
324	7.72E-09	1.54E-13	2.32E-18	6.39E-03
328	8.91E-09	1.78E-13	2.67E-18	7.37E-03
332	1.01E-08	2.02E-13	3.03E-18	8.35E-03
336	1.13E-08	2.26E-13	3.39E-18	9.33E-03
340	1.25E-08	2.49E-13	3.74E-18	1.03E-02
344	1.37E-08	2.73E-13	4.10E-18	1.13E-02
348	1.49E-08	2.97E-13	4.46E-18	1.23E-02
352	1.60E-08	3.21E-13	4.81E-18	1.33E-02
356	1.72E-08	3.45E-13	5.17E-18	1.42E-02
360	1.84E-08	3.68E-13	5.52E-18	1.52E-02
364	1.96E-08	3.92E-13	5.88E-18	1.62E-02
368	2.08E-08	4.16E-13	6.24E-18	1.72E-02
372	2.20E-08	4.40E-13	6.59E-18	1.82E-02
376	2.32E-08	4.63E-13	6.95E-18	1.92E-02
380	2.44E-08	4.87E-13	7.31E-18	2.01E-02
384	2.55E-08	5.11E-13	7.66E-18	2.11E-02
388	2.67E-08	5.35E-13	8.02E-18	2.21E-02
392	2.79E-08	5.58E-13	8.38E-18	2.31E-02
396	2.91E-08	5.82E-13	8.73E-18	2.41E-02
400	3.03E-08	6.06E-13	9.09E-18	2.51E-02

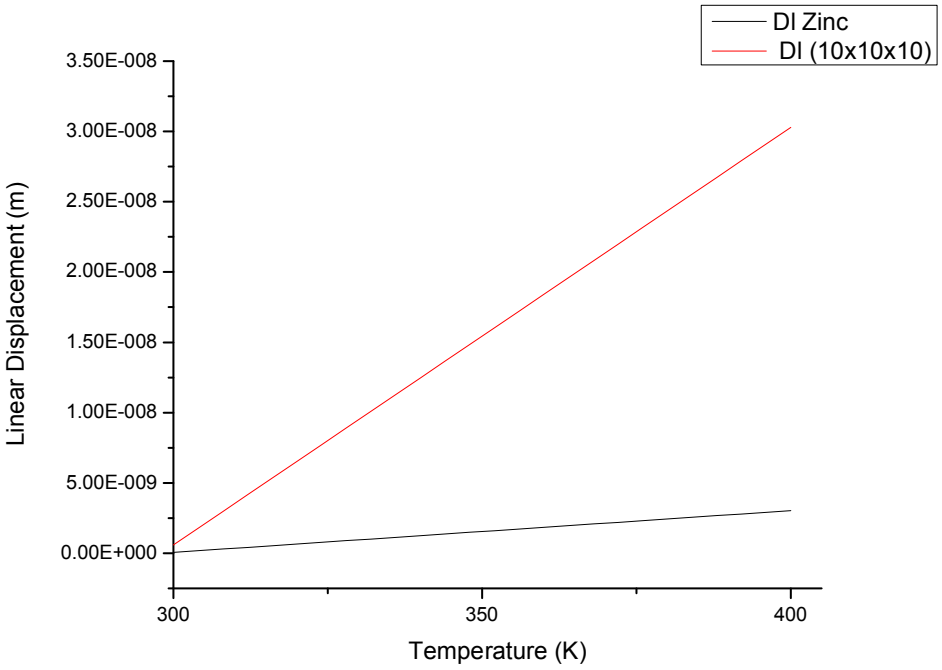

Figure 4.7 Linear displacement of Zinc as a function of temperature.

Table 4.5 Brass - Results 1x1x1 and 10x10x10 (microns)

	1x1x1 (micron)			
T (K)	Δl (m)	ΔA (m^2)	ΔV (m^3)	Stress force (N)
300	3.74E-11	7.48E-17	1.12E-22	4.49E-06
304	1.12E-10	2.24E-16	3.37E-22	1.35E-05
308	1.87E-10	3.74E-16	5.61E-22	2.24E-05
312	2.62E-10	5.24E-16	7.85E-22	3.14E-05
316	3.37E-10	6.73E-16	1.01E-21	4.04E-05
320	4.11E-10	8.23E-16	1.23E-21	4.94E-05
324	4.86E-10	9.72E-16	1.46E-21	5.83E-05
328	5.61E-10	1.12E-15	1.68E-21	6.73E-05
332	6.36E-10	1.27E-15	1.91E-21	7.63E-05
336	7.11E-10	1.42E-15	2.13E-21	8.53E-05
340	7.85E-10	1.57E-15	2.36E-21	9.42E-05
344	8.6E-10	1.72E-15	2.58E-21	1.03E-04
348	9.35E-10	1.87E-15	2.81E-21	1.12E-04
352	1.01E-09	2.02E-15	3.03E-21	1.21E-04
356	1.08E-09	2.17E-15	3.25E-21	1.30E-04
360	1.16E-09	2.32E-15	3.48E-21	1.39E-04
364	1.23E-09	2.47E-15	3.70E-21	1.48E-04
368	1.31E-09	2.62E-15	3.93E-21	1.57E-04
372	1.38E-09	2.77E-15	4.15E-21	1.66E-04
376	1.46E-09	2.92E-15	4.38E-21	1.75E-04
380	1.53E-09	3.07E-15	4.60E-21	1.84E-04
384	1.61E-09	3.22E-15	4.82E-21	1.93E-04
388	1.68E-09	3.37E-15	5.05E-21	2.02E-04
392	1.76E-09	3.52E-15	5.27E-21	2.11E-04
396	1.83E-09	3.67E-15	5.50E-21	2.20E-04
400	1.91E-09	3.81E-15	5.72E-21	2.29E-04

	10x10x10(micron)			
T (K)	Δl (m)	ΔA (m^2)	ΔV (m^3)	Stress Force (N)
300	3.74E-10	7.48E-15	1.12E-19	4.49E-04
304	1.12E-09	2.24E-14	3.37E-19	1.35E-03
308	1.87E-09	3.74E-14	5.61E-19	2.24E-03
312	2.62E-09	5.24E-14	7.85E-19	3.14E-03
316	3.37E-09	6.73E-14	1.01E-18	4.04E-03
320	4.11E-09	8.23E-14	1.23E-18	4.94E-03
324	4.86E-09	9.72E-14	1.46E-18	5.83E-03
328	5.61E-09	1.12E-13	1.68E-18	6.73E-03
332	6.36E-09	1.27E-13	1.91E-18	7.63E-03
336	7.11E-09	1.42E-13	2.13E-18	8.53E-03
340	7.85E-09	1.57E-13	2.36E-18	9.42E-03
344	8.60E-09	1.72E-13	2.58E-18	1.03E-02
348	9.35E-09	1.87E-13	2.81E-18	1.12E-02
352	1.01E-08	2.02E-13	3.03E-18	1.21E-02
356	1.08E-08	2.17E-13	3.25E-18	1.30E-02
360	1.16E-08	2.32E-13	3.48E-18	1.39E-02
364	1.23E-08	2.47E-13	3.70E-18	1.48E-02
368	1.31E-08	2.62E-13	3.93E-18	1.57E-02
372	1.38E-08	2.77E-13	4.15E-18	1.66E-02
376	1.46E-08	2.92E-13	4.38E-18	1.75E-02
380	1.53E-08	3.07E-13	4.60E-18	1.84E-02
384	1.61E-08	3.22E-13	4.82E-18	1.93E-02
388	1.68E-08	3.37E-13	5.05E-18	2.02E-02
392	1.76E-08	3.52E-13	5.27E-18	2.11E-02
396	1.83E-08	3.67E-13	5.50E-18	2.20E-02
400	1.91E-08	3.81E-13	5.72E-18	2.29E-02

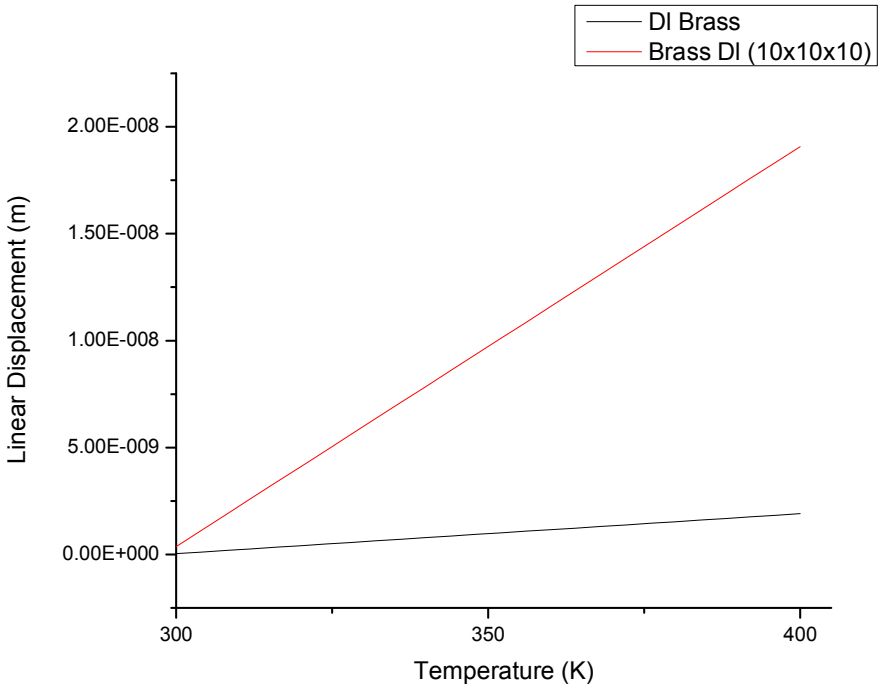

Figure 4.8 Linear displacement of Brass as a function of temperature.

4.4.2 Piezoelectric Material - Voltage Response

In this section, three piezoelectric materials: AlN, $BaTiO_3$ and PZT, in two different sizes 1x1x1 micron^3 and 10x10x10 micron^3, are considered. The strain force from the metal calculated in the previous section is transformed into stress via equation (3.28) and then into strain through equation (3.27). Knowing the strain together with the mechanical, electrical and piezoelectric constants of the piezo material, the output voltage of the piezo, using equation (3.26), is calculated. The capacitance is derived from equation (3.5).

Table 4.6 Voltage Calculations for Cu-AlN Pair

		1x1x1				10x10x10		
T (K)	C (F)	σ (N/m^2)	ε	Voltage (V)	C (F)	σ (N/m^2)	ε	Voltage (V)
300	7.97E-17	3.88E+06	1.13E-05	2.49E-01	7.97E-16	3.88E+06	1.13E-05	2.49E+00
304	7.97E-17	1.17E+07	3.38E-05	7.46E-01	7.97E-16	1.17E+07	3.38E-05	7.46E+00
308	7.97E-17	1.94E+07	5.63E-05	1.24E+00	7.97E-16	1.94E+07	5.63E-05	1.24E+01
312	7.97E-17	2.72E+07	7.89E-05	1.74E+00	7.97E-16	2.72E+07	7.89E-05	1.74E+01
316	7.97E-17	3.50E+07	1.01E-04	2.24E+00	7.97E-16	3.50E+07	1.01E-04	2.24E+01
320	7.97E-17	4.27E+07	1.24E-04	2.73E+00	7.97E-16	4.27E+07	1.24E-04	2.73E+01
324	7.97E-17	5.05E+07	1.46E-04	3.23E+00	7.97E-16	5.05E+07	1.46E-04	3.23E+01
328	7.97E-17	5.83E+07	1.69E-04	3.73E+00	7.97E-16	5.83E+07	1.69E-04	3.73E+01
332	7.97E-17	6.60E+07	1.91E-04	4.23E+00	7.97E-16	6.60E+07	1.91E-04	4.23E+01
336	7.97E-17	7.38E+07	2.14E-04	4.72E+00	7.97E-16	7.38E+07	2.14E-04	4.72E+01
340	7.97E-17	8.16E+07	2.37E-04	5.22E+00	7.97E-16	8.16E+07	2.37E-04	5.22E+01
344	7.97E-17	8.93E+07	2.59E-04	5.72E+00	7.97E-16	8.93E+07	2.59E-04	5.72E+01
348	7.97E-17	9.71E+07	2.82E-04	6.22E+00	7.97E-16	9.71E+07	2.82E-04	6.22E+01
352	7.97E-17	1.05E+08	3.04E-04	6.71E+00	7.97E-16	1.05E+08	3.04E-04	6.71E+01
356	7.97E-17	1.13E+08	3.27E-04	7.21E+00	7.97E-16	1.13E+08	3.27E-04	7.21E+01
360	7.97E-17	1.20E+08	3.49E-04	7.71E+00	7.97E-16	1.20E+08	3.49E-04	7.71E+01
364	7.97E-17	1.28E+08	3.72E-04	8.20E+00	7.97E-16	1.28E+08	3.72E-04	8.20E+01
368	7.97E-17	1.36E+08	3.94E-04	8.70E+00	7.97E-16	1.36E+08	3.94E-04	8.70E+01
372	7.97E-17	1.44E+08	4.17E-04	9.20E+00	7.97E-16	1.44E+08	4.17E-04	9.20E+01
376	7.97E-17	1.51E+08	4.39E-04	9.70E+00	7.97E-16	1.51E+08	4.39E-04	9.70E+01
380	7.97E-17	1.59E+08	4.62E-04	1.02E+01	7.97E-16	1.59E+08	4.62E-04	1.02E+02
384	7.97E-17	1.67E+08	4.84E-04	1.07E+01	7.97E-16	1.67E+08	4.84E-04	1.07E+02
388	7.97E-17	1.75E+08	5.07E-04	1.12E+01	7.97E-16	1.75E+08	5.07E-04	1.12E+02
392	7.97E-17	1.83E+08	5.29E-04	1.17E+01	7.97E-16	1.83E+08	5.29E-04	1.17E+02
396	7.97E-17	1.90E+08	5.52E-04	1.22E+01	7.97E-16	1.90E+08	5.52E-04	1.22E+02
400	7.97E-17	1.98E+08	5.74E-04	1.27E+01	7.97E-16	1.98E+08	5.74E-04	1.27E+02

Table 4.7 Voltage Calculations for Cu-$BaTiO_3$ Pair

	1x1x1			10x10x10		
T (K)	C (F)	ε	Voltage	C (F)	ε	Voltage (V)
300	1.11E-14	5.80E-05	2.74E-02	1.11E-13	5.80E-05	2.74E-01
304	1.11E-14	1.74E-04	8.21E-02	1.11E-13	1.74E-04	8.21E-01
308	1.11E-14	2.90E-04	1.37E-01	1.11E-13	2.90E-04	1.37E+00
312	1.11E-14	4.06E-04	1.92E-01	1.11E-13	4.06E-04	1.92E+00
316	1.11E-14	5.22E-04	2.46E-01	1.11E-13	5.22E-04	2.46E+00
320	1.11E-14	6.38E-04	3.01E-01	1.11E-13	6.38E-04	3.01E+00
324	1.11E-14	7.54E-04	3.56E-01	1.11E-13	7.54E-04	3.56E+00
328	1.11E-14	8.70E-04	4.11E-01	1.11E-13	8.70E-04	4.11E+00
332	1.11E-14	9.86E-04	4.65E-01	1.11E-13	9.86E-04	4.65E+00
336	1.11E-14	1.10E-03	5.20E-01	1.11E-13	1.10E-03	5.20E+00
340	1.11E-14	1.22E-03	5.75E-01	1.11E-13	1.22E-03	5.75E+00
344	1.11E-14	1.33E-03	6.30E-01	1.11E-13	1.33E-03	6.30E+00
348	1.11E-14	1.45E-03	6.84E-01	1.11E-13	1.45E-03	6.84E+00
352	1.11E-14	1.57E-03	7.39E-01	1.11E-13	1.57E-03	7.39E+00
356	1.11E-14	1.68E-03	7.94E-01	1.11E-13	1.68E-03	7.94E+00
360	1.11E-14	1.80E-03	8.49E-01	1.11E-13	1.80E-03	8.49E+00
364	1.11E-14	1.91E-03	9.03E-01	1.11E-13	1.91E-03	9.03E+00
368	1.11E-14	2.03E-03	9.58E-01	1.11E-13	2.03E-03	9.58E+00
372	1.11E-14	2.15E-03	1.01E+00	1.11E-13	2.15E-03	1.01E+01
376	1.11E-14	2.26E-03	1.07E+00	1.11E-13	2.26E-03	1.07E+01
380	1.11E-14	2.38E-03	1.12E+00	1.11E-13	2.38E-03	1.12E+01
384	1.11E-14	2.49E-03	1.18E+00	1.11E-13	2.49E-03	1.18E+01
388	1.11E-14	2.61E-03	1.23E+00	1.11E-13	2.61E-03	1.23E+01
392	1.11E-14	2.72E-03	1.29E+00	1.11E-13	2.72E-03	1.29E+01
396	1.11E-14	2.84E-03	1.34E+00	1.11E-13	2.84E-03	1.34E+01
400	1.11E-14	2.96E-03	1.40E+00	1.11E-13	2.96E-03	1.40E+01

Table 4.8 Voltage Calculations for Cu-PZT Pair

	1x1x1			10x10x10		
T (K)	C (F)	ε	Voltage (V)	C (F)	ε	Voltage (V)
300	1.51E-14	6.17E-05	3.02E-02	1.51E-13	6.17E-05	3.02E-01
304	1.51E-14	1.85E-04	9.06E-02	1.51E-13	1.85E-04	9.06E-01
308	1.51E-14	3.08E-04	1.51E-01	1.51E-13	3.08E-04	1.51E+00
312	1.51E-14	4.32E-04	2.11E-01	1.51E-13	4.32E-04	2.11E+00
316	1.51E-14	5.55E-04	2.72E-01	1.51E-13	5.55E-04	2.72E+00
320	1.51E-14	6.78E-04	3.32E-01	1.51E-13	6.78E-04	3.32E+00
324	1.51E-14	8.02E-04	3.93E-01	1.51E-13	8.02E-04	3.93E+00
328	1.51E-14	9.25E-04	4.53E-01	1.51E-13	9.25E-04	4.53E+00
332	1.51E-14	1.05E-03	5.13E-01	1.51E-13	1.05E-03	5.13E+00
336	1.51E-14	1.17E-03	5.74E-01	1.51E-13	1.17E-03	5.74E+00
340	1.51E-14	1.29E-03	6.34E-01	1.51E-13	1.29E-03	6.34E+00
344	1.51E-14	1.42E-03	6.94E-01	1.51E-13	1.42E-03	6.94E+00
348	1.51E-14	1.54E-03	7.55E-01	1.51E-13	1.54E-03	7.55E+00
352	1.51E-14	1.66E-03	8.15E-01	1.51E-13	1.66E-03	8.15E+00
356	1.51E-14	1.79E-03	8.76E-01	1.51E-13	1.79E-03	8.76E+00
360	1.51E-14	1.91E-03	9.36E-01	1.51E-13	1.91E-03	9.36E+00
364	1.51E-14	2.03E-03	9.96E-01	1.51E-13	2.03E-03	9.96E+00
368	1.51E-14	2.16E-03	1.06E+00	1.51E-13	2.16E-03	1.06E+01
372	1.51E-14	2.28E-03	1.12E+00	1.51E-13	2.28E-03	1.12E+01
376	1.51E-14	2.40E-03	1.18E+00	1.51E-13	2.40E-03	1.18E+01
380	1.51E-14	2.53E-03	1.24E+00	1.51E-13	2.53E-03	1.24E+01
384	1.51E-14	2.65E-03	1.30E+00	1.51E-13	2.65E-03	1.30E+01
388	1.51E-14	2.77E-03	1.36E+00	1.51E-13	2.77E-03	1.36E+01
392	1.51E-14	2.90E-03	1.42E+00	1.51E-13	2.90E-03	1.42E+01
396	1.51E-14	3.02E-03	1.48E+00	1.51E-13	3.02E-03	1.48E+01
400	1.51E-14	3.14E-03	1.54E+00	1.51E-13	3.14E-03	1.54E+01

In Tables 4.6, 4.7 and 4.8, the calculated results for the output voltage of the three piezoelectric materials, when physically attached to copper, are summarized. In Figures 4.9 and 4.10, voltage as a function of temperature, for detector dimensions 1x1x1 and 10x10x10 micron^3, respectively, is presented.

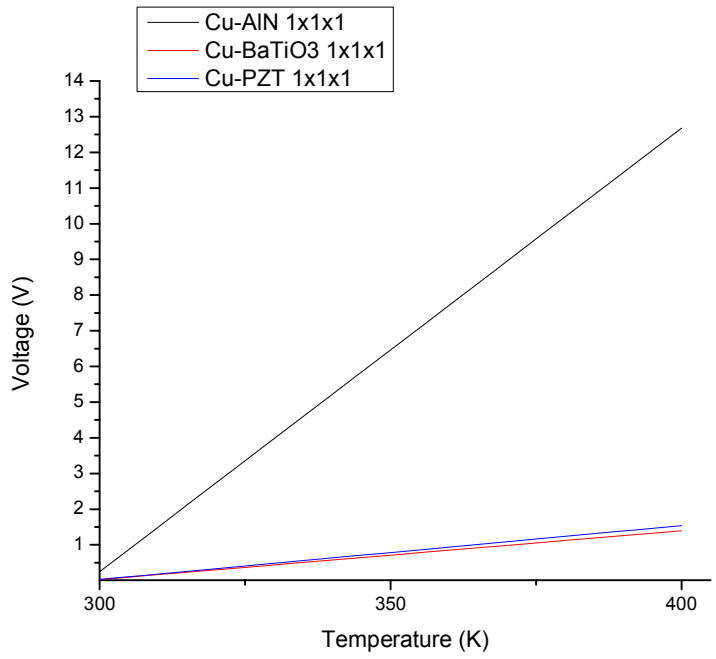

Figure 4.9 Voltage as a function of temperature for 1x1x1 micron^3 Cu-piezo pairs.

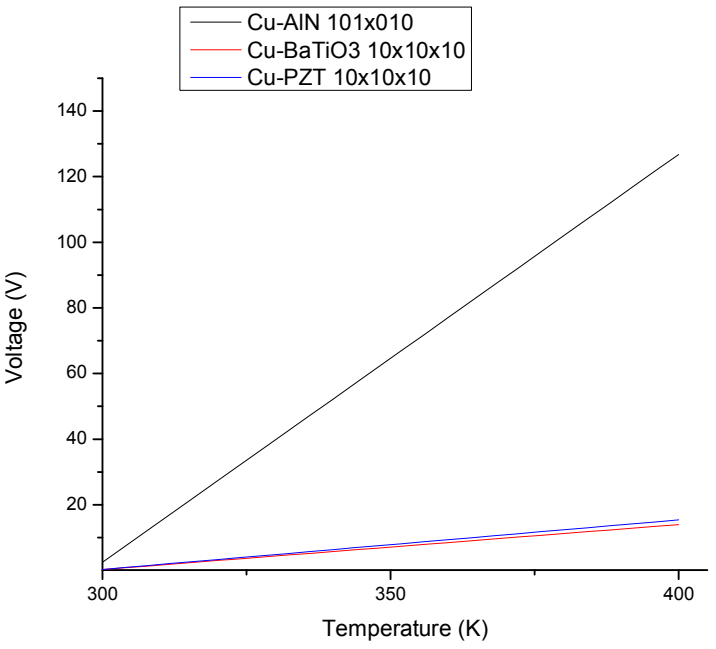

Figure 4.10 Voltage as a function of temperature for 10x10x10 micron^3 Cu-piezo pairs.

Table 4.9 Voltage Calculations for Zinc-AlN Pair

		1x1x1				10x10x10		
T (K)	C (F)	σ (N/m^2)	ε	Voltage (V)	C (F)	σ (N/m^2)	ε	Voltage (V)
300	7.97E-17	4.91E+06	1.42E-05	3.14E-01	7.97E-16	4.91E+06	1.42E-05	3.14E+00
304	7.97E-17	1.47E+07	4.27E-05	9.43E-01	7.97E-16	1.47E+07	4.27E-05	9.43E+00
308	7.97E-17	2.46E+07	7.12E-05	1.57E+00	7.97E-16	2.46E+07	7.12E-05	1.57E+01
312	7.97E-17	3.44E+07	9.97E-05	2.20E+00	7.97E-16	3.44E+07	9.97E-05	2.20E+01
316	7.97E-17	4.42E+07	1.28E-04	2.83E+00	7.97E-16	4.42E+07	1.28E-04	2.83E+01
320	7.97E-17	5.40E+07	1.57E-04	3.46E+00	7.97E-16	5.40E+07	1.57E-04	3.46E+01
324	7.97E-17	6.39E+07	1.85E-04	4.09E+00	7.97E-16	6.39E+07	1.85E-04	4.09E+01
328	7.97E-17	7.37E+07	2.14E-04	4.72E+00	7.97E-16	7.37E+07	2.14E-04	4.72E+01
332	7.97E-17	8.35E+07	2.42E-04	5.34E+00	7.97E-16	8.35E+07	2.42E-04	5.34E+01
336	7.97E-17	9.33E+07	2.71E-04	5.97E+00	7.97E-16	9.33E+07	2.71E-04	5.97E+01
340	7.97E-17	1.03E+08	2.99E-04	6.60E+00	7.97E-16	1.03E+08	2.99E-04	6.60E+01
344	7.97E-17	1.13E+08	3.28E-04	7.23E+00	7.97E-16	1.13E+08	3.28E-04	7.23E+01
348	7.97E-17	1.23E+08	3.56E-04	7.86E+00	7.97E-16	1.23E+08	3.56E-04	7.86E+01
352	7.97E-17	1.33E+08	3.85E-04	8.49E+00	7.97E-16	1.33E+08	3.85E-04	8.49E+01
356	7.97E-17	1.42E+08	4.13E-04	9.12E+00	7.97E-16	1.42E+08	4.13E-04	9.12E+01
360	7.97E-17	1.52E+08	4.42E-04	9.75E+00	7.97E-16	1.52E+08	4.42E-04	9.75E+01
364	7.97E-17	1.62E+08	4.70E-04	1.04E+01	7.97E-16	1.62E+08	4.70E-04	1.04E+02
368	7.97E-17	1.72E+08	4.99E-04	1.10E+01	7.97E-16	1.72E+08	4.99E-04	1.10E+02
372	7.97E-17	1.82E+08	5.27E-04	1.16E+01	7.97E-16	1.82E+08	5.27E-04	1.16E+02
376	7.97E-17	1.92E+08	5.56E-04	1.23E+01	7.97E-16	1.92E+08	5.56E-04	1.23E+02
380	7.97E-17	2.01E+08	5.84E-04	1.29E+01	7.97E-16	2.01E+08	5.84E-04	1.29E+02
384	7.97E-17	2.11E+08	6.13E-04	1.35E+01	7.97E-16	2.11E+08	6.13E-04	1.35E+02
388	7.97E-17	2.21E+08	6.41E-04	1.41E+01	7.97E-16	2.21E+08	6.41E-04	1.41E+02
392	7.97E-17	2.31E+08	6.70E-04	1.48E+01	7.97E-16	2.31E+08	6.70E-04	1.48E+02
396	7.97E-17	2.41E+08	6.98E-04	1.54E+01	7.97E-16	2.41E+08	6.98E-04	1.54E+02
400	7.97E-17	2.51E+08	7.27E-04	1.60E+01	7.97E-16	2.51E+08	7.27E-04	1.60E+02

Table 4.10 Voltage Calculations for Zinc-$BaTiO_3$ Pair

	1x1x1			10x10x10		
T (K)	C (F)	ε	Voltage	C (F)	ε	Voltage (V)
300	1.11E-14	7.33E-05	3.46E-02	1.11E-13	7.33E-05	3.46E-01
304	1.11E-14	2.20E-04	1.04E-01	1.11E-13	2.20E-04	1.04E+00
308	1.11E-14	3.67E-04	1.73E-01	1.11E-13	3.67E-04	1.73E+00
312	1.11E-14	5.13E-04	2.42E-01	1.11E-13	5.13E-04	2.42E+00
316	1.11E-14	6.60E-04	3.12E-01	1.11E-13	6.60E-04	3.12E+00
320	1.11E-14	8.07E-04	3.81E-01	1.11E-13	8.07E-04	3.81E+00
324	1.11E-14	9.53E-04	4.50E-01	1.11E-13	9.53E-04	4.50E+00
328	1.11E-14	1.10E-03	5.19E-01	1.11E-13	1.10E-03	5.19E+00
332	1.11E-14	1.25E-03	5.89E-01	1.11E-13	1.25E-03	5.89E+00
336	1.11E-14	1.39E-03	6.58E-01	1.11E-13	1.39E-03	6.58E+00
340	1.11E-14	1.54E-03	7.27E-01	1.11E-13	1.54E-03	7.27E+00
344	1.11E-14	1.69E-03	7.96E-01	1.11E-13	1.69E-03	7.96E+00
348	1.11E-14	1.83E-03	8.66E-01	1.11E-13	1.83E-03	8.66E+00
352	1.11E-14	1.98E-03	9.35E-01	1.11E-13	1.98E-03	9.35E+00
356	1.11E-14	2.13E-03	1.00E+00	1.11E-13	2.13E-03	1.00E+01
360	1.11E-14	2.27E-03	1.07E+00	1.11E-13	2.27E-03	1.07E+01
364	1.11E-14	2.42E-03	1.14E+00	1.11E-13	2.42E-03	1.14E+01
368	1.11E-14	2.57E-03	1.21E+00	1.11E-13	2.57E-03	1.21E+01
372	1.11E-14	2.71E-03	1.28E+00	1.11E-13	2.71E-03	1.28E+01
376	1.11E-14	2.86E-03	1.35E+00	1.11E-13	2.86E-03	1.35E+01
380	1.11E-14	3.01E-03	1.42E+00	1.11E-13	3.01E-03	1.42E+01
384	1.11E-14	3.15E-03	1.49E+00	1.11E-13	3.15E-03	1.49E+01
388	1.11E-14	3.30E-03	1.56E+00	1.11E-13	3.30E-03	1.56E+01
392	1.11E-14	3.45E-03	1.63E+00	1.11E-13	3.45E-03	1.63E+01
396	1.11E-14	3.59E-03	1.70E+00	1.11E-13	3.59E-03	1.70E+01
400	1.11E-14	3.74E-03	1.77E+00	1.11E-13	3.74E-03	1.77E+01

Table 4.11 Voltage Calculations for Zinc-PZT Pair

	1x1x1			10x10x10		
T (K)	C (F)	ε	Voltage	C (F)	ε	Voltage (V)
300	1.51E-14	7.80E-05	3.82E-02	1.51E-13	7.80E-05	3.82E-01
304	1.51E-14	2.34E-04	1.15E-01	1.51E-13	2.34E-04	1.15E+00
308	1.51E-14	3.90E-04	1.91E-01	1.51E-13	3.90E-04	1.91E+00
312	1.51E-14	5.46E-04	2.67E-01	1.51E-13	5.46E-04	2.67E+00
316	1.51E-14	7.02E-04	3.44E-01	1.51E-13	7.02E-04	3.44E+00
320	1.51E-14	8.58E-04	4.20E-01	1.51E-13	8.58E-04	4.20E+00
324	1.51E-14	1.01E-03	4.96E-01	1.51E-13	1.01E-03	4.96E+00
328	1.51E-14	1.17E-03	5.73E-01	1.51E-13	1.17E-03	5.73E+00
332	1.51E-14	1.33E-03	6.49E-01	1.51E-13	1.33E-03	6.49E+00
336	1.51E-14	1.48E-03	7.26E-01	1.51E-13	1.48E-03	7.26E+00
340	1.51E-14	1.64E-03	8.02E-01	1.51E-13	1.64E-03	8.02E+00
344	1.51E-14	1.79E-03	8.78E-01	1.51E-13	1.79E-03	8.78E+00
348	1.51E-14	1.95E-03	9.55E-01	1.51E-13	1.95E-03	9.55E+00
352	1.51E-14	2.11E-03	1.03E+00	1.51E-13	2.11E-03	1.03E+01
356	1.51E-14	2.26E-03	1.11E+00	1.51E-13	2.26E-03	1.11E+01
360	1.51E-14	2.42E-03	1.18E+00	1.51E-13	2.42E-03	1.18E+01
364	1.51E-14	2.57E-03	1.26E+00	1.51E-13	2.57E-03	1.26E+01
368	1.51E-14	2.73E-03	1.34E+00	1.51E-13	2.73E-03	1.34E+01
372	1.51E-14	2.89E-03	1.41E+00	1.51E-13	2.89E-03	1.41E+01
376	1.51E-14	3.04E-03	1.49E+00	1.51E-13	3.04E-03	1.49E+01
380	1.51E-14	3.20E-03	1.57E+00	1.51E-13	3.20E-03	1.57E+01
384	1.51E-14	3.35E-03	1.64E+00	1.51E-13	3.35E-03	1.64E+01
388	1.51E-14	3.51E-03	1.72E+00	1.51E-13	3.51E-03	1.72E+01
392	1.51E-14	3.66E-03	1.79E+00	1.51E-13	3.66E-03	1.79E+01
396	1.51E-14	3.82E-03	1.87E+00	1.51E-13	3.82E-03	1.87E+01
400	1.51E-14	3.98E-03	1.95E+00	1.51E-13	3.98E-03	1.95E+01

In Tables 4.9, 4.10 and 4.11, the calculated results, for the output voltage of the three piezoelectric materials when physically attached to Zinc, are presented. In Figures 4.11 and 4.12 the output voltage as a function of temperature for the two different dimensions of the detector (1x1x1 micron^{3}and 10x10x10 micron^3) are shown.

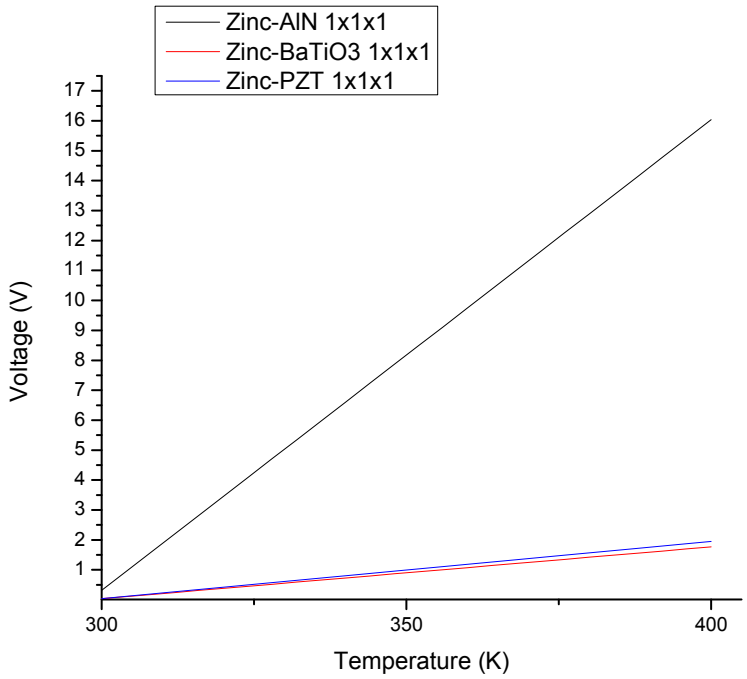

Figure 4.11 Voltage as a function of temperature for 1x1x1 micron^3 Zinc-piezo pairs.

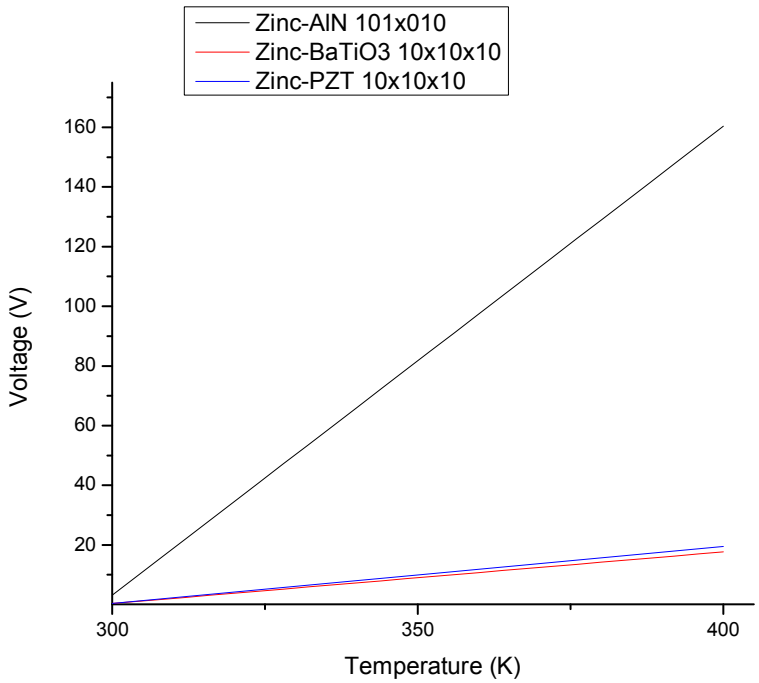

Figure 4.12 Voltage as a function of temperature for 10x10x10 micron^3 Zinc-piezo pairs.

Table 4.12 Voltage Calculations for Brass-AlN Pair

		1x1x1				10x10x10		
T (K)	C (F)	σ (N/m^2)	ε	Voltage (V)	C (F)	σ (N/m^2)	ε	Voltage (V)
300	7.97E-17	4.49E+06	1.30E-05	2.87E-01	7.97E-16	4.49E+06	1.30E-05	2.87E+00
304	7.97E-17	1.35E+07	3.90E-05	8.62E-01	7.97E-16	1.35E+07	3.90E-05	8.62E+00
308	7.97E-17	2.24E+07	6.51E-05	1.44E+00	7.97E-16	2.24E+07	6.51E-05	1.44E+01
312	7.97E-17	3.14E+07	9.11E-05	2.01E+00	7.97E-16	3.14E+07	9.11E-05	2.01E+01
316	7.97E-17	4.04E+07	1.17E-04	2.59E+00	7.97E-16	4.04E+07	1.17E-04	2.59E+01
320	7.97E-17	4.94E+07	1.43E-04	3.16E+00	7.97E-16	4.94E+07	1.43E-04	3.16E+01
324	7.97E-17	5.83E+07	1.69E-04	3.73E+00	7.97E-16	5.83E+07	1.69E-04	3.73E+01
328	7.97E-17	6.73E+07	1.95E-04	4.31E+00	7.97E-16	6.73E+07	1.95E-04	4.31E+01
332	7.97E-17	7.63E+07	2.21E-04	4.88E+00	7.97E-16	7.63E+07	2.21E-04	4.88E+01
336	7.97E-17	8.53E+07	2.47E-04	5.46E+00	7.97E-16	8.53E+07	2.47E-04	5.46E+01
340	7.97E-17	9.42E+07	2.73E-04	6.03E+00	7.97E-16	9.42E+07	2.73E-04	6.03E+01
344	7.97E-17	1.03E+08	2.99E-04	6.61E+00	7.97E-16	1.03E+08	2.99E-04	6.61E+01
348	7.97E-17	1.12E+08	3.25E-04	7.18E+00	7.97E-16	1.12E+08	3.25E-04	7.18E+01
352	7.97E-17	1.21E+08	3.51E-04	7.76E+00	7.97E-16	1.21E+08	3.51E-04	7.76E+01
356	7.97E-17	1.30E+08	3.77E-04	8.33E+00	7.97E-16	1.30E+08	3.77E-04	8.33E+01
360	7.97E-17	1.39E+08	4.03E-04	8.90E+00	7.97E-16	1.39E+08	4.03E-04	8.90E+01
364	7.97E-17	1.48E+08	4.29E-04	9.48E+00	7.97E-16	1.48E+08	4.29E-04	9.48E+01
368	7.97E-17	1.57E+08	4.56E-04	1.01E+01	7.97E-16	1.57E+08	4.56E-04	1.01E+02
372	7.97E-17	1.66E+08	4.82E-04	1.06E+01	7.97E-16	1.66E+08	4.82E-04	1.06E+02
376	7.97E-17	1.75E+08	5.08E-04	1.12E+01	7.97E-16	1.75E+08	5.08E-04	1.12E+02
380	7.97E-17	1.84E+08	5.34E-04	1.18E+01	7.97E-16	1.84E+08	5.34E-04	1.18E+02
384	7.97E-17	1.93E+08	5.60E-04	1.24E+01	7.97E-16	1.93E+08	5.60E-04	1.24E+02
388	7.97E-17	2.02E+08	5.86E-04	1.29E+01	7.97E-16	2.02E+08	5.86E-04	1.29E+02
392	7.97E-17	2.11E+08	6.12E-04	1.35E+01	7.97E-16	2.11E+08	6.12E-04	1.35E+02
396	7.97E-17	2.20E+08	6.38E-04	1.41E+01	7.97E-16	2.20E+08	6.38E-04	1.41E+02
400	7.97E-17	2.29E+08	6.64E-04	1.46E+01	7.97E-16	2.29E+08	6.64E-04	1.46E+02

Table 4.13 Voltage Calculations for Brass-$BaTiO_3$ Pair

	1x1x1			10x10x10		
T (K)	C (F)	ε	Voltage	C (F)	ε	Voltage (V)
300	1.11E-14	6.70E-05	3.16E-02	1.11E-13	6.70E-05	3.16E-01
304	1.11E-14	2.01E-04	9.49E-02	1.11E-13	2.01E-04	9.49E-01
308	1.11E-14	3.35E-04	1.58E-01	1.11E-13	3.35E-04	1.58E+00
312	1.11E-14	4.69E-04	2.21E-01	1.11E-13	4.69E-04	2.21E+00
316	1.11E-14	6.03E-04	2.85E-01	1.11E-13	6.03E-04	2.85E+00
320	1.11E-14	7.37E-04	3.48E-01	1.11E-13	7.37E-04	3.48E+00
324	1.11E-14	8.71E-04	4.11E-01	1.11E-13	8.71E-04	4.11E+00
328	1.11E-14	1.00E-03	4.74E-01	1.11E-13	1.00E-03	4.74E+00
332	1.11E-14	1.14E-03	5.38E-01	1.11E-13	1.14E-03	5.38E+00
336	1.11E-14	1.27E-03	6.01E-01	1.11E-13	1.27E-03	6.01E+00
340	1.11E-14	1.41E-03	6.64E-01	1.11E-13	1.41E-03	6.64E+00
344	1.11E-14	1.54E-03	7.27E-01	1.11E-13	1.54E-03	7.27E+00
348	1.11E-14	1.67E-03	7.91E-01	1.11E-13	1.67E-03	7.91E+00
352	1.11E-14	1.81E-03	8.54E-01	1.11E-13	1.81E-03	8.54E+00
356	1.11E-14	1.94E-03	9.17E-01	1.11E-13	1.94E-03	9.17E+00
360	1.11E-14	2.08E-03	9.81E-01	1.11E-13	2.08E-03	9.81E+00
364	1.11E-14	2.21E-03	1.04E+00	1.11E-13	2.21E-03	1.04E+01
368	1.11E-14	2.34E-03	1.11E+00	1.11E-13	2.34E-03	1.11E+01
372	1.11E-14	2.48E-03	1.17E+00	1.11E-13	2.48E-03	1.17E+01
376	1.11E-14	2.61E-03	1.23E+00	1.11E-13	2.61E-03	1.23E+01
380	1.11E-14	2.75E-03	1.30E+00	1.11E-13	2.75E-03	1.30E+01
384	1.11E-14	2.88E-03	1.36E+00	1.11E-13	2.88E-03	1.36E+01
388	1.11E-14	3.01E-03	1.42E+00	1.11E-13	3.01E-03	1.42E+01
392	1.11E-14	3.15E-03	1.49E+00	1.11E-13	3.15E-03	1.49E+01
396	1.11E-14	3.28E-03	1.55E+00	1.11E-13	3.28E-03	1.55E+01
400	1.11E-14	3.42E-03	1.61E+00	1.11E-13	3.42E-03	1.61E+01

Table 4.14 Voltage Calculations for Brass-PZT Pair

1x1x1			10x10x10			
T (K)	C (F)	ε	Voltage	C (F)	ε	Voltage (V)
300	1.51E-14	7.12E-05	3.49E-02	1.51E-13	7.12E-05	3.49E-01
304	1.51E-14	2.14E-04	1.05E-01	1.51E-13	2.14E-04	1.05E+00
308	1.51E-14	3.56E-04	1.74E-01	1.51E-13	3.56E-04	1.74E+00
312	1.51E-14	4.99E-04	2.44E-01	1.51E-13	4.99E-04	2.44E+00
316	1.51E-14	6.41E-04	3.14E-01	1.51E-13	6.41E-04	3.14E+00
320	1.51E-14	7.84E-04	3.84E-01	1.51E-13	7.84E-04	3.84E+00
324	1.51E-14	9.26E-04	4.54E-01	1.51E-13	9.26E-04	4.54E+00
328	1.51E-14	1.07E-03	5.23E-01	1.51E-13	1.07E-03	5.23E+00
332	1.51E-14	1.21E-03	5.93E-01	1.51E-13	1.21E-03	5.93E+00
336	1.51E-14	1.35E-03	6.63E-01	1.51E-13	1.35E-03	6.63E+00
340	1.51E-14	1.50E-03	7.33E-01	1.51E-13	1.50E-03	7.33E+00
344	1.51E-14	1.64E-03	8.02E-01	1.51E-13	1.64E-03	8.02E+00
348	1.51E-14	1.78E-03	8.72E-01	1.51E-13	1.78E-03	8.72E+00
352	1.51E-14	1.92E-03	9.42E-01	1.51E-13	1.92E-03	9.42E+00
356	1.51E-14	2.07E-03	1.01E+00	1.51E-13	2.07E-03	1.01E+01
360	1.51E-14	2.21E-03	1.08E+00	1.51E-13	2.21E-03	1.08E+01
364	1.51E-14	2.35E-03	1.15E+00	1.51E-13	2.35E-03	1.15E+01
368	1.51E-14	2.49E-03	1.22E+00	1.51E-13	2.49E-03	1.22E+01
372	1.51E-14	2.64E-03	1.29E+00	1.51E-13	2.64E-03	1.29E+01
376	1.51E-14	2.78E-03	1.36E+00	1.51E-13	2.78E-03	1.36E+01
380	1.51E-14	2.92E-03	1.43E+00	1.51E-13	2.92E-03	1.43E+01
384	1.51E-14	3.06E-03	1.50E+00	1.51E-13	3.06E-03	1.50E+01
388	1.51E-14	3.21E-03	1.57E+00	1.51E-13	3.21E-03	1.57E+01
392	1.51E-14	3.35E-03	1.64E+00	1.51E-13	3.35E-03	1.64E+01
396	1.51E-14	3.49E-03	1.71E+00	1.51E-13	3.49E-03	1.71E+01
400	1.51E-14	3.63E-03	1.78E+00	1.51E-13	3.63E-03	1.78E+01

In Tables 4.12, 4.13 and 4.14, the calculated results, for the output voltage of the three piezoelectric materials when physically attached to brass, are presented. In Figures 4.13 and 4.14, voltage as a function of temperature for detector dimensions 1x1x1 micron^3 and 10x10x10 micron^3, respectively, are shown.

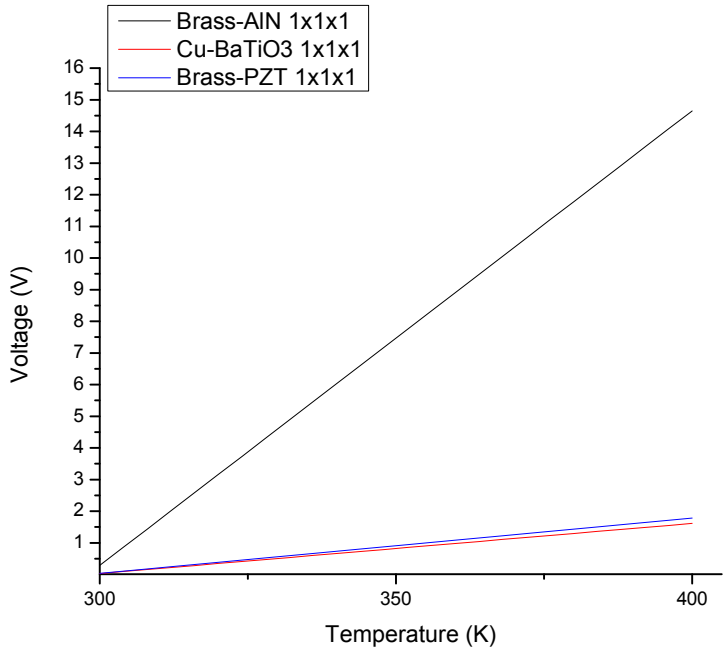

Figure 4.13 Voltage as a function of temperature for 1x1x1 micron^3 Brass-piezo pairs.

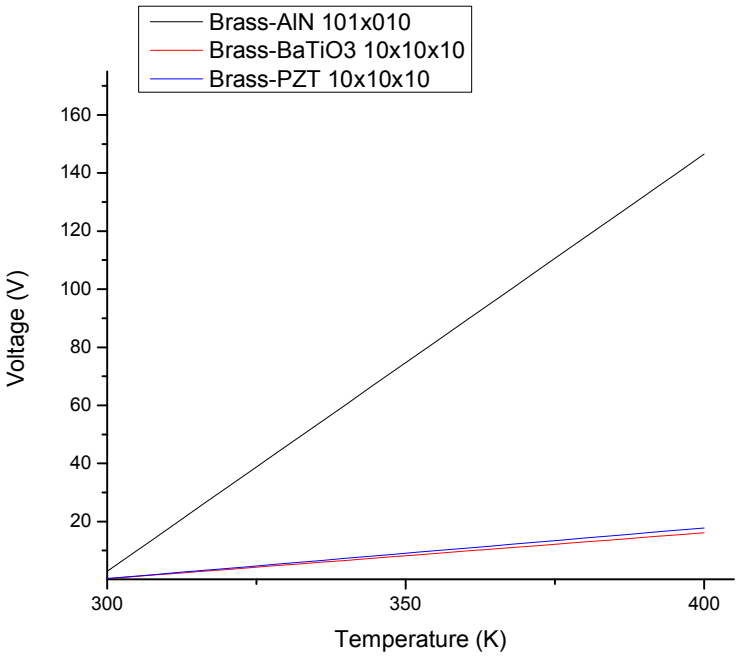

Figure 4.14 Voltage as a function of temperature for 10x10x10 micron^3 Brass-piezo pairs.

4.4.3 Frequency Response

In order to test the frequency response of the pixel, Equation 3.30 is utilized as well as Equations 3.27a, 3.27b and 3.28 in order to calculate the change in the piezo dimensions (distance between the electrodes). The results are shown in Tables 4.18a, 4.18b, 4.19a 4.19b, 4.20a and 4.20b for copper, zinc and brass as the metal component of the detector respectively. a and b point to the detector dimensions (1x1x1 micron^3 and 10x10x10 micron^3, respectively). Resonance frequencies at room temperature (298 K) and density of the piezoelectric materials are listed in Table 4.15.

Table 4.15 Resonance Frequency of AlN, $BaTiO_3$ and PZT at Room Temperature

	AlN (Hz)	BatiO3 (Hz)	PZT (Hz)
F_0 (298)	514237478.26	1666804881.76	1449137674.62
ρ(Kg/m^3)	3260	6029	7500

Table 4.16a Frequency Response of AlN, $BaTiO_3$ and PZT with Cu as the Metal Part Dimensions 1x1x1 micron^3

T (K)	ΔL(AlN) (m)	ΔL(BaTiO3) (m)	ΔL(PZT) (m)	Fq (AlN) (Hz)	Fq(BaTiO3) (Hz)	Fq(PZT) (Hz)	ΔF (AlN) (Hz)	ΔF (BaTiO3) (Hz)	ΔF (PZT) (Hz)
300	1.13E-11	5.80E-11	6.17E-11	5142432710.48	1666901522.24	1449227029.82	57927.86	96640.48	89355.20
304	3.38E-11	1.74E-10	1.85E-10	5142548570.13	1667094836.83	1449405773.28	173787.51	289955.07	268098.66
308	5.63E-11	2.90E-10	3.08E-10	5142664434.99	1667288196.25	1449584560.83	289652.38	483314.50	446886.21
312	7.89E-11	4.06E-10	4.32E-10	5142780305.08	1667481600.54	1449763392.50	405522.46	676718.79	625717.88
316	1.01E-10	5.22E-10	5.55E-10	5142896180.39	1667675049.71	1449942268.30	521397.77	870167.95	804593.68
320	1.24E-10	6.38E-10	6.78E-10	5143012060.92	1667868543.76	1450121188.24	637278.30	1063662.00	983513.62
324	1.46E-10	7.54E-10	8.02E-10	5143127946.67	1668062082.72	1450300152.35	753164.05	1257200.96	1162477.73
328	1.69E-10	8.70E-10	9.25E-10	5143243837.65	1668255666.60	1450479160.63	869055.03	1450784.85	1341486.01
332	1.91E-10	9.86E-10	1.05E-09	5143359733.84	1668449295.42	1450658213.11	984951.23	1644413.66	1520538.49
336	2.14E-10	1.10E-09	1.17E-09	5143475635.27	1668642969.19	1450837309.80	1100852.65	1838087.44	1699635.18
340	2.37E-10	1.22E-09	1.29E-09	5143591541.91	1668836687.93	1451016450.72	1216759.29	2031806.18	1878776.10
344	2.59E-10	1.33E-09	1.42E-09	5143707453.78	1669030451.66	1451195635.88	1332671.16	2225569.90	2057961.26
348	2.82E-10	1.45E-09	1.54E-09	5143823370.87	1669224260.38	1451374865.30	1448588.25	2419378.63	2237190.69
352	3.04E-10	1.57E-09	1.66E-09	5143939293.19	1669418114.12	1451554139.00	1564510.57	2613232.37	2416464.38
356	3.27E-10	1.68E-09	1.79E-09	5144055220.73	1669612012.89	1451733457.00	1680438.11	2807131.14	2595782.38
360	3.49E-10	1.80E-09	1.91E-09	5144171153.50	1669805956.71	1451912819.30	1796370.88	3001074.96	2775144.68
364	3.72E-10	1.91E-09	2.03E-09	5144287091.49	1669999945.59	1452092225.93	1912308.88	3195063.84	2954551.31
368	3.94E-10	2.03E-09	2.16E-09	5144403034.71	1670193979.55	1452271676.90	2028252.10	3389097.80	3134002.28
372	4.17E-10	2.15E-09	2.28E-09	5144518983.16	1670388058.61	1452451172.23	2144200.54	3583176.85	3313497.61
376	4.39E-10	2.26E-09	2.40E-09	5144634936.83	1670582182.77	1452630711.93	2260154.22	3777301.01	3493037.31
380	4.62E-10	2.38E-09	2.53E-09	5144750895.73	1670776352.06	1452810296.03	2376113.12	3971470.30	3672621.41
384	4.84E-10	2.49E-09	2.65E-09	5144866859.86	1670970566.49	1452989924.53	2492077.24	4165684.73	3852249.92
388	5.07E-10	2.61E-09	2.77E-09	5144982829.22	1671164826.07	1453169597.46	2608046.60	4359944.32	4031922.85
392	5.29E-10	2.72E-09	2.90E-09	5145098803.80	1671359130.83	1453349314.84	2724021.18	4554249.08	4211640.22
396	5.52E-10	2.84E-09	3.02E-09	5145214783.61	1671553480.78	1453529076.67	2840000.99	4748599.03	4391402.05
400	5.74E-10	2.96E-09	3.14E-09	5145330768.65	1671747875.94	1453708882.97	2955986.04	4942994.18	4571208.35

Table 4.16b Frequency Response of AlN, $BaTiO_3$ and PZT with Cu as the Metal Part Dimensions 10x10x10 micron^3

T (K)	ΔL(AlN) (m)	ΔL(BaTiO3) (m)	ΔL(PZT) (m)	Fq (AlN) (Hz)	Fq(BaTiO3) (Hz)	Fq(PZT) (Hz)	ΔF (AlN) (Hz)	ΔF (BaTiO3) (Hz)	ΔF (PZT) (Hz)
300	1.13E-10	5.80E-10	6.17E-10	514243271.05	166685320.06	144922702.98	5792.79	4831.88	8935.52
304	3.38E-10	1.74E-09	1.85E-09	514254857.01	166694984.67	144940577.33	17378.75	14496.49	26809.87
308	5.63E-10	2.90E-09	3.08E-09	514266443.50	166704650.40	144958456.08	28965.24	24162.22	44688.62
312	7.89E-10	4.06E-09	4.32E-09	514278030.51	166714317.25	144976339.25	40552.25	33829.07	62571.79
316	1.01E-09	5.22E-09	5.55E-09	514289618.04	166723985.22	144994226.83	52139.78	43497.04	80459.37
320	1.24E-09	6.38E-09	6.78E-09	514301206.09	166733654.31	145012118.82	63727.83	53166.14	98351.36
324	1.46E-09	7.54E-09	8.02E-09	514312794.67	166743324.53	145030015.23	75316.41	62836.35	116247.77
328	1.69E-09	8.70E-09	9.25E-09	514324383.76	166752995.86	145047916.06	86905.50	72507.69	134148.60
332	1.91E-09	9.86E-09	1.05E-08	514335973.38	166762668.32	145065821.31	98495.12	82180.15	152053.85
336	2.14E-09	1.10E-08	1.17E-08	514347563.53	166772341.90	145083730.98	110085.26	91853.73	169963.52
340	2.37E-09	1.22E-08	1.29E-08	514359154.19	166782016.60	145101645.07	121675.93	101528.43	187877.61
344	2.59E-09	1.33E-08	1.42E-08	514370745.38	166791692.43	145119563.59	133267.12	111204.25	205796.13
348	2.82E-09	1.45E-08	1.54E-08	514382337.09	166801369.38	145137486.53	144858.83	120881.20	223719.07
352	3.04E-09	1.57E-08	1.66E-08	514393929.32	166811047.45	145155413.90	156451.06	130559.27	241646.44
356	3.27E-09	1.68E-08	1.79E-08	514405522.07	166820726.64	145173345.70	168043.81	140238.47	259578.24
360	3.49E-09	1.80E-08	1.91E-08	514417115.35	166830406.96	145191281.93	179637.09	149918.78	277514.47
364	3.72E-09	1.91E-08	2.03E-08	514428709.15	166840088.40	145209222.59	191230.89	159600.22	295455.13
368	3.94E-09	2.03E-08	2.16E-08	514440303.47	166849770.96	145227167.69	202825.21	169282.79	313400.23
372	4.17E-09	2.15E-08	2.28E-08	514451898.32	166859454.65	145245117.22	214420.05	178966.48	331349.76
376	4.39E-09	2.26E-08	2.40E-08	514463493.68	166869139.47	145263071.19	226015.42	188651.29	349303.73
380	4.62E-09	2.38E-08	2.53E-08	514475089.57	166878825.40	145281029.60	237611.31	198337.23	367262.14
384	4.84E-09	2.49E-08	2.65E-08	514486685.99	166888512.46	145298992.45	249207.72	208024.29	385224.99
388	5.07E-09	2.61E-08	2.77E-08	514498282.92	166898200.65	145316959.75	260804.66	217712.48	403192.28
392	5.29E-09	2.72E-08	2.90E-08	514509880.38	166907889.96	145334931.48	272402.12	227401.79	421164.02
396	5.52E-09	2.84E-08	3.02E-08	514521478.36	166917580.40	145352907.67	284000.10	237092.22	439140.20
400	5.74E-09	2.96E-08	3.14E-08	514533076.87	166927271.96	145370888.30	295598.60	246783.78	457120.83

Table 4.17a Frequency Response of AlN, $BaTiO_3$ and PZT with Zinc as the Metal Part Dimensions 1x1x1 micron^3

T (K)	ΔL(AlN) (m)	ΔL(BaTiO3) (m)	ΔL(PZT) (m)	Fq (AlN) (Hz)	Fq(BaTiO3) (Hz)	Fq(PZT) (Hz)	ΔF (AlN) (Hz)	ΔF (BaTiO3) (Hz)	ΔF (PZT) (Hz)
300	1.42E-11	7.33E-11	7.80E-11	5142448040.92	1666927099.36	1449250678.91	73258.30	122217.60	113004.29
304	4.27E-11	2.20E-10	2.34E-10	5142594563.77	1667171588.34	1449476740.36	219781.16	366706.58	339065.74
308	7.12E-11	3.67E-10	3.90E-10	5142741094.98	1667416149.05	1449702872.35	366312.36	611267.29	565197.73
312	9.97E-11	5.13E-10	5.46E-10	5142887634.54	1667660781.52	1449929074.91	512851.92	855899.77	791400.29
316	1.28E-10	6.60E-10	7.02E-10	5143034182.45	1667905485.79	1450155348.07	659399.83	1100604.03	1017673.45
320	1.57E-10	8.07E-10	8.58E-10	5143180738.71	1668150261.87	1450381691.86	805956.09	1345380.12	1244017.24
324	1.85E-10	9.53E-10	1.01E-09	5143327303.33	1668395109.82	1450608106.32	952520.71	1590228.06	1470431.70
328	2.14E-10	1.10E-09	1.17E-09	5143473876.30	1668640029.65	1450834591.48	1099093.68	1835147.89	1696916.86
332	2.42E-10	1.25E-09	1.33E-09	5143620457.62	1668885021.40	1451061147.38	1245675.00	2080139.64	1923472.76
336	2.71E-10	1.39E-09	1.48E-09	5143767047.30	1669130085.10	1451287774.04	1392264.68	2325203.34	2150099.42
340	2.99E-10	1.54E-09	1.64E-09	5143913645.33	1669375220.78	1451514471.51	1538862.71	2570339.02	2376796.89
344	3.28E-10	1.69E-09	1.79E-09	5144060251.72	1669620428.47	1451741239.80	1685469.10	2815546.72	2603565.18
348	3.56E-10	1.83E-09	1.95E-09	5144206866.47	1669865708.22	1451968078.96	1832083.85	3060826.46	2830404.35
352	3.85E-10	1.98E-09	2.11E-09	5144353489.57	1670111060.03	1452194989.03	1978706.95	3306178.28	3057314.41
356	4.13E-10	2.13E-09	2.26E-09	5144500121.03	1670356483.96	1452421970.02	2125338.41	3551602.21	3284295.40
360	4.42E-10	2.27E-09	2.42E-09	5144646760.86	1670601980.03	1452649021.99	2271978.24	3797098.27	3511347.37
364	4.70E-10	2.42E-09	2.57E-09	5144793409.04	1670847548.27	1452876144.95	2418626.42	4042666.52	3738470.33
368	4.99E-10	2.57E-09	2.73E-09	5144940065.58	1671093188.72	1453103338.94	2565282.96	4288306.96	3965664.32
372	5.27E-10	2.71E-09	2.89E-09	5145086730.48	1671338901.40	1453330604.00	2711947.87	4534019.65	4192929.38
376	5.56E-10	2.86E-09	3.04E-09	5145233403.75	1671584686.36	1453557940.16	2858621.13	4779804.60	4420265.54
380	5.84E-10	3.01E-09	3.20E-09	5145380085.38	1671830543.61	1453785347.45	3005302.76	5025661.85	4647672.84
384	6.13E-10	3.15E-09	3.35E-09	5145526775.37	1672076473.19	1454012825.91	3151992.75	5271591.43	4875151.30
388	6.41E-10	3.30E-09	3.51E-09	5145673473.73	1672322475.14	1454240375.57	3298691.11	5517593.38	5102700.95
392	6.70E-10	3.45E-09	3.66E-09	5145820180.45	1672568549.48	1454467996.47	3445397.83	5763667.73	5330321.85
396	6.98E-10	3.59E-09	3.82E-09	5145966895.54	1672814696.26	1454695688.62	3592112.92	6009814.50	5558014.01
400	7.27E-10	3.74E-09	3.98E-09	5146113618.99	1673060915.49	1454923452.08	3738836.37	6256033.73	5785777.46

Table 4.17b Frequency Response of AlN, $BaTiO_3$ and PZT with Zinc as the Metal Part Dimensions 10x10x10 micron^3

T (K)	ΔL(AlN) (m)	ΔL(BaTiO3) (m)	ΔL(PZT) (m)	Fq (AlN) (Hz)	Fq(BaTiO3) (Hz)	Fq(PZT) (Hz)	ΔF (AlN) (Hz)	ΔF (BaTiO3) (Hz)	ΔF (PZT) (Hz)
300	1.42E-10	7.33E-10	7.80E-10	514244804.09	166692709.94	144925067.89	7325.83	12221.76	11300.43
304	4.27E-10	2.20E-09	2.34E-09	514259456.38	166717158.83	144947674.04	21978.12	36670.66	33906.57
308	7.12E-10	3.67E-09	3.90E-09	514274109.50	166741614.91	144970287.23	36631.24	61126.73	56519.77
312	9.97E-10	5.13E-09	5.46E-09	514288763.45	166766078.15	144992907.49	51285.19	85589.98	79140.03
316	1.28E-09	6.60E-09	7.02E-09	514303418.25	166790548.58	145015534.81	65939.98	110060.40	101767.34
320	1.57E-09	8.07E-09	8.58E-09	514318073.87	166815026.19	145038169.19	80595.61	134538.01	124401.72
324	1.85E-09	9.53E-09	1.01E-08	514332730.33	166839510.98	145060810.63	95252.07	159022.81	147043.17
328	2.14E-09	1.10E-08	1.17E-08	514347387.63	166864002.96	145083459.15	109909.37	183514.79	169691.69
332	2.42E-09	1.25E-08	1.33E-08	514362045.76	166888502.14	145106114.74	124567.50	208013.96	192347.28
336	2.71E-09	1.39E-08	1.48E-08	514376704.73	166913008.51	145128777.40	139226.47	232520.33	215009.94
340	2.99E-09	1.54E-08	1.64E-08	514391364.53	166937522.08	145151447.15	153886.27	257033.90	237679.69
344	3.28E-09	1.69E-08	1.79E-08	514406025.17	166962042.85	145174123.98	168546.91	281554.67	260356.52
348	3.56E-09	1.83E-08	1.95E-08	514420686.65	166986570.82	145196807.90	183208.38	306082.65	283040.43
352	3.85E-09	1.98E-08	2.11E-08	514435348.96	167011106.00	145219498.90	197870.70	330617.83	305731.44
356	4.13E-09	2.13E-08	2.26E-08	514450012.10	167035648.40	145242197.00	212533.84	355160.22	328429.54
360	4.42E-09	2.27E-08	2.42E-08	514464676.09	167060198.00	145264902.20	227197.82	379709.83	351134.74
364	4.70E-09	2.42E-08	2.57E-08	514479340.90	167084754.83	145287614.49	241862.64	404266.65	373847.03
368	4.99E-09	2.57E-08	2.73E-08	514494006.56	167109318.87	145310333.89	256528.30	428830.70	396566.43
372	5.27E-09	2.71E-08	2.89E-08	514508673.05	167133890.14	145333060.40	271194.79	453401.96	419292.94
376	5.56E-09	2.86E-08	3.04E-08	514523340.38	167158468.64	145355794.02	285862.11	477980.46	442026.55
380	5.84E-09	3.01E-08	3.20E-08	514538008.54	167183054.36	145378534.75	300530.28	502566.19	464767.28
384	6.13E-09	3.15E-08	3.35E-08	514552677.54	167207647.32	145401282.59	315199.28	527159.14	487515.13
388	6.41E-09	3.30E-08	3.51E-08	514567347.37	167232247.51	145424037.56	329869.11	551759.34	510270.10
392	6.70E-09	3.45E-08	3.66E-08	514582018.05	167256854.95	145446799.65	344539.78	576366.77	533032.18
396	6.98E-09	3.59E-08	3.82E-08	514596689.55	167281469.63	145469568.86	359211.29	600981.45	555801.40
400	7.27E-09	3.74E-08	3.98E-08	514611361.90	167306091.55	145492345.21	373883.64	625603.37	578577.75

Table 4.18a Frequency Response of AlN, $BaTiO_3$ and PZT with Brass as the Metal Part Dimensions 1x1x1 micron^3

T (K)	ΔL(AlN) (m)	ΔL(BaTiO3) (m)	ΔL(PZT) (m)	Fq (AlN) (Hz)	Fq(BaTiO3) (Hz)	Fq(PZT) (Hz)	ΔF (AlN) (Hz)	ΔF (BaTiO3) (Hz)	ΔF (PZT) (Hz)
300	1.30E-11	6.70E-11	7.12E-11	5142441712.06	1666916540.29	1449240915.78	66929.44	111658.53	103241.16
304	3.90E-11	2.01E-10	2.14E-10	5142575576.16	1667139902.23	1449447442.24	200793.54	335020.47	309767.62
308	6.51E-11	3.35E-10	3.56E-10	5142709447.24	1667363324.04	1449654027.58	334664.62	558442.28	516352.96
312	9.11E-11	4.69E-10	4.99E-10	5142843325.28	1667586805.74	1449860671.81	468542.66	781923.99	722997.19
316	1.17E-10	6.03E-10	6.41E-10	5142977210.29	1667810347.36	1450067374.96	602427.68	1005465.61	929700.34
320	1.43E-10	7.37E-10	7.84E-10	5143111102.28	1668033948.92	1450274137.06	736319.66	1229067.16	1136462.44
324	1.69E-10	8.71E-10	9.26E-10	5143245001.24	1668257610.44	1450480958.13	870218.62	1452728.69	1343283.51
328	1.95E-10	1.00E-09	1.07E-09	5143378907.17	1668481331.96	1450687838.19	1004124.55	1676450.20	1550163.58
332	2.21E-10	1.14E-09	1.21E-09	5143512820.07	1668705113.48	1450894777.28	1138037.45	1900231.72	1757102.67
336	2.47E-10	1.27E-09	1.35E-09	5143646739.94	1668928955.04	1451101775.42	1271957.33	2124073.28	1964100.80
340	2.73E-10	1.41E-09	1.50E-09	5143780666.79	1669152856.66	1451308832.63	1405884.18	2347974.90	2171158.01
344	2.99E-10	1.54E-09	1.64E-09	5143914600.62	1669376818.36	1451515948.94	1539818.00	2571936.61	2378274.32
348	3.25E-10	1.67E-09	1.78E-09	5144048541.42	1669600840.18	1451723124.37	1673758.80	2795958.42	2585449.75
352	3.51E-10	1.81E-09	1.92E-09	5144182489.19	1669824922.13	1451930358.96	1807706.57	3020040.37	2792684.34
356	3.77E-10	1.94E-09	2.07E-09	5144316443.94	1670049064.23	1452137652.71	1941661.32	3244182.47	2999978.09
360	4.03E-10	2.08E-09	2.21E-09	5144450405.67	1670273266.52	1452345005.67	2075623.05	3468384.76	3207331.05
364	4.29E-10	2.21E-09	2.35E-09	5144584374.37	1670497529.01	1452552417.85	2209591.75	3692647.25	3414743.23
368	4.56E-10	2.34E-09	2.49E-09	5144718350.05	1670721851.73	1452759889.28	2343567.43	3916969.98	3622214.66
372	4.82E-10	2.48E-09	2.64E-09	5144852332.71	1670946234.71	1452967419.98	2477550.09	4141352.95	3829745.36
376	5.08E-10	2.61E-09	2.78E-09	5144986322.35	1671170677.97	1453175009.99	2611539.73	4365796.21	4037335.37
380	5.34E-10	2.75E-09	2.92E-09	5145120318.97	1671395181.53	1453382659.32	2745536.35	4590299.77	4244984.70
384	5.60E-10	2.88E-09	3.06E-09	5145254322.57	1671619745.41	1453590368.01	2879539.95	4814863.66	4452693.39
388	5.86E-10	3.01E-09	3.21E-09	5145388333.14	1671844369.65	1453798136.07	3013550.53	5039487.89	4660461.45
392	6.12E-10	3.15E-09	3.35E-09	5145522350.70	1672069054.27	1454005963.54	3147568.08	5264172.51	4868288.92
396	6.38E-10	3.28E-09	3.49E-09	5145656375.24	1672293799.28	1454213850.43	3281592.62	5488917.52	5076175.81
400	6.64E-10	3.42E-09	3.63E-09	5145790406.77	1672518604.72	1454421796.78	3415624.15	5713722.96	5284122.16

Table 4.18b Frequency Response of AlN, $BaTiO_3$ and PZT with Brass as the Metal Part Dimensions 10x10x10 micron^3

T (K)	ΔL(AlN)	ΔL(BaTiO3)	ΔL(PZT)	Fq (AlN)	Fq(BaTiO3)	Fq(PZT)	ΔF (AlN)	ΔF (BaTiO3)	ΔF (PZT)
300	1.30E-10	6.70E-10	7.12E-10	514244171.21	166691654.03	144924091.58	6692.94	11165.85	10324.12
304	3.90E-10	2.01E-09	2.14E-09	514257557.62	166713990.22	144944744.22	20079.35	33502.05	30976.76
308	6.51E-10	3.35E-09	3.56E-09	514270944.72	166736332.40	144965402.76	33466.46	55844.23	51635.30
312	9.11E-10	4.69E-09	4.99E-09	514284332.53	166758680.57	144986067.18	46854.27	78192.40	72299.72
316	1.17E-09	6.03E-09	6.41E-09	514297721.03	166781034.74	145006737.50	60242.77	100546.56	92970.03
320	1.43E-09	7.37E-09	7.84E-09	514311110.23	166803394.89	145027413.71	73631.97	122906.72	113646.24
324	1.69E-09	8.71E-09	9.26E-09	514324500.12	166825761.04	145048095.81	87021.86	145272.87	134328.35
328	1.95E-09	1.00E-08	1.07E-08	514337890.72	166848133.20	145068783.82	100412.45	167645.02	155016.36
332	2.21E-09	1.14E-08	1.21E-08	514351282.01	166870511.35	145089477.73	113803.75	190023.17	175710.27
336	2.47E-09	1.27E-08	1.35E-08	514364673.99	166892895.50	145110177.54	127195.73	212407.33	196410.08
340	2.73E-09	1.41E-08	1.50E-08	514378066.68	166915285.67	145130883.26	140588.42	234797.49	217115.80
344	2.99E-09	1.54E-08	1.64E-08	514391460.06	166937681.84	145151594.89	153981.80	257193.66	237827.43
348	3.25E-09	1.67E-08	1.78E-08	514404854.14	166960084.02	145172312.44	167375.88	279595.84	258544.98
352	3.51E-09	1.81E-08	1.92E-08	514418248.92	166982492.21	145193035.90	180770.66	302004.04	279268.43
356	3.77E-09	1.94E-08	2.07E-08	514431644.39	167004906.42	145213765.27	194166.13	324418.25	299997.81
360	4.03E-09	2.08E-08	2.21E-08	514445040.57	167027326.65	145234500.57	207562.30	346838.48	320733.10
364	4.29E-09	2.21E-08	2.35E-08	514458437.44	167049752.90	145255241.78	220959.18	369264.73	341474.32
368	4.56E-09	2.34E-08	2.49E-08	514471835.01	167072185.17	145275988.93	234356.74	391697.00	362221.47
372	4.82E-09	2.48E-08	2.64E-08	514485233.27	167094623.47	145296742.00	247755.01	414135.30	382974.54
376	5.08E-09	2.61E-08	2.78E-08	514498632.24	167117067.80	145317501.00	261153.97	436579.62	403733.54
380	5.34E-09	2.75E-08	2.92E-08	514512031.90	167139518.15	145338265.93	274553.64	459029.98	424498.47
384	5.60E-09	2.88E-08	3.06E-08	514525432.26	167161974.54	145359036.80	287953.99	481486.37	445269.34
388	5.86E-09	3.01E-08	3.21E-08	514538833.31	167184436.97	145379813.61	301355.05	503948.79	466046.15
392	6.12E-09	3.15E-08	3.35E-08	514552235.07	167206905.43	145400596.35	314756.81	526417.25	486828.89
396	6.38E-09	3.28E-08	3.49E-08	514565637.52	167229379.93	145421385.04	328159.26	548891.75	507617.58
400	6.64E-09	3.42E-08	3.63E-08	514579040.68	166965685.50	145442179.68	341562.41	285197.33	528412.22

In Figures 4.15 - 4.20, the frequency response with pixel temperature, for the three piezo when combined with each metal, are shown.

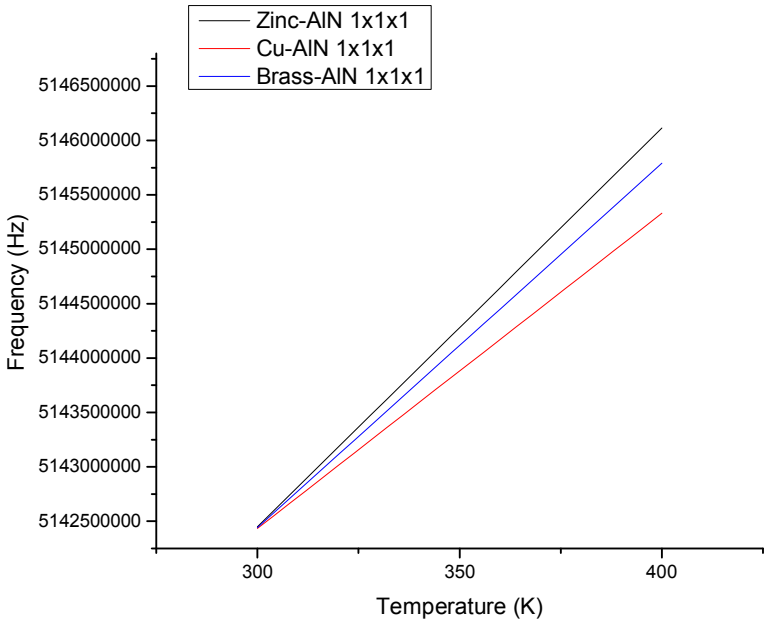

Figure 4.15 Frequency response of AlN (1x1x1 micron^3).

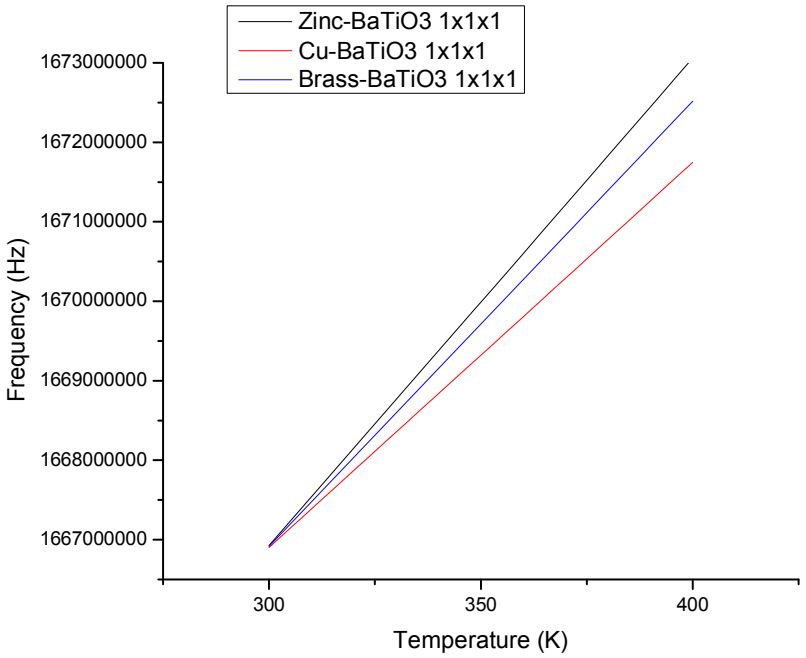

Figure 4.16 Frequency response of $BaTiO_3$ (1x1x1 micron^3).

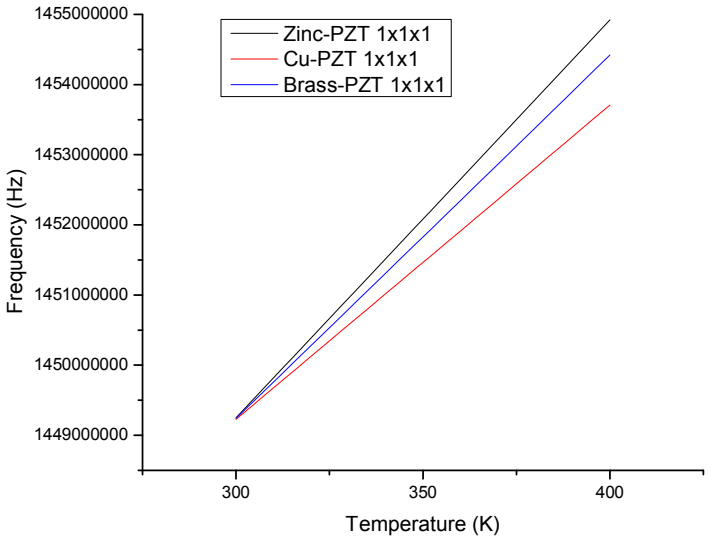

Figure 4.17 Frequency response of PZT (1x1x1 micron^3).

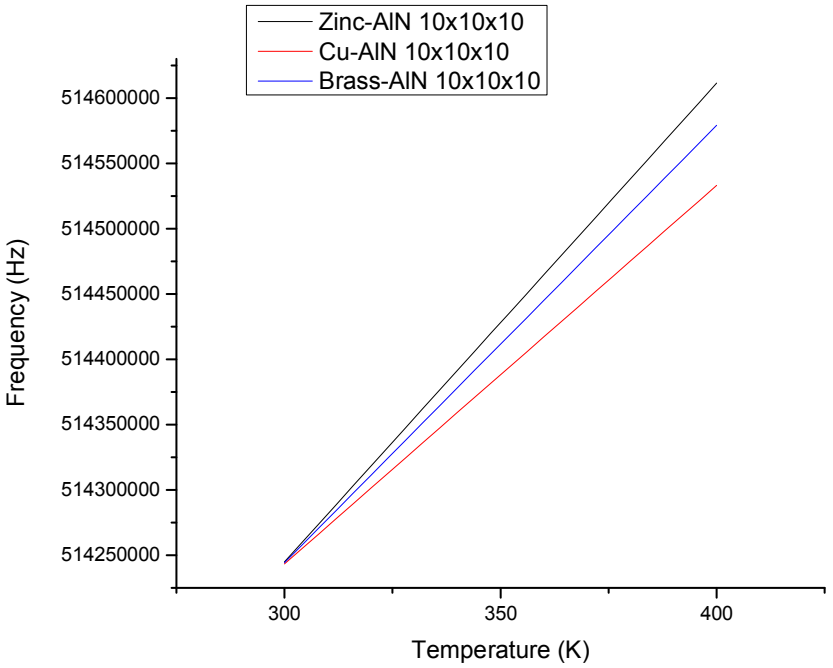

Figure 4.18 Frequency response of AlN (10x10x10 micron^3).

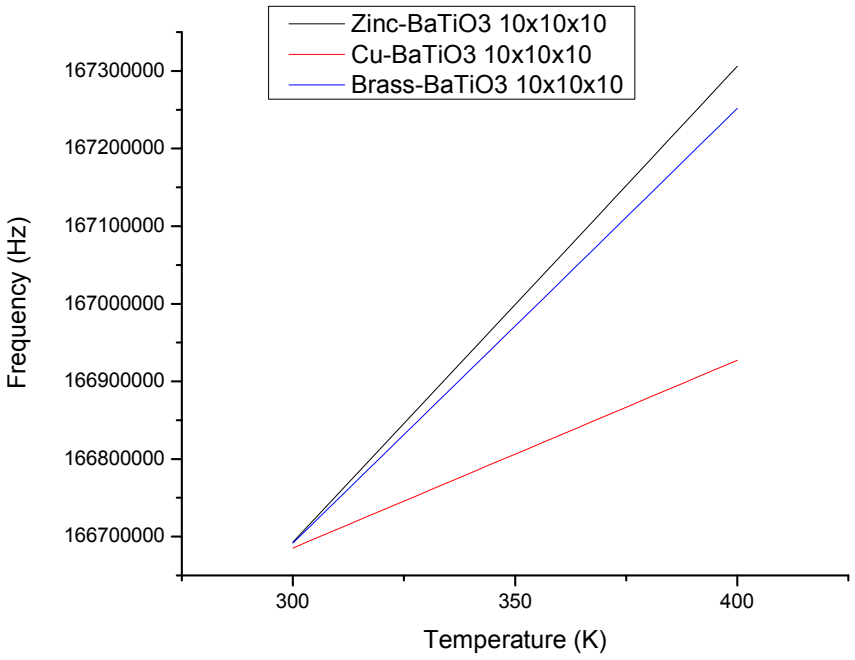

Figure 4.19 Frequency response of $BaTiO_3$ (10x10x10 micron^3).

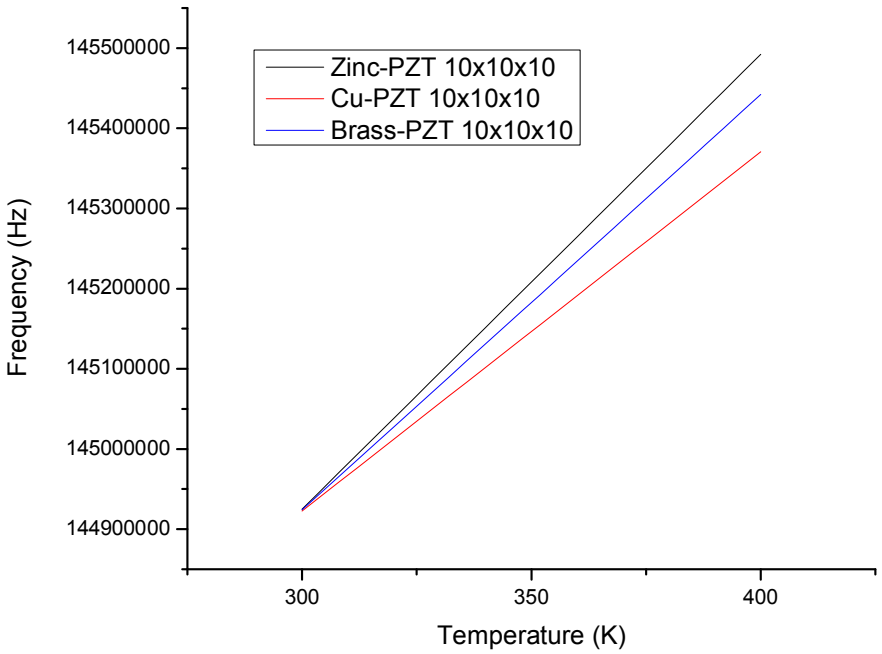

Figure 4.20 Frequency response of PZT (10x10x10 micron^3).

4.5 Discussion of the Results

The *Black Body Calculator* (BBC) [35] was utilized to calculate the amount of energy that reaches the detector. By choosing the parameters, BBC outputs the thermal flux available to the *focal array plane* (FPA). Because of their large thermal conductivities copper, zinc and brass cannot be exposed directly to ambient. Hence a bridge made of PbSe [36] was designed with a thermal conductivity of 1.6 W/m K at 300 K. The thermal conductivity coefficient, λ, of PbSe can be seen in Figures 4.21, along with that of PbS and PbTe.

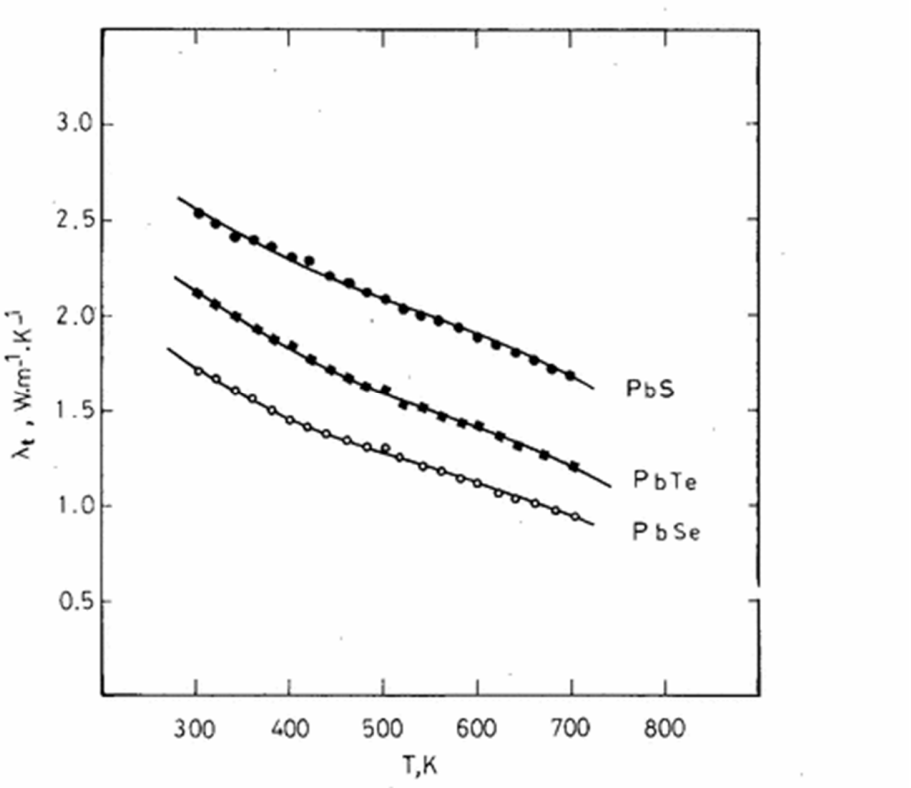

Figure 4.21 Variation in total thermal conductivity of polycrystalline PbS, PbSe and PbTe.
Source: [36]

The temperature sensitivity is approximately 0.2 K of pixel temperature per 1 K of scene temperature change which is 200mK per 1 K of scene temperature change.

As expected from the linear expansion coefficients, the performance of zinc in terms of displacement is better than that of copper and brass. Zinc and brass show a better response as the pixel temperature rises above ambient. Since zinc has a lower melting point, questions on the performance of the metal may arise (although pixel temperatures will not attain temperatures close to its melting point). Brass is a mixture of Cu and Zn, usually 70% copper and 30% zinc, which makes brass harder than copper. However, because heat transfer will occur at higher rates, across materials of high thermal

conductivity, the use of copper as the detecting pixel element outperforms the others in terms of response time.

In the piezoelectric part, it is clear that AlN has the best performance over $BaTiO_3$ and PZT. The performances of PZT and $BaTiO_3$ are almost close to each other and this is due to their comparable mechanical and electrical properties. In summary, the combination of copper and AlN provides the best configuration for the proposed infrared detector based on coefficient of thermal expansion. In Table 4.19, the performance characteristics, i.e., voltage response, of this metal-piezo configuration is summarized.

Table 4.19 Voltage Calculations for Pixel Temperature above Ambient of Table 4.2

Scene temp (K)	pixel temp above ambient (K)	Stress (N/m^2)	Strain	Capacitance (F)	Voltage (V)
300	1.94E+00	1.88E+07	5.46E-05	1.99E-14	1.20E+01
305	2.09E+00	2.03E+07	5.90E-05	1.99E-14	1.30E+01
310	2.25E+00	2.18E+07	6.34E-05	1.99E-14	1.40E+01
315	2.41E+00	2.34E+07	6.80E-05	1.99E-14	1.50E+01
320	2.59E+00	2.51E+07	7.28E-05	1.99E-14	1.61E+01
325	2.77E+00	2.69E+07	7.79E-05	1.99E-14	1.72E+01
330	2.95E+00	2.87E+07	8.32E-05	1.99E-14	1.84E+01
335	3.17E+00	3.07E+07	8.91E-05	1.99E-14	1.97E+01
340	3.34E+00	3.25E+07	9.42E-05	1.99E-14	2.08E+01
345	3.55E+00	3.44E+07	9.99E-05	1.99E-14	2.20E+01
350	3.76E+00	3.65E+07	1.06E-04	1.99E-14	2.34E+01
355	3.98E+00	3.87E+07	1.12E-04	1.99E-14	2.48E+01
360	4.21E+00	4.09E+07	1.19E-04	1.99E-14	2.62E+01
365	4.44E+00	4.31E+07	1.25E-04	1.99E-14	2.76E+01
370	4.68E+00	4.54E+07	1.32E-04	1.99E-14	2.91E+01

From the above Table, a voltage change of approximately 1 V for 5 K change in scene temperature is determined, which is a promising resolution.

As far as the frequency response of the piezo materials is concerned, AlN displays the highest resonance frequency in the pixel temperature range of 300 to 400 K. Performing frequency calculations, for data in Table 4.2, we get:

Table 4.20 Frequency Response for Pixel Temperature Above Ambient of Table 4.2 for AlN

Scene temp (K)	F(Hz)	ΔF(Hz)
300	514392274.4	154796.1434
305	514394536.9	157058.6243
310	514396799.4	159321.1251
315	514399163.7	161685.4597
320	514401663.8	164185.5692
325	514404265.8	166787.5189
330	514406980.9	169502.6249
335	514410058	172579.7797
340	514412637.4	175159.1879
345	514415578.9	178100.6498
350	514418633.5	181155.2804
355	514421914.5	184436.2204
360	514425195.5	187717.2023
365	514428476.5	190998.226
370	514431979.3	194501.0478

Table 4.21 Frequency Response for Pixel Temperature Above Ambient of Table 4.2 for PZT

Scene temp (K)	F(Hz)	ΔF(Hz)
300	144957059.1	43291.68646
305	144960551.5	46784.07847
310	144964044.1	50276.63876
315	144967694	53926.54409
320	144971553.7	57786.2133
325	144975570.7	61803.28187
330	144979762.7	65995.24294
335	144984513.9	70746.42522
340	144988496.7	74729.27383
345	144993038.8	79271.38579
350	144997756	83988.49558
355	145002822.8	89055.3628
360	145007890	94122.58415
365	145012957.6	99190.15966
370	145018368.1	104600.6243

Table 4.22 Frequency Response for Pixel Temperature above Ambient of Table 4.2 for $BaTiO_3$

Scene temp (K)	F(Hz)	ΔF(Hz)
300	166727308.8	46820.66743
305	166731085.8	50597.67393
310	166734863	54374.85157
315	166738810.4	58322.18506
320	166742984.5	62496.36302
325	166747328.9	66840.75207
330	166751862.4	71374.26897
335	166757000.7	76512.55281
340	166761308.1	80819.88764
345	166766220.2	85732.03226
350	166771321.6	90833.41183
355	166776801.2	96313.01901
360	166782281.2	101792.9863
365	166787761.5	107273.3137
370	166793612.6	113124.4332

Therefore, for a scene temperature change of 5K, a frequency change of approximately 3 kHz is determined for AlN, 4.4 kHz for PZT and 4.8 kHz for $BaTiO_3$. AlN performs well at higher frequencies than $BaTiO_3$ and PZT. The clock speed of the circuit developed will be determined by the piezo material. Measuring higher frequencies is always more expensive. From the results, it is also clear that the resolution of the lower frequency materials (PZT and $BaTiO_3$) is higher.

CHAPTER 5

CONCLUSIONS AND FUTURE WORK

5.1 Summary

The design and simulation of a MEMS based IR detector was discussed. Theoretical analysis and simulation suggests that good resolution and sensitivity can be obtained in the wavelength range of 8 to 14 microns.

In the present study, three different materials were considered for the detector metal part and three for the piezoelectric part, in the simulations for the voltage displacement and frequency response.

Further investigation on the bridge design has to be conducted since significant changes to its thermal resistance and the overall improvement in detector performance is attainable. Combined with the conceptual design of the detector and further research on the piezoelectric ceramic alloys, the proposed resolution for both frequency and pixel temperature may even be exceeded.

An issue that needs further investigation is the potential need for a thermal insulation layer between the metal and the piezoelectric material. In the present design, it is certain that the piezo part will counteract to the metal displacement due to the fact that heat will be exchanged between the metal and the piezo. The heat transfer will cause a thermal expansion of the piezo and will change its resonance frequency.

The effects of the shear and bulk modulus were also ignored in the present study, but will have to be considered in the future. A key feature of the thermal expansion

material is also the product between Young's modulus and the coefficient of thermal expansion as it determines the induced stress intensity by being proportional to it.

$$\sigma = E\alpha\Delta T \tag{5.1}$$

Future work which involves fabrication of the device, experimental tests and research on potential material and different more complex designs, may provide better results.

5.2 Multiple Rod Design

A more complex design that annihilates a few of the problems mentioned above and improves the overall performance is being investigated. The model can be seen in Figure 5.1.

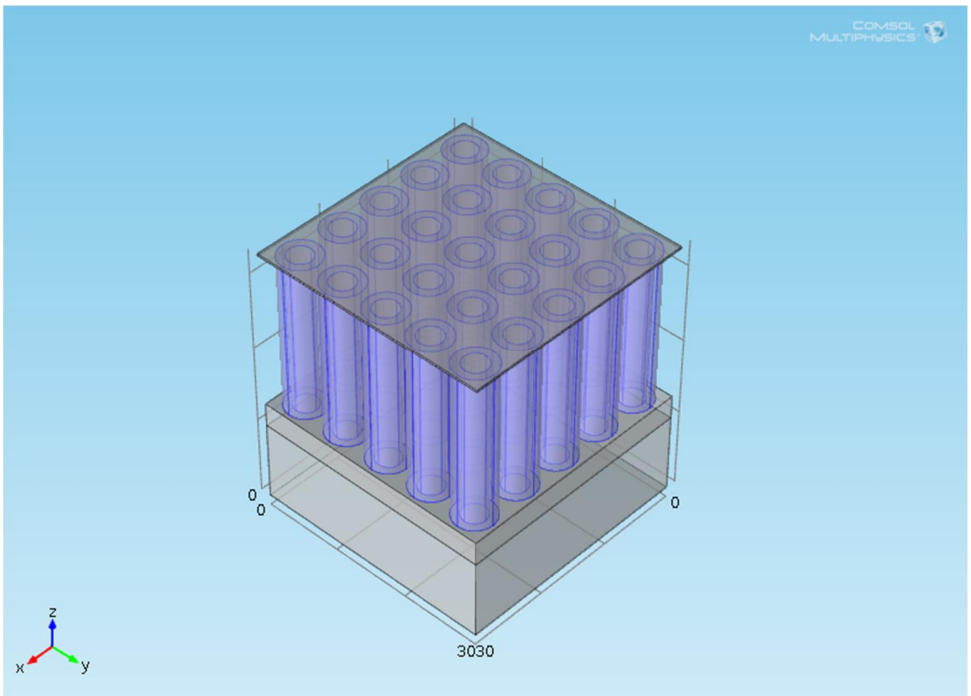

Figure 5.1 COMSOL model of a multi pillar MEMS IR imager design.

In this design, multiple pillars made of a thermal expanding material are physically attached to a Si_3N_4 layer. The Si_3N_4 layer is grown on a piezoelectric block layer (Quartz, PZT, AlN etc). The pillars are coated with an IR absorbing material (PbSe for MIR, or of BCB/PolyAnilene (PANI)[37] for 10 μm IR). On top of the pillars, there is a cubic shaped IR trap (AR coating) which acts like a perfect black body (SiC, CaF_2 ZnSe, ZnS). Its intention is to absorb and trap the incident IR photons between 3-14 μm. The trapped IR photons will be absorbed by the pillar coating material, which acts like a Fabry-Perot cavity and its intention is to heat up the metal rod-core. Each rod will expand applying a stress to the Si_3N_4 layer. This layer has to be hard, with a low thermal expansion coefficient. Its dual purpose is to provide insulation between the thermal expanding material and the resonator and uniformly transport the stress to the resonator. The key element of the structure is the mechanical and thermal properties of the core material of the pillars. The material must have a high Young's modulus and thermal expansion coefficient and a large bulk modulus value, as mentioned in the previous section. At the same time, it must act as a perfect thermal sink in order to quickly absorb the thermal energy from the coating material.

The advantages of the design over the block model are many. First of all, by using a pillar model for the expanding material, potential shear stresses can be avoided. The multi rod design provides significantly better resolution and the pixel size can be chosen, depending on the range of wavelengths. Finally, the pillar coatings do not have to be all from the same material, which means that the same structure can be sensitive to different IR spectral regions. In this way, the design can serve as a multi-region IR imager. Future COMSOL simulations and research on the material candidates will determine the right

course of material choices and provide the necessary calibration data, as well as information on the performance and integrity.

REFERENCES

1. Ujihara, K. (1972). *Reflectivity of Metals at High Temperatures*. Journal of Applied Physics, 43, 2376-2383.
2. Takenaka, K. (2011). *Negative thermal expansion materials: technological key for control of thermal expansion*. Science and Technology of Advanced Materials, 013001 (11pages).
3. Serway, R.A. and J.W. Jewett (2004). Physics for Scientists and Engineers. Upper Saddle River, NJ: Pearson Education. Inc.
4. Hummel, R.E. (2011). Electronic Properties of Materials. New York, NY: Springer.
5. Machine, I.A.W. *Thermal Expansion*. Access date: [09/10/2013]; Available from: http://web.archive.org/web/20090417003154/http://www.ac.wwu.edu/~vawter/PhysicsNet/Topics/Thermal/ThermExpan.html.
6. Murphy, D.B., et al. *Introduction to Optical Birefringence*. Access date: [23/9/2013]; Available from: http://www.microscopyu.com/articles/polarized/birefringenceintro.html.
7. Ferraris, G. *Symmetry Constraints on the physical Properties Of An Anisotropic Material*. 2006 Access date: [09/23/2013]; Available from: http://www.crystallography.fr/mathcryst/pdf/AsCA-MaThCryst-Tsukuba-06_Ferraris.pdf.
8. Wortman, J.J. and R.A. Evans (1965). *Young's Modulus, Shear Modulus, and Poisson's Ratio in Silicon and Germanium*. Journal of Applied Physics, 36, 153-156.

9. Roylance, D. (1995). Mechanical Properties Of Materials. Hoboken, NJ Wiley.

10. Toolbox, E. *Modulus of Elasticity - Young modulus for some common elements*. Access date: [09/23/2013]; Available from: http://www.engineeringtoolbox.com/young-modulus-d_417.html.

11. Toolbox, T.E. *Poissons Ratio*. Access date: [09/10/2013]; Available from: http://www.engineeringtoolbox.com/poissons-ratio-d_1224.html.

12. Norris, A.N. (2006). *Poisson's Ratio in Cubic Materials*. Proceedings of the Royal a Society, 3385-3405.

13. R Nave, G.S.U. *Bulk Elastic Properties*. Access date: [11/3/2013]; Available from: hyperphysics.phy-astr.gsu.edu/hbase/permot3.html.

14. Crandall, D., Lander (1959). An Introduction to the Mechanins of Solids. New York, NY: McGraw-Hill Science.

15. Lind, C. (2012). *Two Decades of Negative Thermal Expansion Research: Where Do We Stand?* Materials, 5, 1125-1154.

16. Zeghbroeck, B.J.V. *Temperature Dependence of the Energy Bandgap*. Access date: [09/10/2013]; Available from: http://ecee.colorado.edu/~bart/book/eband5.htm.

17. Schilling, J.S. (2007). High-Pressure Effects. New York, NY: Springer

18. Nathan, M.I. and W. Paul (1962). *Effect of Pressure on the Energy Levels of Impurities in Semiconductors. II. Gold in Silicon*. Physical Review, 128, 38-42.

19. Samara, G.A. (1968). *Temperature and Pressure Dependence of the Dielectric Constants of the Thallous Halides*. Physical Review, 165, 959-969.

20. Lueng, C.M., et al. (2000). *Piezoelectric Coefficient of Aluminum Nitride and Gallium Nitride*. Journal of Applied Physics, 88, 5360-5363.

21. Heywang, W., K. Lubitz, and W. Wersing (2008). Piezoelectricity: Evolution and Future of a Technology. New York, NY: Springer.
22. Ceramic, P. *Piezo Technology*. [Tutorial] Access date: [09/20/2013]; Available from: http://www.piceramic.com/pdf/Piezoelectric_Effect_Piezo_Techlology_Tutorial_PI_Ceramic.pdf.
23. Ceramic, P. *Piezo Materials Tutorial: The Piezoelectric Effect*. 2013 Access date: [09/30/2013]; Available from: http://www.piceramic.com/piezo_effect.php.
24. Mohammadi, V., S. Mohammadi, and F. Barghi (2013). Piezoelectric Pressure Sensor Based on Enhanced Thin-Film PZT Diaphragm Containing Nanocrystalline Powders. Rijeka, Croatia: InTech.
25. Gad-el-Hak, M. (2001). The MEMS Handbook. Boca Raton, FL: CRC Press.
26. Preumont, A. (2002). Vibration Control of Active Structures: An Introduction. New York, NY: Springer.
27. Moheimani, S.O.R. and Andrew J. Fleming (2006). Piezoelectric Transdusers For Vibration control and Damping New York, NY: Springer.
28. Sirohi, J. and I. Chopra (2000). *Fundamental understanding of piezoelectric strain sensors*. Journal of Intelligent Material Systems and Structures, 11, 246-257.
29. APC International, L. *Piezoelectric ceramics: principles and applications*. 2002 Access date: [09/30/2013]; Available from: http://books.google.com/books?id=HPPtAAAAMAAJ.

30. Ivan Puchades, S.K., *Prototyping of a MEMS Resonant Thermal Imaging Sensor*. 2013, Rochester Institute of Technology, Sponsored Student Research Agreement Statement of Work.

31. Onoe, M. and H. Jumonji (1967). *Useful Formulas for Piezoelectric Ceramic Resonators and Their Application to Measurement of Parameters*. The Journal of the Acoustical Society of America, 41, 974-980.

32. Kutiš, V., et al. (2012). *MEMS Piezoelectric Pressure Sensor-modelling and Simulation*. Procedia Engineering, 48, 338-345.

33. Hui, Y. and M. Rinaldi (2013). *Fast and high resolution thermal detector based on an aluminum nitride piezoelectric microelectromechanical resonator with an integrated suspended heat absorbing element*. Applied Physics Letters, 102, 093501 (4 pages).

34. Kaufman, P.N., N.M. Ravindra, and B. Jamieson (2013). *Coefficient of Thermal Expansion Based MEMS Infrared Detector*. Accepted Manuscript, Emerging Materials Research.

35. Santa Barbara Focalplane, L.M. *Extended Blackbody Calculator*. Access date: [10/10/2013]; Available from: http://www.sbfp.com/fluxcalc/fluxcalculator.html.

36. El-Sharkawy, A.A., et al. (1983). *Thermophysical properties of polycrystalline PbS, PbSe, and PbTe in the temperature range 300–700 K*. International Journal of Thermophysics, 4, 261-269.

37. Kamineni, V.K., et al. (2011). *Investigation of Optical Properties of Benzocyclobutene Wafer Bonding Layer Used for 3D Interconnects Via Infrared Spectroscopic Ellipsometry*. Thin Solid Films, 519, 2924-2928.